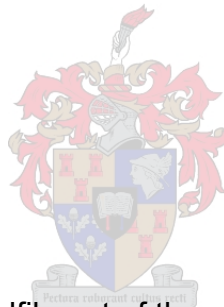


**A NUMERICAL ANALYSIS OF THE FLOW FIELD  
SURROUNDING A SOLAR CHIMNEY POWER PLANT**

by

Rhydar Lee Harris



Thesis presented in partial fulfilment of the requirements for the degree of  
Master of Science in Engineering at the University of Stellenbosch

Thesis Supervisors: Dr T M Harms

Prof. D. G. Kröger

Department of Mechanical Engineering  
University of Stellenbosch

April 2004

## Declaration

I, the undersigned declare that the work contained in this thesis is my own original work and that I have not previously, in its entirety or in part, submitted it at any university for degree.

Signature: \_\_\_\_\_

(R. L. Harris)

Date: \_\_\_\_\_

## Abstract

This study investigated the flow field above a proposed solar chimney power plant, without a cross wind, using a commercial numerical solver in the form of CFX 4-4 by AEA Technology plc. The governing equations solved are for an incompressible steady state solution. Variation in density due to buoyant effects is modelled with the Boussinesq approximation, and turbulence is approximated by the k- $\epsilon$  model with modifications due to buoyancy. The effect of different turbulence conditions at atmospheric inflows is also investigated.

Modifications to the k- $\epsilon$  turbulence model in the context of atmospheric turbulence are investigated and applied to the standard k- $\epsilon$  model. These modifications include the addition of source terms in the turbulence kinetic energy and the turbulence dissipation rate equations to allow for the production/destruction of turbulence due to buoyancy. Other modifications include an additional source term in the turbulence dissipation rate equation accounting for atmospheric stability and the specification of model constants relevant to atmospheric flows.

Initial results for the flow field using the Boussinesq approximation show reasonable correlation between the current study and the study by Thiart (2002) whereby the flow field exhibits characteristics of the axially symmetric turbulent jet. One of the primary and most noticeable differences between the current study and that of Thiart (2002) is the difference in height at which air is drawn into the collector.

In order to account for variation in density with height, a modification on the Boussinesq approximation, the Deep Boussinesq model, Montavon (1998), is applied to a simplified 100 m by 100 m rectangular geometry. The results obtained are compared to a similar model using the Boussinesq approximation and it is seen that the average velocities reached in the deep Boussinesq model are significantly larger than those obtained in the Boussinesq approximation.

## Abstrak

Hierdie studie ondersoek die vloeiveld bo 'n aangewese son-skoorsteen kragstasie, deur die gebruik van 'n kommersiële numeriese oplosser in die vorm van CFX 4-4; van AEA Technology plc. Die heersende vergelykings wat opgelos moet word, is vir 'n nie-saampersbare, tyd-onafhanklike oplossing. Die wisseling in digtheid as gevolg van saamdrukbaarheids effekte, word gemodelleer met die Boussinesq benadering en turbulensie-skatting deur die  $k-\epsilon$  model met aanpassings as gevolg van dryfkrag. Die effek van die verskillende turbulensie-toestande teen atmosferiese invloeing word ook ondersoek.

Aanpassings op die  $k-\epsilon$  turbulensie-model in die konteks van atmosferies turbulensie word ondersoek en toegepas op die standaard  $k-\epsilon$  model. Hierdie veranderinge sluit die byvoeging van bron terme in die turbulente kinetiese energie en die turbulensie-verspillings vergelykings om ruimte te laat vir die produksie/afbreking van turbulensie as gevolg van dryfkrag in. Ander aanpassings sluit in 'n bykomende bron term in die turbulensie-verspillings vergelyking wat rekenskap gee vir atmosferiese stabiliteit en die spesifikasie van model onveranderlikes met betrekking tot atmosferiese vloei.

Aanvanklike resultate vir die vloeiveld met die gebruik van die Boussinesq benadering dui op geredelike ooreenstemming tussen de huidige studie en die studie van Thiart (2002), waar die vloeiveld eienskappe toon van 'n simmetriese turbulente spilpunt. Een van die mees primêre en duidelikste verskille tussen die huidige studie en diè van Thiart (2002) is die verskil in die hoogte waarteen die lug in die samesteller ingesuiig word.

Om rekenskap te kan gee vir die verskil in digtheid met betrekking tot hoogte is 'n aanpassing van die Boussinesq benadering, die Diep Bussinesq model, Montavon (1998), aangebring. Hierdie aanpassing word toegepas op 'n vereenvoudigde 100 m by 100 m reghoek. Die resultate wat verkry word, word vergelyk met 'n soortgelyke model waar die algemene snelheid wat met die diep Boussinesq model bereik word merkbaar groter is as die in die Boussinesq benadering.

## Acknowledgements

I am grateful for my parents who supported me.

Thanks to Dr T M Harms for insightful discussions and his patience.

To Prof D Kröger for increasing my understanding.

To Dr C Montavon and Dr P Witt for technical help

Table of Contents	pg
Declaration	i
Abstract	ii
Acknowledgments	iv
Table of Contents	v
List of Symbols	ix
List of Figures	xii
List of Tables	xiv
 <b>CHAPTER 1. INTRODUCTION</b>	
1.1. Motivation	1-1
1.2. Layout of the Thesis	1-4
1.3. Conventions Used	1-5
 <b>CHAPTER 2. LITERATURE STUDY</b>	
2.1. Solar Chimney	2-1
2.2. Atmospheric Flow Modelling	2-2
2.3. Turbulence and Buoyancy	2-3
 <b>CHAPTER 3. SOLAR CHIMNEY</b>	

3.1. Introduction	3-1
3.2. Physical Geometry	3-2
3.3. Operation	3-3
3.4. Physical Boundaries and Model Assumptions	3-4
3.5. Numerical Modelling of Free Boundaries	3-7



## **CHAPTER 4. ATMOSPHERIC MODELLING**

4.1. Introduction	4-1
4.2. Physical Aspects of the Atmosphere	4-2
4.3. Stability of the Atmosphere	4-5
4.4. Buoyancy	4-7
4.5. Atmospheric Turbulence	4-8
4.6. Conclusions and Discussion	4-9

## **CHAPTER 5. BUOYANCY AND TURBULENCE**

5.1. Introduction	5-1
5.2. Variable Density	5-2
5.3. Buoyancy	5-7
5.4. Turbulence Modelling	5-10
5.5. Discussions and Conclusions	5-14

## **CHAPTER 6. SOLAR CHIMNEY NUMERICAL MODEL**

6.1. Introduction	6-1
6.2. Axisymmetric Geometry	6-2
6.3. Boundary Conditions	6-6
6.4. Model Assumptions	6-9
6.5. Numerical Control	6-10
6.6. Results	6-13
6.7. Conclusion	6-21

## **CHAPTER 7. DEEP BOUSSINESQ MODEL**

7.1. Introduction	7-1
7.2. Theoretical Considerations	7-2
7.3. CFX 4-4 Application	7-5
7.4. Sample Test Case	7-7
7.5. Results	7-11
7.6. Discussion and Conclusions	7-20

## **CHAPTER 8. FURTHER WORK**

8.1. Three-dimensional Model	8-1
8.2. Large Eddy Simulation Turbulence Model	8-3
8.3. Variable Density	8-4

## **CHAPTER 9. CONCLUSION**

9.1. Conclusion	9-1
-----------------	-----

## **REFERENCES**

## **APPENDIX A. ATMOSPHERIC LAPSE RATE**

A.1 Fully Compressible DALR	A-2
A.2 Weakly Compressible DALR	A-4

## **APPENDIX B. CFD BASICS**

B.1 Introduction	B-2
B.2 Governing Equations	B-2
B.3 Discretization of Differential Equations	B-4
B.4 Pressure Velocity Coupling	B-6
B.5 Components of a CFD Code	B-7

## **APPENDIX C. TURBULENCE MODELLING**

C.1 Turbulence Models	C-2
C.2 Reynolds Averaged Navier-Stokes Equations	C-4
C.3 k- $\epsilon$ Turbulence Model	C-6

## **APPENDIX D. ERRORS**

D.1 Errors in CFD Simulations	D-2
D.2 Grid Independence	D-3

## **APPENDIX E. DEEP BOUSSINESQ**

E.1 Energy Equation in Terms of Potential Temperature	E-1
---	-----

## APPENDIX F. USER FORTRAN ROUTINES

F.1	Hydrostatic Density Profile	F-2
F.2	Specification of Potential Temperature Diffusivity	F-3
F.3	Addition of Source Terms in Transport Equations	F-4

## List of Symbols

<i>Symbol</i>	<i>Description</i>	<i>Units</i>
C	Constant	
$c_p$	Specific heat at constant pressure	$\text{J kg}^{-1} \text{K}^{-1}$
$c_v$	Specific heat at constant volume	$\text{J kg}^{-1} \text{K}^{-1}$
D	Diameter	m
d	Characteristic length based on diameter	m
g	Gravitational acceleration	$\text{m s}^{-2}$
H	Total enthalpy	$\text{J kg}^{-1}$
h	Enthalpy, height	$\text{J kg}^{-1}, \text{m}$
$h_0$	Collector inlet height	m
k	Turbulent kinetic energy	$\text{m}^2 \text{s}^{-2}$
l	Characteristic length	m
N	Number of control volumes	
p	Pressure	$\text{N m}^{-2}$
R	Gas constant,	$\text{J kg}^{-1} \text{K}^{-1}$
R	Residual error	
$R_0$	Maximum radius	m
$R_u$	Universal gas constant,	$\text{J mol}^{-1} \text{K}^{-1}$
r	Radius	m
S	Source terms in the transport equations	
T	Real Temperature	K
t	Time	s
U	Free stream velocity	$\text{m s}^{-1}$
u	Internal energy, velocity in the x direction	$\text{J kg}^{-1}, \text{m.s}^{-1}$
w	Velocity component in the z direction	$\text{m s}^{-1}$
x	Horizontal co-ordinate direction	m
y	Horizontal co-ordinate direction	m
z	Vertical co-ordinate direction	m

### *Dimensionless Numbers*

Pe	Péclet number	$Pe = \frac{\rho u \Delta x}{\Gamma}$
Pr	Prandtl number	$Pr = \frac{c_p \mu}{\lambda}$
Re	Reynolds number	$Re = \frac{\rho U d}{\mu}$
Ri	Richardson number	$Ri = \frac{g}{T_o} \frac{\partial \bar{T} / \partial z}{(\partial \bar{u} / \partial z)^2}$

### *Greek symbols*

$\Delta$	Difference	m
$\Gamma$	Diffusivity, Dry Adiabatic Lapse Rate	$\text{kg m}^{-1} \text{s}^{-1}$ , $\text{K m}^{-1}$
$\alpha$	Specific volume	$\text{m}^3 \text{kg}^{-1}$
$\beta$	Thermal expansion co-efficient	$\text{K}^{-1}$
$\varepsilon$	Turbulence dissipation rate	$\text{m}^2 \text{s}^{-3}$
$\phi$	Independent variable	
$\gamma$	Ratio of specific heats	
$\lambda$	Conductivity	$\text{W m}^{-1} \text{K}^{-1}$
$\mu$	Dynamic viscosity	$\text{kg m}^{-1} \text{s}^{-1}$
$\nu$	Kinematic viscosity	$\text{m}^2 \text{s}^{-1}$
$\theta$	Potential Temperature	K
$\rho$	Fluid density	$\text{kg m}^{-3}$
$\sigma$	Prandtl number	
$\partial$	Partial derivative	

*Sub-scripts*

0	Reference or ground value
ave	Average
c	Chimney
eff	Effective
fb	Free Boundary
h	Hydrostatic
i	Index notation
inl	Inlet
j	Index notation
o	Outer
ref	Reference value
T	Turbulent
$\infty$	Ambient value



## List of Figures

Figure 3-1: Solar chimney power plant physical geometry	3-3
Figure 3-2: Boundary condition assumptions	3-4
Figure 4-1: Diagram of troposphere subdivision	4-2
Figure 4-2: Stability representation - Guyot (1998)	4-6
Figure 5-1: Comparison of hydrostatic pressure	5-4
Figure 5-2: Comparison of temperature profiles for an adiabatic process	5-5
Figure 5-3: Density comparison – Adiabatic process	5-5
Figure 5-4: Density comparison – Adiabatic temp	5-6
Figure 6-1: Axisymmetric section of the solar chimney	6-2
Figure 6-2: Coarse grid	6-3
Figure 6-3: Grid at chimney exit	6-4
Figure 6-4: Grid at collector inlet	6-4
Figure 6-5: Grid expansion in the x-direction above the chimney	6-5
Figure 6-6: Convergence history	6-12
Figure 6-7: u Velocity comparison above collector	6-14
Figure 6-8: Temperature comparison above collector	6-14
Figure 6-9: Normalised u-velocity above the outlet of the chimney	6-15
Figure 6-10: Normalised temperature above the outlet of the chimney	6-15
Figure 6-11: Temperature contours	6-16
Figure 6-12: Pressure contours	6-17
Figure 6-13: Velocity vectors and speed contours	6-18
Figure 6-14: Streamlines	6-19
Figure 6-15: Turbulent viscosity contours – Neumann boundary	6-20
Figure 6-16: Turbulent viscosity contours – Dirichlet boundary	6-21
Figure 7-1: Test model boundary conditions	7-8
Figure 7-2: Turbulent viscosity – Boussinesq approximation	7-11
Figure 7-3: Comparison of density	7-12
Figure 7-4: Residual plot for "zero" flow test	7-13
Figure 7-5: Potential temperature contour plot	7-13

Figure 7-6: Speed contours and vector plot	7-13
Figure 7-7: Residual plot - $\Delta\theta = 1\text{K}$	7-14
Figure 7-8: Potential temperature contour plot	7-14
Figure 7-9: Speed contours	7-15
Figure 7-10: Potential temperature contours	7-15
Figure 7-11: Speed contours	7-15
Figure 7-12: $k$ - no additional source terms	7-16
Figure 7-13: $\varepsilon$ - no additional source terms	7-16
Figure 7-14: $k$ buoyancy and dissipation source terms	7-16
Figure 7-15: $\varepsilon$ buoyancy and dissipation source terms	7-16
Figure 7-16: Complete model - $\mu_{\text{eff}}$	7-17
Figure 7-17: Complete model - Potential temperature	7-17
Figure 7-18: Complete model - Speed contours	7-18
Figure 7-19: Boussinesq approximation - Speed contours	7-18
Figure 7-20: Boussinesq approximation - Potential temperature contours	7-19
Figure 8-1: Model geometry and boundaries	8-1
Figure 8-2: Top view of model	8-2
Figure 8-3: Front view and chimney detail	8-3

## List of Tables

Table 5-1: Modified k- $\epsilon$ model constants	5-11
Table 5-2: Boundary conditions for turbulence	5-13
Table 6-1: Grid refinement	6-5
Table 6-2: Number of control volumes	6-6
Table 6-3: Turbulence constants	6-10
Table 6-4: Differencing schemes	6-11
Table 6-5: Under-relaxation factors	6-11
Table 7-1: Under-relaxation factors	7-10
Table C-1: Standard k- $\epsilon$ model constants	C-8

# CHAPTER 1. INTRODUCTION

---

## 1.1. Motivation

A strong global opinion as well as scientific research holds that the burning of fossil fuels in power plants, automobiles and production processes is causing an increase in global temperature and the exacerbation of the greenhouse effect, Wilks (2001). Coupled with this is the increase in industrialization and the subsequent need for electricity in developing nations of the world. International treaties on the reduction of fossil fuel power generation and on the increase of renewable and sustainable sources of energy have led to the development of “greener” and more environmentally friendly power plants.

One of the friendliest of these; releasing zero pollutants into the atmosphere and requiring significantly less maintenance than conventional power stations; could be considered to be the solar chimney power plant proposed by J Schlaich in the late 1970's, Schlaich (1995). This relatively simple design comprises of three known technologies: a raised, circular, transparent collector, a central chimney and a shrouded turbine at the base of the chimney. Short wavelength solar radiation is transmitted through the glass of the collector and causes the temperature of the ground underneath to rise. Heat is then transferred to the air above the ground, inside the collector. Density differences between the external air and the hot, low density, air in the chimney induces a radial flow from the periphery to the centre of the collector, where the kinetic energy of the air is converted to electrical energy by the turbine.

This thesis attempts to numerically model the flow field above the collector and the chimney of the power plant. The primary influences on the structure of the flow field are expected to be buoyancy driven, due to the hot collector and entrainment due to the buoyant jet of the chimney outlet. An attempt has been made to answer a number of questions relating to small to medium scale atmospheric processes: How is buoyancy modelled in the context of a variable density atmosphere? Linked to this question is that of what boundary conditions are appropriate and similarly if a compressible flow field can be

calculated using the assumption of an incompressible CFD model. Furthermore the effects of variations on turbulence models are investigated. With respect to the performance of the solar chimney power plant an important question is that of the height at which air is drawn into the collector.

There are numerous reasons why a numerical model is important. Generically a numerical model is usually more cost effective than an experimental one. In some cases, such as environmental flow modelling, it is not possible to conduct experiments due to scaling constraints. The cost of a numerical model is usually proportional to the complexity of the model. For this reason numerical models are most effectively used when comparing only certain parameters. Consequently it becomes necessary to make assumptions regarding the nature of the flow field and the predominant flow parameters, Ferziger et al. (2002)

Most, if not all, environmental processes are turbulent due to the low viscosity of air and the large associated length scales. The correct implementation of a turbulence model to the solution of the flow field is therefore critical in obtaining accurate results.

Another important aspect in the modelling of the solar chimney is correctly modelling the buoyant effects caused by the density difference due to the hot collector roof and the ambient air. The most common buoyancy model is based on the Boussinesq approximation, Kays and Crawford (1993), which approximates density differences to temperature differences utilising the thermal expansion co-efficient of the fluid. This model is limited however to the assumption of an incompressible fluid and small temperature differences, (Jaluria, 1980). Considering an atmosphere with a dry adiabatic lapse rate, the density decreases as a function of the linear temperature decrease and the hydrostatic pressure. The assumption of incompressibility then, becomes less valid with increasing height. At approximately 1000 m, the density difference between a constant reference density at ground level and the actual density is approximately 8 % of the actual density. At the proposed height at the exit of the chimney of the power plant shown in figure 3-1, the error would be just over 13 %. For a numerical model, the upper vertical boundary must be far enough away from the chimney so that it does not affect the results. Considering a height of 5000 m, the actual density is less than half that at ground level. At

these heights, the density differences cannot be ignored in the solution of the governing equations of the flow, and a method of accounting for the density variation should be sought.

Montavon (1998) utilised a modified Boussinesq buoyancy model, referred to as a “Deep Boussinesq” approximation, Montavon (1998), in modelling of hydrostatic mountain waves with a vertical dimension of 15 km. The basis of the deep Boussinesq model is that flow variables do not change significantly from a hydrostatic equilibrium condition. It then becomes possible to linearise the pressure, density and temperature as a deviation from this hydrostatic state. The conservation and Navier-Stokes equations are then solved with density being specified as a function of height only, based on a real temperature profile. Buoyant momentum forces in the vertical direction caused by differences in density from the hydrostatic condition are approximated by differences in potential temperature from the hydrostatic potential temperature. This model has the advantage of the simplifications utilised by the Boussinesq approximation, whereby the assumption of constant density decouples the momentum and energy equations, yet still allows for the modelling of a variable density.

The flow field surrounding the solar chimney is characterised by a number of flow processes such as unstable horizontal flat plate convection, entrainment of air at the chimney exit and buoyancy driven natural circulation. An analytical solution to this problem is therefore very difficult to obtain. A numerical solution is thus necessary. In obtaining the numerical solution, the commercial code CFX 4-4 by AEA Technologies was utilised. Two personal computers were used independently when solving flow cases. The decision was based on the scale of the particular model. The “smaller” of these uses a Pentium II 400 Mhz processor with 516 Mbytes of RAM. For larger models a Pentium III 1 Ghz processor with 786 Mbytes of RAM was used.

## 1.2. Layout of the Thesis

There are many references and papers written concerning small scale atmospheric flow modelling and flow due to buoyant forces in an environmental context. Chapter 2, attempts to summarise the primary assumptions used in these models and the dependent parameters for atmospheric flow phenomena.

As the focus of the thesis is on the solution of the flow surrounding the solar chimney it is necessary to investigate the physical aspects of a standard design. In chapter 3, a brief description of the scale, geometry and workings of a 200 MW power plant are discussed, standard operating conditions are then defined. Numerically it is required to specify boundary conditions to be solved, thus it is necessary to define the physical boundaries for the actual model. This aspect is also discussed in chapter 3.

Chapter 4 deals with the description of an analytical solution for pressure and temperature of dry air in an adiabatic process. Commonly made assumptions for environmental flow phenomena are also discussed in this chapter. Atmospheric stability based on buoyancy effects and the deviation of local temperature gradients to a dry adiabatic lapse rate is also investigated.

The important aspects of an accurate model for atmospheric turbulence, buoyancy and compressibility are detailed in chapter 5. Throughout, the k- $\epsilon$  model is used in the modelling of turbulent processes. Modifications to the k- $\epsilon$  model with respect to production and dissipation of turbulence due to buoyancy and with regards to atmospheric flows are described along with available buoyancy models.

The development of a two-dimensional axisymmetric model of the solar chimney power plant is detailed in chapter 6. Results shown are based on the Boussinesq approximation for the modelling of buoyancy.

Implementation of a potential temperature based deep Boussinesq model is developed in chapter 7 for a simple 100 m by 100 m, two-dimensional rectangular block. Results

obtained for the deep Boussinesq model are compared to results from the same boundary conditions using the Boussinesq approximation.

Chapter 8 briefly describes some of the work started on further modelling challenges for an accurate representation of the flow field above the solar chimney power plant. These include a three-dimensional model, turbulence models and models that better account for the variation in density in atmospheric flow processes.

### **1.3. Conventions Used**

In the description of governing equations, and in their derivations the normal conventions of horizontal plane variables in the  $x,y$  directions are used, with  $z$  being the vertical component. The exception to this occurs in the description of flow processes in the numerical model of the solar chimney, where the positive  $x$  axis is defined as the vertical co-ordinate direction. The reason for this is that CFX 4-4 specifies the  $x$ -axis as the axis of symmetry for an axisymmetric model; in order to maintain consistency in FORTRAN subroutines this convention has been used for *all* the numerical models. SI units are used throughout.

The term CFX 4-4 is used to describe the operation of the program and the program itself. If any references are made to theoretical aspects of the modelling or information contained in the documentation of CFX 4-4, the reference CFX 4-4 (2001) is used. In a similar manner the post-processing program Tecplot 7-5 by Amtec is described. The reference Tecplot 7-5 refers to the program itself and Tecplot 7-5 (1998) refers to the documentation.



## CHAPTER 2. LITERATURE STUDY

---

### 2.1. Solar Chimney

In order to develop a numerical model, the physical dimensions of the model need to be known. Information regarding sizing of the components was obtained from numerous sources including, Schlaich (1995), and Gannon and von Backström (2000). Hedderwick (2001) numerically investigated the flow field through the collector and chimney of the power plant. The results obtained included transient data for collector temperature, air temperature in the collector and outlet velocity and temperature of the air at the chimney exit. The standard operating conditions for the model are taken from the values calculated for solar noon on the summer equinox, the 21<sup>st</sup> of December, for a hypothetical power plant at a reference location near Sishen in South Africa.

Thiart (2002) modelled the flow above a solar chimney power plant using the assumption of incompressible flow and utilising the Boussinesq approximation to account for the buoyancy terms. The free boundary was modelled by a pressure boundary, whereby the pressure and temperature were explicitly stated as the hydrodynamic pressure and temperature. Turbulence was modelled with the k- $\epsilon$  model.

There are many papers and articles available for numerically modelling large scale problems that involve interaction with the atmosphere, physically unconstrained problems. Schreüder (1986) modelled the airflow through and around the air-cooled condenser of a 4 000 MWe generic power station. The primary focus was on the problems associated with the free boundaries and possible numerical approaches to specifying conditions on these. The approach used in calculating the boundary conditions for the current model of the solar chimney uses a method specified by Schreuder (1986).

## 2.2. Atmospheric Flow Modelling

König and Mokhtarzadeh-Dehgahn (2002) modelled flow from and around a multi-flue chimney using the assumption of weak compressibility. This assumes that the density of air is a function of the temperature only, described by a related equation of state. Turbulence is modelled using the k- $\epsilon$  model and the boundary conditions are stipulated with the use of an inlet/outlet condition and three symmetry boundaries for the remaining free boundaries associated with their three-dimensional model. A turbulent atmospheric boundary layer was set for the atmospheric inlet boundary. Temperature was assumed to be constant for the inlet condition. As will be seen in the following chapters, this assumption greatly simplifies the numerical computation of the problem.

Huser et al. (1997) utilised a buoyancy modified k- $\epsilon$  model in the application of CFD to a pollution model over complex terrain. Once again the weakly compressible flow option was utilised. Huser et al. (1997) also introduce the concept of calculating the potential temperature,  $\theta$ , in order to compensate for using the weakly compressible flow option. The atmospheric boundary conditions follow those used by König and Mokhtarzadeh-Dehgahn (2002), namely using inlet/outlet, and three symmetry boundary conditions. Huser et al. (1997) specify a pressure value for the outlet boundary and impose zero gradients in the flow direction on other variables. A turbulent velocity profile is specified at the inlet as well as specification of inlet potential temperature and functions for the calculation of turbulence parameters, k and  $\epsilon$ . Buoyancy is not modelled in the vertical direction, as this causes complications with the outlet pressure boundaries.

Sinai (2000) obtained results for the flow field above a pool fire. Buoyancy is modelled with the Boussinesq approximation and the standard buoyancy modified k- $\epsilon$  model is used for turbulence. The model is axisymmetric, and a zero cross wind condition is used. For the boundary conditions on the perimeter of the model and at the upper horizontal boundary, pressure boundaries are applied. This configuration is similar to the approach used in this work.



### 2.3. Turbulence and Buoyancy

The textbook by Rodi (1980) is considered to be the definitive text in describing the buoyancy extension of the  $k$ - $\epsilon$  model for turbulence. Yan and Holmstedt (1999) developed a modified  $k$ - $\epsilon$  turbulence model to improve the modelling of buoyancy in the standard model. They found that the standard model seriously under-predicts the spreading rate of the vertical thermal plume. Shabbir and Taulbee (1990) have evaluated turbulence models for the prediction of buoyant flows and also found that the rate of production of turbulence kinetic energy by buoyancy is several times larger than that predicted by the simple gradient diffusion term in the standard buoyancy modified equation.

Values of the constants in the  $k$ - $\epsilon$  model are usually modified for specific flow situations. Duynkerke (1988) experimentally obtained values for turbulence constants for the neutral and stable boundary layer. Duynkerke (1988) also introduces a modification to the standard  $k$ - $\epsilon$  model to take into account stability of the atmosphere. This source term in the turbulence dissipation rate,  $\epsilon$  equation relates the gradients of the turbulence kinetic energy,  $k$ , to the dissipation of turbulence. It is only applied when positive, for a stable atmosphere.

Montavon (1998) uses the above-mentioned modifications and model constants in the turbulence model applied to flow over a mountain range for wind power analysis. Coupled to this is the use of the potential temperature for the modelling of buoyancy and the use of the deep Boussinesq model. The vertical scale of the problem described by Montavon (1998) is approximately 15 km. The deep Boussinesq model assumes incompressible flow, but specifies the density as a function of a hydrostatic pressure and an actual temperature profile in order to account for the density changes over such a large vertical domain.

The use of Large Eddy Simulation (LES) in the modelling of turbulence for atmospheric application is becoming popular. Van Stijn and Nieuwstadt (1986) utilise LES for atmospheric flows and Ferziger et al. (2002) insists on the use of LES for the modelling of environmental and atmospheric turbulence. Wilcox (1994) suggests that LES needs approximately 10% of the computational resources that direct numerical simulation, DNS,

requires. For a model the size of the flow field above and around the solar chimney power plant a more economical model for turbulence, such as the  $k-\epsilon$ , though not as accurate, would have to be used.

## CHAPTER 3. SOLAR CHIMNEY POWER PLANT

---

### 3.1. Introduction

This chapter describes the physical geometry and operation of a proposed 200 MW solar chimney power plant. As there are many papers and books on the plant, specifically the book by Schlaich (1995), these topics are only briefly covered. The results of the numerical model of Hedderwick (2001) of the solar chimney power plant are used in order to specify a set of standard operating values at solar noon for the collector temperature and the chimney outlet velocity and temperature. These values are used in the final numerical model of the flow field above the collector as boundary conditions.

An important aspect of this chapter is determining a method of modelling the free boundaries. These are numerically the most difficult to model, as they must be specified such that they have little effect on the flow field caused by the collector and close enough to the plant in order to minimise computations where there is little or no interest in the results. The possible options for the free boundaries are investigated and a method of approach is selected.

For a geometrically symmetric model, as in the case of the solar chimney power plant, the usual convention is to simplify the model to a two-dimensional case. In reality, for a model of the dimensions of the solar chimney the effect of Coriolis forces on the flow field will not be negligible for this study. However, this would complicate the model and exceed the computational resources available by forcing the modelling of a three dimensional field. The assumption then, in order to simplify the modelling, is that the flow results would be symmetric about the axis of the chimney.

Another simplifying assumption for the model is that a quasi-steady state solution exists. Poreh (1996) investigated the use of small-scale models in order to assimilate the phenomena of the Urban Heat Island (UHI). UHIs are localised atmospheric effects, which occur over urban areas due to differences in the heat flux between the urban and the

surrounding rural areas. In order to simplify the modelling of the UHI, Poreh (1996) defined a Simple Heat Island (SHI) as being geometrically well bounded; Poreh (1996) considers a circular area. It is also assumed in the modelling that UHI's have uniform surface characteristics and a uniform vertical sensible heat flux from the surface to the atmosphere. Another assumption used by Poreh (1996) was of a zero vertical sensible heat flux from the surrounding area and a neutrally stratified, calm ambient atmosphere. Further assumptions are that the flow is turbulent above the SHI and that the effects of Coriolis acceleration and radiation have a negligible influence on the flow above the SHI.

It seems plausible that the same assumptions can be applied to the collector of the solar chimney power plant. Poreh (1996) calculated the time needed for an urban heat island, with an effective radius of 5000 m, to establish steady-state conditions as approximately 70 minutes and for a radius of 1000 m, approximately 25 minutes, based on the rate of change of the ground heat flux. When the change in heat flux is low, around the middle of the day, a quasi-steady state solution would probably exist.

### 3.2. Physical Geometry

The solar chimney power plant is an amalgamation of three known technologies. A circular transparent, either glass or clear plastic, collector, raised above the ground, a tall chimney and a shrouded wind turbine at the base of the chimney. According to Schlaich (1995) and Gannon and von Backström (2000), a power plant with a design output of 200 MW would require a 7 km diameter collector and a 1500 m chimney, with a flue diameter of 160 m. In order to facilitate airflow through the chimney the height of the collector would increase with decreasing radius. Thiart (2002) suggests the following function to describe the curvature of the collector, where  $h_0$  is the collector height at the outer perimeter and is approximately 10 m high.

$$h = h_0 \left( \frac{R_o}{r} \right)^{0.5} \quad (3-1)$$

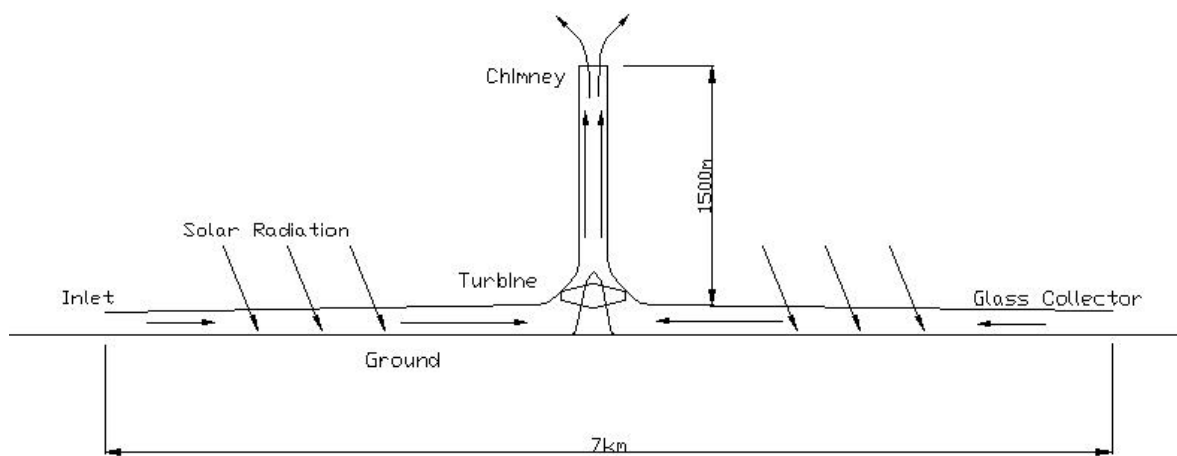


Figure 3-1: Solar chimney power plant physical geometry

The chimney would be constructed as a stand-alone structure and would not rely on guy cables for support. Geographically, the plant would be situated on a large, flat, semi-desert area.

### 3.3. Operation

Short wavelength solar radiation transmits through the collector to the ground below, causing heating of the ground surface. This heating of the ground causes the so-called greenhouse effect, leading to a convective flow field in underneath the collector. As the air heats up its density decreases and there exists a subsequent density difference between the hot collector air and the cold ambient air.

A buoyancy induced flow due to the difference in density between the column of colder ambient air surrounding the collector and the column of hot air in the chimney, causes a driving force, which tends to accelerate the air under the collector from the periphery to the centre. The turbine at the base of the chimney then converts this kinetic energy to electrical power by means of a generator situated in the turbine hub.



As power output is directly related to solar radiation, the power curve of the plant follows the diurnal movement of the sun, with peak power at around mid-day, Gannon and von Backström (2000). Schlaich (1995) has shown that nighttime operation is possible with the inclusion of a thermal storage system under the collector. Even without an additional system, the thermal storage in the ground under the collector means that some power is available even at night.

A 50 kW test plant was constructed in Manzanarez, Spain, in 1981 and was operational until the end of 1989, Schlaich (1995).

### 3.4. Physical Boundaries and Model Assumptions

There are a number of physical boundaries, which need to be defined and specified for any model of the chimney. As can be seen in the figure below three wall conditions exist: the collector wall, the ground and the chimney wall. Mass will leave the model at the collector inlet and enter at the chimney outlet at a certain velocity and temperature. The boundaries surrounding the plant are open to the atmosphere and must allow for mass flow into and out of the flow domain depending on the flow field above the collector.

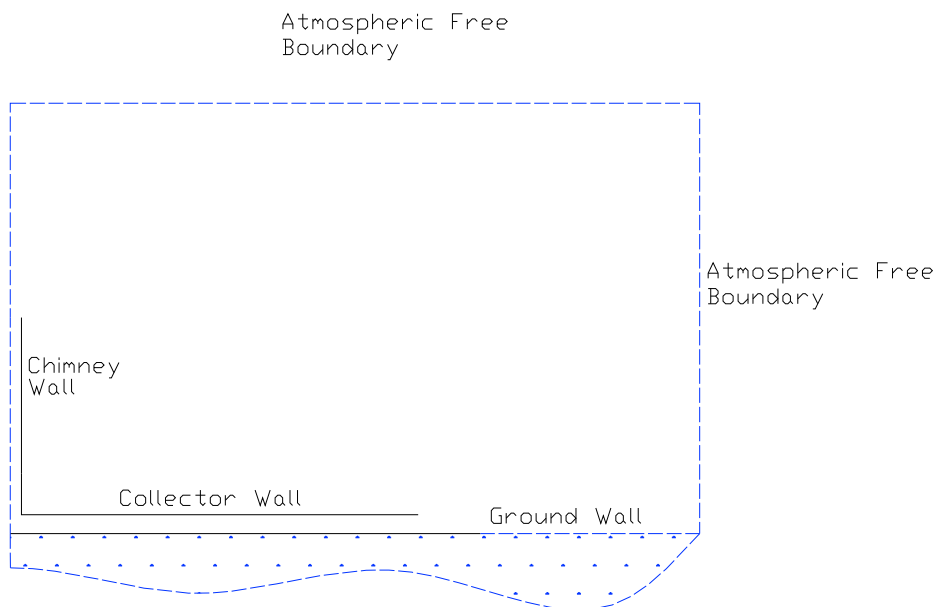


Figure 3-2: Boundary condition assumptions

### 3.4.1. Walls

Considering the size of the flow domain, and the relative size of surface undulations compared to the height of the chimney, the wall boundaries can be idealised as smooth. Surface roughness of the glass and the sand surrounding the plant is of the order of  $10^{-4}$ , Guyot (1997). Hedderwick (2001) has shown that the temperature of the collector surface stays relative constant, as a function of the radius from the chimney axis, during operation of the plant. At solar noon, the temperature varies little from an average value of approximately  $47\text{ }^{\circ}\text{C}$  or about  $320\text{ K}$ . The ground surrounding the collector is also assumed to have a constant temperature of  $300\text{ K}$  or  $27\text{ }^{\circ}\text{C}$ .

Due to the high velocity of air in the chimney and the insulating properties of concrete it is reasonable to assume that the chimney wall is at the same temperature as the surrounding air. For the purpose of the model, the chimney wall is also considered smooth. The curvature of the collector is assumed not to have a significant effect on the flow pattern and can be idealised as flat and parallel to the ground.

### 3.4.2. Mass Flow

Hedderwick (2001) has further demonstrated that at solar noon, the chimney outlet velocity is approximately  $14.5\text{ m s}^{-1}$ . For an adiabatic process the temperature drop through the chimney is approximately  $1\text{ }^{\circ}\text{C}$  per  $100\text{ m}$ . This would be the same temperature decrease in the ambient air around the chimney. Therefore the temperature difference between the chimney outlet and the ambient air, at the same height, is approximately  $20\text{ }^{\circ}\text{C}$  for the ground and collector temperature defined above.

Using a temperature of  $305\text{ K}$ ; the temperature that  $320\text{ K}$  air from the collector would adiabatically cool to at the chimney outlet; to obtain density and viscosity, the outlet velocity stated and the chimney diameter as a characteristic length, the Reynolds number for the chimney outlet is calculated from:

$$\text{Re} = \frac{\rho U d}{\mu} \quad (3-2)$$

This is in the order of  $10^9$  and is therefore turbulent. The level of turbulent fluctuations will be a function of the outlet velocity and the dissipation will have a characteristic length defined by the diameter of the chimney. König and Mokhtarzadeh-Dehghan (2002) use the following functions to calculate  $k$  and  $\varepsilon$  values for a buoyant plume from a chimney into an atmospheric boundary layer:

$$k = 0.002 \bar{w}^2 \quad (3-3)$$

$$\varepsilon = \frac{k^{3/2}}{l} \quad (3-4)$$

Where  $l$  is defined in terms of the chimney diameter as  $0.1d_{\text{ch}}$ .

In the absence of a louvre system to control mass flow through the roof of the collector, there will be local mass conservation between collector inlet and the chimney outlet. This means that no mass will enter the flow domain through the collector. In the event of re-circulation of air from the collector back into the surroundings, it is assumed that the air will be at the same temperature, 300 K, as the ground.

### 3.4.3. Free Boundaries

For a characteristic length of the height of the chimney, and assuming a constant average density for a dry adiabatic lapse rate, a Reynolds number calculation gives a value in the order of  $10^6$  for an inlet velocity of  $0.1 \text{ m s}^{-1}$ . The air entering into the flow domain will therefore be turbulent and it is necessary to ascertain what level of turbulence exists for this particular configuration. Chapter 5 explains the modelling of turbulence for atmospheric flows and possible values for the specification thereof for the free boundaries.

#### **3.4.4. Standard operating values**

With the above information it is possible to specify a set of standard operating values for the wall and mass flow boundary conditions at solar noon. For the purpose of this numerical model, standard operating values of 320 K for the collector temperature have been used. A ground temperature of 300 K or 27 °C is assumed

An outlet velocity of 15 m s<sup>-1</sup> for the chimney outlet and an outlet temperature 20 °C less than the ambient air at the collector height is used. This is based on the above given values for the air at the base of the chimney being at 320 K and the surrounding air at 300 K, from the same vertical height, cooling adiabatically to the height at the chimney outlet.

Further assumptions regarding variation of thermal properties in the atmosphere around the chimney are discussed in chapter 4.

### **3.5. Numerical Modelling of Free Boundaries**

According to Schreüder (1986), it is common to view the atmosphere as a semi-infinite air mass bounded below by an infinite flat surface, which may either be rough or smooth depending on the scale of the problem. Analytically the concept of an infinite domain may be used as an advantage, in a numerical investigation, however, it is very difficult to treat an infinite domain. Usually the domain boundaries are fixed at some distance away from the object such that, in general the disturbance created by the object at that boundary is not zero. Boundary conditions can either be described with Dirichlet conditions, where the values of the variables of velocity, pressure, temperature and turbulence are specified explicitly; or Neumann conditions where the gradients of the variables are specified.

It is in the specification of the boundary conditions for free boundaries; where the numerical model is open to the atmosphere surrounding; where most of the problems of atmospheric flow arise, Schreüder (1986). The major problem is the lack of knowledge of the variables at a distance far removed from the part of the flow where the major interest lies. For all practical purposes, if the boundary were positioned far enough away, the disturbance created by the boundary condition would die away. The problem lies in the

fact that an impractical amount of nodes are then needed in an area where the least interest in the flow patterns exists, thus extending the required computing and storage. A strong cross velocity, or wind, greatly simplifies the problem as the extent of vertical movements in the flow is thus reduced, subsequently reducing the vertical domain needed. Failing this, Schreuder (1986) describes three methods for modelling free atmospheric boundaries.

1. The potential flow extension method splits the flow domain into two regions. In the inner region, the area of interest, the standard governing equations are solved. In the outer region a simplified inviscid potential flow solution is used in order to calculate velocities, and pressure, through Bernoulli's equation. This method still requires a large amount of computational effort and the inner zone needs to be extended in order to act as a buffer region for the outer zone perturbations to die down.
2. The second method involves using general analytical solutions in order to specify the variables in terms of each other and then solving the required variables.
3. Thirdly it is possible to calculate the boundary value of the variable using the normal momentum and energy equations followed by the solution of the mass conservation equation in order to correct for the overall values of mass and or heat flux.

Schreuder (1986) then divides the above methods into three general classes, illustrated below.

1.  $u_{fb}$  specified,  $v_{fb} = 0$ ,  $\left(\frac{\partial p}{\partial y}\right)_{fb} = 0$
2.  $u_{fb}$  specified,  $v_{fb}$  calculated,  $\left(\frac{\partial p}{\partial y}\right)_{fb} = 0$
3.  $u_{fb}$  specified,  $v_{fb}$  calculated,  $p_{fb}$  specified

The above-mentioned methods impose fewer restrictions on the boundaries; consequently less needs to be known about the boundary beforehand. As can be seen in the specifications above, the velocity and pressure values are specified or calculated, with other variables being calculated from these. There are restrictions on each of the boundary conditions. Option one, while well behaved, effectively puts a limit on the mass flow into

or out of the boundary. The second boundary conditions allow for mass flow across the boundary, but limit large velocities across the boundary due to the zero pressure gradient term. The third condition allows for the specification of the pressure term, which could lead to large gradients in the velocity and pressure.

Due to the restriction imposed by the commercial numerical fluid dynamics package used, CFX 4-4, the boundary conditions specified for the numerical model of the solar chimney power plant are of the third type.

If the flow field of the numerical problem under consideration is driven by buoyancy forces a further complication to the numerical model is added, Cook and Lomas (1997). There are two main reasons for this: firstly the flow field is implicitly specified, the sources of buoyancy must calculate a velocity field, and secondly, there is uncertainty on how accurately turbulence is modelled. The implications of these statements on the specifications of the boundary conditions are that the inlet values for velocity and turbulence are not known *a priori*. This makes specifications of boundary conditions on the free boundaries for velocity, pressure and turbulence properties difficult, and certain assumptions to the flow field, and inlet conditions, need to be made. Specification of values for the pressure at the free boundary is discussed further in chapter 5.

## CHAPTER 4. ATMOSPHERIC MODELLING

---

### 4.1. Introduction

As seen in the previous chapter, the top of the chimney of the solar chimney power plant is approximately 1500 m above ground level. The atmospheric, or planetary, boundary layer, (PBL), extends from the ground to approximately 1 – 2 km, depending on the time of day, surface heating and atmospheric stability. It is in this region that most thermal, pollutant and water vapour mixing takes place. As this is the region most affected by the solar chimney power plant, and the processes in this region have the most effect on the plant itself, a brief description of the PBL is given in this chapter. An important characteristic of the PBL is the concept of atmospheric stability, and the effects of surface heating and buoyancy on stability. Coupled with buoyancy is the production or destruction of turbulence due to unstable or stable atmospheres respectively. Atmospheric turbulence and buoyancy are qualitatively introduced in this chapter.

According to Ferziger et al. (2002) the smallest scale of interest in atmospheric flow modelling is the atmospheric boundary layer. In the horizontal direction, the computational domain must be several kilometres wide in order to reasonably represent the physical aspects of the flow. For modelling of the atmospheric state above urban areas and surroundings, the scale must be even larger than this. These typical dimensions needed for an accurate representation of what Ferziger et al. (2002) calls small-scale atmospheric flows, dictates a limit on the accuracy that can be expected in the modelling. This limit manifests itself in the computational resources available. Another factor, which makes environmental flow modelling difficult, is the large number of parameters that need to be specified. It is very difficult, with present computing resources, to model all of these processes. This chapter outlines the predominant features of atmospheric flow modelling and the associated models, including variation in properties and stratification of density and temperature.

## 4.2. Physical Aspects of the Atmosphere

### 4.2.1. Planetary Boundary Layer

The planetary boundary layer, PBL, extends from the earth surface to approximately 1km into the troposphere. It is strongly influenced by the earth's surface due to shear stresses. Heat is released into the atmosphere through the PBL via surface heat flux and turbulent eddies or thermal plumes. During the day, the PBL is characterised by turbulent transport of mass and thermal energy.

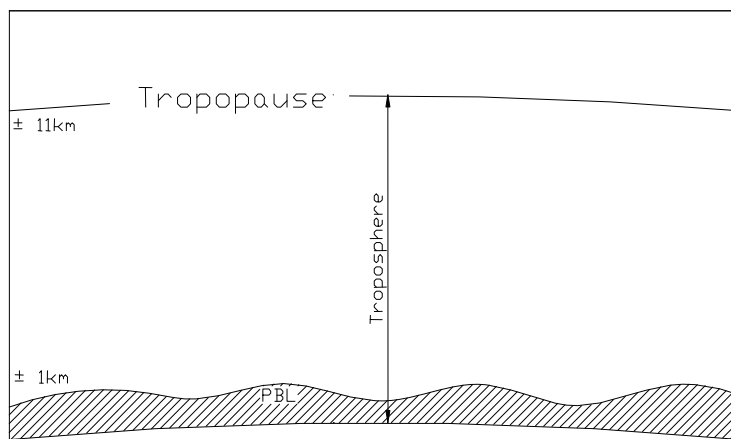


Figure 4-1: Diagram of troposphere subdivision

Further investigation of the PBL shows the existence of three regions. These regions vary throughout the day. During the day the following divisions can be made. The first layer is the surface layer, which extends to approximately 100 m. It is in this region that the vertical fluxes are nearly constant. The next layer is the convective mixed layer, which extends to a height slightly less than the top of the PBL; it is in this layer that the potential temperature and mixing ratio are nearly uniform. Temperature profiles are nearly adiabatic and the water vapour mixing ratio is nearly constant. The division between the PBL and the free atmosphere, the continuation of the troposphere, is the entrainment zone.

At night, the convective mixed layer is replaced by a stable boundary layer. The top of the PBL, at night, is seen to be a capping inversion.



#### 4.2.2. Composition

The atmosphere of the earth is made up of about 78% nitrogen, 21% oxygen and other trace gases, including argon and carbon dioxide. There is also a large amount of water vapour present in the earth's atmosphere.

#### 4.2.3. Variation of properties

##### *Viscosity*

Viscosity of a fluid is known to vary as a function of temperature and pressure, White (1994). The increase of viscosity with increasing pressure is very small, approximately 10 percent for a pressure difference of 5000 kPa, White (1994), and can effectively be neglected for environmental flows. There is however a relatively strong dependence of viscosity with temperature, with  $\mu$  increasing with temperature for gasses.

The variation of viscosity in the atmosphere can be calculated from Rayleigh's formula, Houghton and Carpenter (1993), given below:

$$\frac{\mu_2}{\mu_1} = \left( \frac{T_2}{T_1} \right)^{3/4} \quad (4-1)$$

Even though molecular viscosity is seen to change with temperature, the apparent eddy-viscosity of turbulent flow is orders of magnitude larger than the molecular viscosity, and this temperature dependence can be ignored, Wilcox (1994).

##### *Specific heat*

The specific heat of air varies slightly with temperature, Mills (1995), and can be considered constant for atmospheric processes.

### ***Temperature Profiles***

Atmospheric air is characterised by a vertical variation of temperature profiles and distinct layers. Many textbooks, Guyot (1998), give details on these layers, the most important, as far as meteorological phenomena is concerned is the Troposphere. The troposphere extends from the earth's surface to approximately 11 km and is characterised by a linear temperature profile. The temperature profile varies throughout the day depending on, among other factors, the surface heat flux and the relative humidity of the air. The saturated adiabatic lapse rate, SALR, is the temperature gradient for completely saturated atmospheric air and decreases at approximately 5 °C per 1000 m. For completely dry air, the dry adiabatic lapse rate, DALR, applies, which can later be seen to correspond to a temperature decrease of approximately 10 °C per 1000 m. The atmospheric lapse rate lies somewhere between these two extremes and an international standard lapse rate is defined as 6.5 °C per 1000 m. For a solar chimney, which would be built in an arid region, the use of the DALR in modelling is the more appropriate option.

### ***Density***

Atmospheric air behaves practically as a perfect gas, and thus verifies the equation of state linking pressure, temperature and density. For dry air this is:

$$\rho = \frac{p}{RT} \quad (4-2)$$

For a particle of slowly rising air, the pressure gradient in the vertical direction is equal to the product of the density of the parcel and the gravitational acceleration:

$$\frac{dp}{dz} = -\rho g \quad (4-3)$$

### ***Dry Adiabatic Lapse Rate***

Utilising the perfect gas law approximation for a parcel of air subjected to a pressure gradient as described above, and assuming an isentropic expansion process for the air, it is possible to derive equations for the temperature and pressure field for a fully compressible atmosphere, Kröger (1998). The complete derivation is given in appendix A. The temperature profile is known as the dry adiabatic lapse rate, due to the assumptions of dry air and an adiabatic, reversible process. The pressure and temperature profiles are shown below.

$$T = T_1 - 0.00975z \quad (4-4)$$

$$p = p_1 \left( 1 - \frac{0.00975z}{T_1} \right)^{3.5} \quad (4-5)$$

The equations for the temperature and pressure profiles can then be used to calculate air density at any altitude using the perfect gas law. As mentioned above, this is known as a neutrally stable condition.

### **4.3. Stability of the Atmosphere**

Variation in the temperature of the air with altitude involves vertical stratification of the density of the atmospheric air. An air parcel displaced either upwards or downwards will enter into an environment with differing density from the parcel. Depending on the surrounding air temperature and density, the air will either accelerate or decelerate, due to this difference in density after adiabatic cooling or heating. If the air parcel continues to accelerate the atmosphere is unstable, if the parcel decelerates the atmosphere is considered stable. Guyot (1998) demonstrates that the stability of the atmosphere can be based on the potential temperature gradients and the variation of the temperature gradient from the dry adiabatic lapse rate. The dry adiabatic lapse rate is considered neutrally stable.

In the figure below, the shaded arrows represent the motion of the air parcel after an initial displacement.

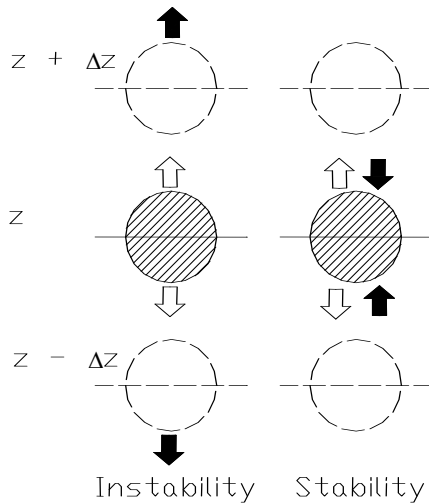


Figure 4-2: Stability representation - Guyot (1998)

For a local temperature gradient,  $\partial T/\partial z$ , and  $\Gamma$  being the dry adiabatic lapse rate the stability of the atmosphere is shown below.

$$\frac{\partial T}{\partial z} < \Gamma \quad \text{Unstable} \quad (4-6)$$

$$\frac{\partial T}{\partial z} = \Gamma \quad \text{Neutrally stable} \quad (4-7)$$

$$\frac{\partial T}{\partial z} > \Gamma \quad \text{Stable} \quad (4-8)$$

### 4.3.1. Richardson Number

The Richardson number represents the ratio of forces of buoyancy due to vertical thermal gradient to the forces of inertia resulting from the interaction of eddies with the mean vertical velocity gradient.

$$Ri = \frac{g}{T_o} \frac{\partial \bar{T} / \partial z}{(\partial \bar{u} / \partial z)^2} \quad (4-9)$$

The Richardson number is negative when the thermal profile is super-adiabatic and positive in inversion conditions. It is zero for conditions of thermal neutrality. The value of the Richardson number can be used to determine the transition between different convection types, Guyot (1998).

The Richardson number is also used to indicate the relative importance of turbulence intensity in a particular stably stratified flow field with the anisotropy of the turbulence, rewritten in terms of densities, this becomes.

$$Ri_g = \frac{g}{\rho} \frac{\partial \rho / \partial z}{(\partial U / \partial z)^2} \quad (4-10)$$

#### 4.3.2. Potential Temperature

Potential temperature is a variable, which is conserved along flow trajectories for processes without radiative heat flux or latent heat release and for adiabatic processes, see appendix E for details. The definition of potential temperature is given below:

$$\theta(z) = T(z) \left( \frac{P_0}{p(z)} \right)^{R/C_p} \quad (4-11)$$

Using potential temperature to model thermal fluxes in atmospheric processes is preferred, Hoffman (1997), since the gradient is a true reflection of the actual heat flux in the atmospheric boundary layer.

#### 4.4. Buoyancy

Buoyancy forces play a dominant role in the determination of atmospheric motions, Batchelor (1954). Buoyancy effects are generated due to density differences from temperature or concentration gradients in a fluid. This buoyancy force is linked to convective transfer of heat and mass in a fluid. Convection can be divided into two main categories. The first is forced convection, where the movement of air is caused by an external force, such as a wind, a fan or even the induced flow field caused by the temperature difference from the object to the surrounding atmosphere. Free convection is the process whereby the motion of fluid around a particular object is due primarily to the temperature difference of the object in the presence of an external body force, such as gravity. In many practical cases of interest the convective heat transfer is a combination of free and mixed convection. The main difficulty in the analysis of convective heat transfer processes is the coupling of the energy equation to the governing equations of motion and mass conservation of the fluid through the variation of density,  $\rho$  (Jaluria,1980). The distributions of velocity and temperature are interdependent.

An important class of natural convection flows is one which relates to buoyancy driven flows moving freely in the atmosphere without the constraining influence of a surface. These flows occur frequently in nature and are termed free boundary flows (Jaluria ,1980). Natural convective flows are considerably affected by a stratification of the ambient, surrounding fluid. This stratification often arises due to the processes of heat and mass transfer from the surface itself. A stable stratified medium is one where the lighter, less dense fluid is lying above heavier, fluid.

According to Batchelor (1954), hot columns of air intermittently ascend from heated plates into ambient atmospheric conditions. These hot columns are non-stationary and appear to move at random across the plate, developing from small disturbances.

## 4.5. Atmospheric Turbulence

Turbulence is a disorderly motion of flow characterized by high Reynolds numbers. It is a three-dimensional phenomenon and is extremely complex. White (1991) gives 5 characteristics of turbulent flow as being:

- Fluctuations in pressure, velocity and temperature (for heat transfer). Fluctuations in three directions superimposed on the mean value of the flow properties.
- The existence of a large range of fluid 'packets' known as eddies. Varying sizes of eddies from the shear layer thickness,  $\delta$  to the Kolmogorov length scale,  $L = (\nu^3 \delta / U^3)^{1/4}$ .
- Random variation in fluid properties, which have a particular form. Each property has a specific continuous energy spectrum, which decreases to zero at high wave number, small eddy sizes.
- Self-sustaining motion. After the initial formation of turbulence, the flow can maintain turbulence by the production of new eddies to replace those lost by viscous dissipation.
- Mixing which is much stronger than due to laminar action. Due to the three dimensional nature of the flow, rapid diffusion of mass, momentum and energy is possible. Heat transfer and friction are much greater for turbulent flow than for laminar flow.

Turbulent flows need not be confined to wall boundaries. Boundary free flows, such as jets, wakes and mixing layers also exhibit turbulent flow patterns and characteristics.

Due to the large scale of atmospheric flow phenomena and the low viscosity of air, atmospheric flows are almost always turbulent. The large variation in mixing length and turbulent vortices guarantees effective mixing of heat, and the dispersion of particulates and effluent into the atmosphere, Van Stijn and Nieuwstadt (1986).

## 4.6. Conclusions and Discussion

This chapter has introduced some of the concepts in modelling atmospheric processes. In particular is the variation of temperature, density and pressure with height.

The most important concept is the fact that a local temperature profile has an effect on the stability of the atmosphere. Atmospheric stability has been defined as being related to the temperature gradient for an adiabatic process. For a gradient less than the adiabatic gradient the atmosphere is unstable and for a gradient greater than the adiabatic gradient, the atmosphere is considered stable.

Buoyancy forces are directly related to the local temperature gradient. Buoyancy has been qualitatively defined in this chapter. It is important to realise that buoyancy is a local phenomenon, in as much as the movement of a parcel of air is dependant on the density differences between the parcel and surrounding air.

Atmospheric turbulence has also been introduced in the chapter. Atmospheric processes are almost always turbulent due to large length scales and low viscosity of air. In the following chapter the numerical aspects of modelling buoyancy, turbulence and density stratifications will be discussed.



## CHAPTER 5. BUOYANCY AND TURBULENCE

---

### 5.1. Introduction

The previous chapter has shown that there are three main criteria for the modelling of flow processes on the scale of the solar chimney. These are: variable density of atmospheric air, buoyancy effects in the atmosphere and atmospheric turbulence. Due to the fact that a commercial code in the form of CFX 4-4 is being used, the available models in the program limit the specification of how these processes are implemented. Radical alterations to the available default models are also beyond the scope of this thesis. In this chapter the available models are investigated in order to ascertain the most applicable for the modelling of the flow field above the solar chimney. Buoyancy effects and compressibility are linked through, primarily, the momentum equation. For this reason these two effects will be investigated together. There is also a tenuous link between buoyancy and the production and destruction of turbulence. Turbulence generation is however a secondary effect of a buoyant flow, rather than, as is the case with the level of compressibility, a fundamental characteristic of the modelling thereof.

Four possible compressibility-buoyancy options are investigated. The first three are the default options available in CFX 4-4, while the fourth is a modification on the incompressible assumption to account for a variation in density.

In the case of turbulence the well-known  $k-\epsilon$  model, detailed in appendix C, is used. In this chapter the modifications to the turbulence model, due to the effects of buoyancy and for the application in atmospheric flow processes, are discussed. These modifications entail the addition of source terms to account for production and dissipation due to buoyancy, and the use of non-standard equation constants based on atmospheric flow. A further source term is introduced into the dissipation equation to take into account atmospheric stability.

As the specifications of boundary conditions for free boundaries are dependent on the model used, the final part of this chapter details the free boundary values associated with the numerical model of the solar chimney.

## 5.2. Variable Density

There are three default methods of modelling compressibility in CFX 4-4. The first is that the flow is incompressible and that the density is constant.

$$\rho = \rho_{ref} \quad (5-1)$$

The second method of modelling compressibility is under the assumption that the density is only a function of the temperature. This is accomplished by using a modified equation of state with the variable pressure term being replaced by a constant reference pressure.

$$\rho = \frac{P_{ref}}{RT} \quad (5-2)$$

The implication of this is that density is independent of pressure fluctuations and the speed of sound is assumed infinite. This option is prescribed for flow where the Mach number is small, usually less than 0.3 and where large temperature differences are expected in the flow. Combustion processes are an example of the applicability of this assumption, particularly when the physical space is limited.

A further assumption for weakly compressible flow is that the kinetic energy term is ignored in the energy equation with respect to the internal energy.

$$H = h + \frac{1}{2} \vec{u}^2 \approx h \quad (5-3)$$

The energy equation, where  $\lambda$  is the thermal conductivity, for weakly compressible flows is:

$$\frac{\partial}{\partial t}(\rho h) + \bar{\nabla}(\rho \bar{u} h) - \bar{\nabla}(\lambda \nabla T) = 0 \quad (5-4)$$

The energy equation is transformed into an advection diffusion equation for  $h$ , by replacing the temperature gradient with an enthalpy gradient.

$$\lambda \nabla T = \frac{\lambda}{c_p} \nabla h \quad (5-5)$$

The final compressibility option is the ideal gas law equation of state. In this instance density is related to both pressure and temperature:

$$\rho = \frac{P}{RT} \quad (5-6)$$

The pressure in the above equation refers to the absolute pressure and not the pressure used in calculations by CFX 4-4, the modifications to the pressure term can be seen in appendix B.

In appendix A, temperature and pressure functions have been derived for an adiabatic process for the above mentioned compressibility options. Substituting the pressure and temperature into the relevant equations of state yields the density. In the case of incompressible flow the temperature is independent of the pressure and the pressure is simply the hydrostatic pressure for a constant density.

$$P = P_0 - \rho_{ref} g z \quad (5-7)$$

These functions are shown graphically below. As can be seen in figure 5-1, the fully compressible and weakly compressible hydrostatic pressure compares exactly in the assumption of an adiabatic process.

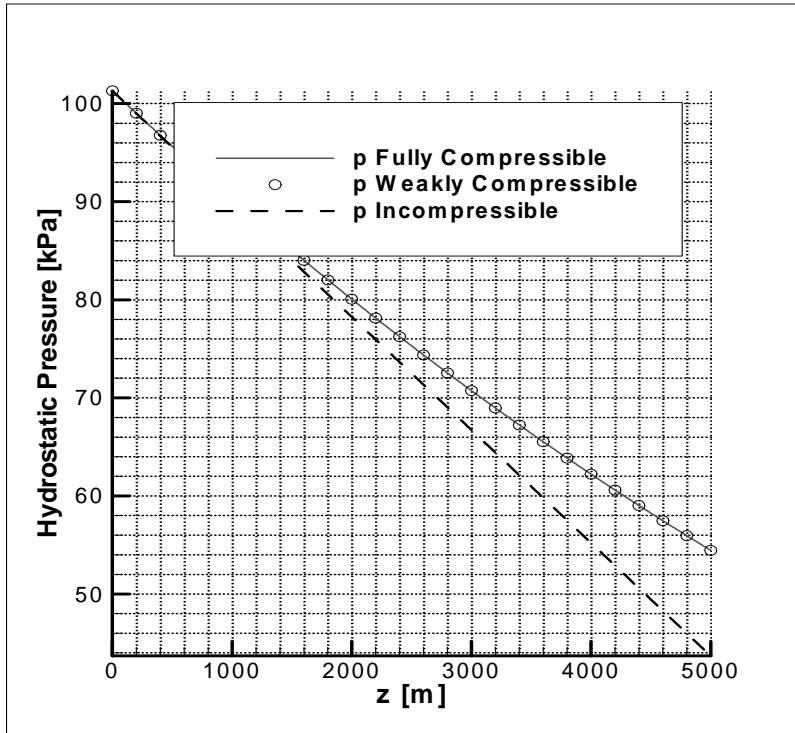


Figure 5-1: Comparison of hydrostatic pressure

Figures 5-2 and 5-3 compare the derived adiabatic temperature profile and the subsequent density profile from equations A-11 and A-22, and the integration of the pressure gradient for a constant density. As can be seen in figure 5-2 the temperature solved for an isentropic process under the assumption of weak compressibility the temperature increases for an increasing height. The temperature gradient is also not constant, as can be seen in the figure and in the derivation in appendix A.

The density functions, as seen in figure 5-3 below, are exact for the compressible options. This is due to the assumption, in the derivation, of an isentropic process.

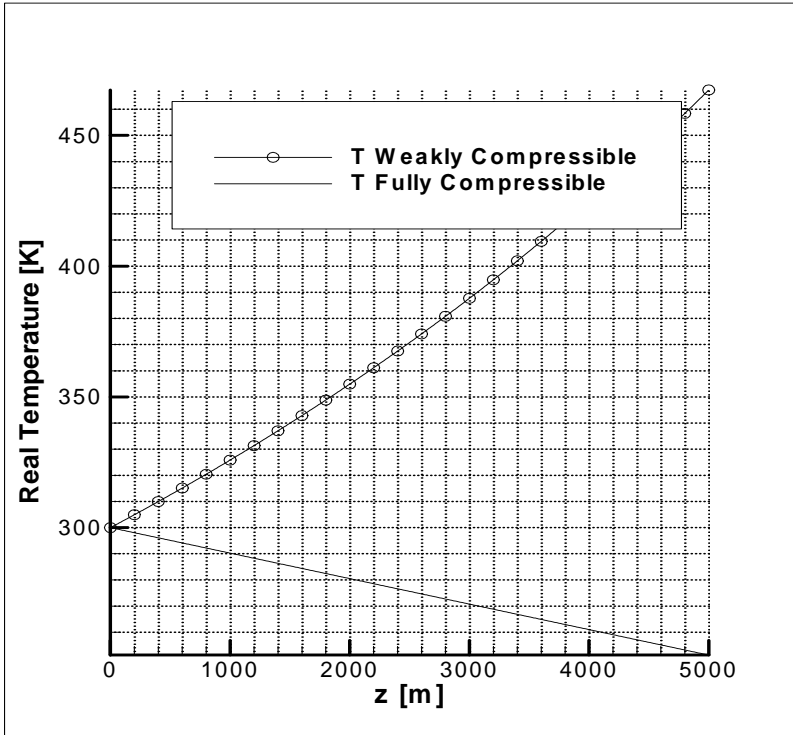


Figure 5-2: Comparison of temperature profiles for an adiabatic process

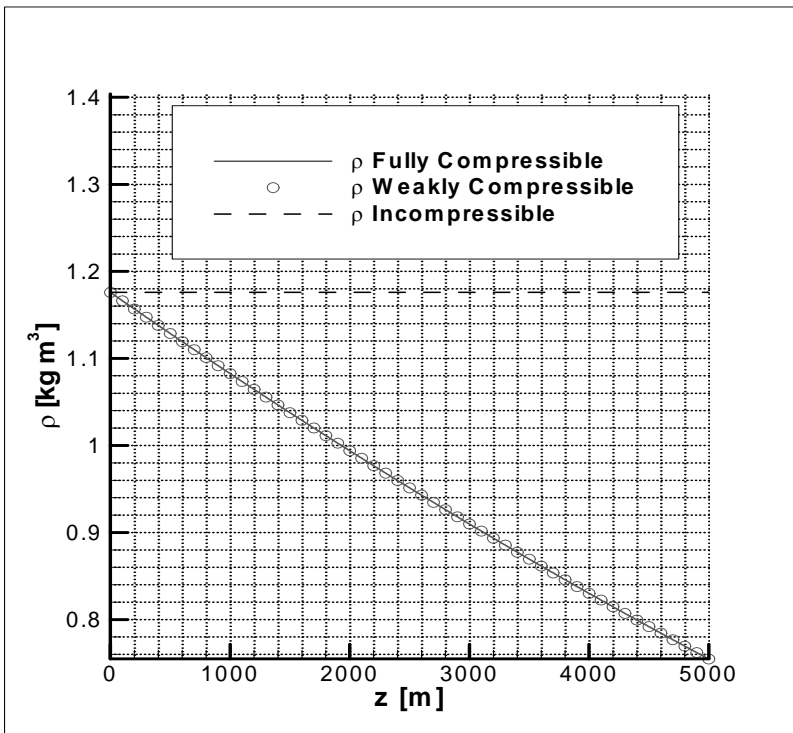


Figure 5-3: Density comparison – Adiabatic process

It is instructive to compare density of the compressibility options in the event of a dry adiabatic lapse rate as the temperature function for the weakly compressible option.

This is done by simply setting the temperature in the weakly compressible equation of state as the dry adiabatic lapse rate. The density is shown in figure 5-4.

As can be seen in the figure below, the density values for an adiabatic temperature profile for the weakly compressible flow option result in an increase in density with height. It is therefore not possible, without modifications to the weakly compressible equation of state, to correctly model adiabatic processes under the weakly compressible flow assumption.

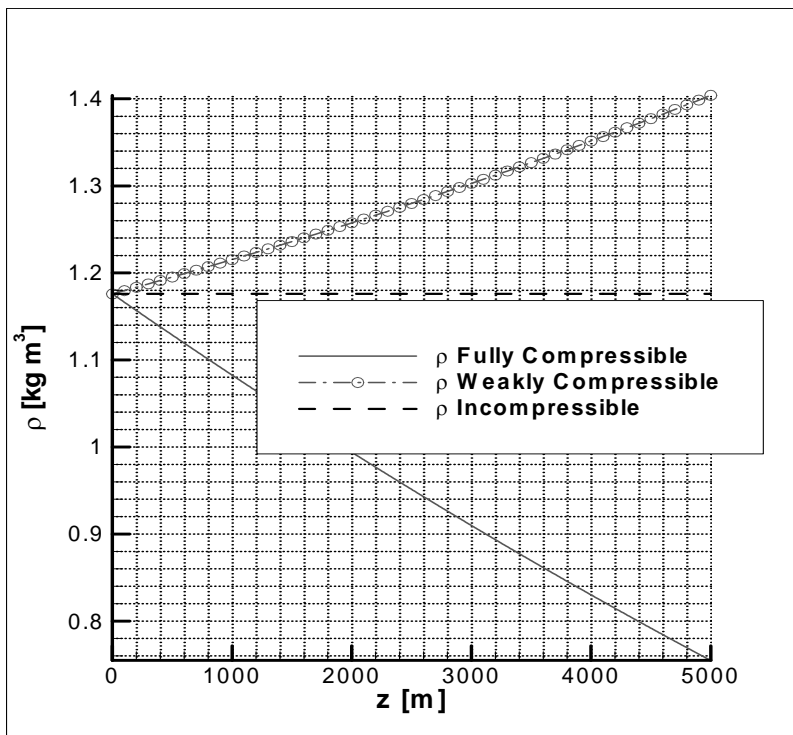


Figure 5-4: Density comparison – Adiabatic temp

In this respect, Huser et al. (1997) used an equation of state modified in terms of the potential temperature in order to compensate for the weakly compressible assumption. This equation is given below.

$$\rho = \frac{P_{ref} W}{R_u \theta} \quad (5-8)$$

An important consideration is that Huser et al. (1997) neglected the effects of buoyancy in the vertical direction because it requires “special treatment in the pressure outflow boundary condition”.

### 5.3. Buoyancy

Buoyancy driven flows are notoriously difficult to model, Cook and Lomas (1997), using CFD techniques. There are three main reasons for this: Firstly, the fact that the driving force for the induction of the flow field is small compared to other CFD models, this leads to numerical instability. Secondly, creation of turbulence due to buoyancy effects is not fully understood, but uncertainty exists regarding which turbulence model to use and what the values of the empirically derived constants should be. Finally, and perhaps most significantly, the flow field is implicitly specified. Unlike flow conditions where the flow field is specified with a known pressure at the boundary conditions or inlet velocity field the CFD code must calculate the flow field from supplied buoyancy sources.

The boundary layer equations governing free convection flows are given by Kays and Crawford (1993), for variable density and the assumption of constant specific heat and a steady two-dimensional flow field.

$$\frac{\partial(\rho u)}{\partial x} + \frac{\partial(\rho v)}{\partial y} = 0 \quad \text{Continuity} \quad (5-9)$$

$$\rho u \frac{\partial u}{\partial x} + \rho v \frac{\partial u}{\partial y} + \frac{dP}{dx} = \frac{\partial}{\partial y} \left( \mu \frac{\partial u}{\partial y} \right) - \rho g \quad \text{Momentum} \quad (5-10)$$

$$\rho u c_p \frac{\partial T}{\partial x} + \rho v c_p \frac{\partial T}{\partial y} - \frac{\partial}{\partial y} \left( k \frac{\partial T}{\partial y} \right) = 0 \quad \text{Energy} \quad (5-11)$$

The pressure gradient term in the momentum term represents the hydrostatic contribution, and can be written with respect to the ambient density as:

$$\frac{dp}{dx} = -\rho_0 g \quad (5-12)$$

A combination of the hydrostatic pressure gradient term and the body force term,  $\rho g$ , leads to the following momentum equation:

$$\rho u \frac{\partial u}{\partial x} + \rho v \frac{\partial u}{\partial y} + g(\rho - \rho_0) = \frac{\partial}{\partial y} \left( \mu \frac{\partial u}{\partial y} \right) \quad (5-13)$$

### ***Boussinesq approximation***

The Boussinesq approximation is used for incompressible flows where the density is assumed constant throughout the flow field, except in the vertical momentum equation, where the density is a function of the change in temperature for a parcel of air.

$$\rho - \rho_0 = -\rho_0 \beta (T - T_0) \quad (5-14)$$

where  $T$  and  $T_0$  are the local and buoyancy reference temperatures respectively, and  $\beta$  is the thermal expansion co-efficient of air.

The Boussinesq approximation is only valid for marginally compressible flows at best, and also where temperature differences from the reference temperature are small. Jaluria (1980) gives the following conditions for the applicability of the Boussinesq approximation.

- $\beta(T - T_0) \ll 1$



- $(g\beta z)/R \ll 1$

### ***Compressible buoyancy model***

Buoyancy is calculated the same for both compressible flow options. For compressible flows the density is given, as an equation of state and the buoyancy force is simply,  $\rho\mathbf{g}$ , with the gravitational vector prescribed in the command file.

For density calculated by an equation of state, the density can be expressed in relation to a reference density by:

$$\rho = \rho_0 + (\rho - \rho_0) \tag{5-15}$$

Where  $\rho_0$ , is a reference density, also prescribed in the command file, details of which are given in appendix B. The  $\rho_0\mathbf{g}$  part is absorbed into the pressure gradient. In both the Boussinesq approximation and the compressible case, the body force is simplified to:

$$\vec{B} = (\rho - \rho_0)\vec{g} \tag{5-16}$$

This is done in order to reduce the size of the momentum source due to buoyancy forces in the momentum equation, which can be beneficial for convergence of the solution.

In the definitions of the models above it can be seen that the standard version of CFX 4-4 calculates the energy conservation equation and the buoyancy term in the vertical momentum equation in terms of the real temperature, T, CFX 4-4 (2001) The pressure term appearing in the momentum conservation equation is defined as a deviation from a constant density hydrostatic state, i.e. a linear pressure decrease with increasing altitude. This makes it inappropriate for simulating stratified atmospheric flows with large vertical length scales, Montavon (1998), where the density and temperature vary with height.

### ***Deep Boussinesq model***

The primary assumption for the deep Boussinesq model is that density is constant as a function of height rather than a thermodynamic property of pressure and temperature and that the buoyancy source term in the momentum equation is defined in terms of the potential temperature gradients of the flow.

$$\rho_h = \frac{p_h}{RT_h(z)} \quad \text{Hydrostatic density} \quad (5-17)$$

$$(\rho_h - \rho) = \frac{\rho_h}{\theta_h} (\theta - \theta_h) \quad \text{Buoyancy source term} \quad (5-18)$$

It can be seen in the equations above that buoyancy is modelled as a change from a hydrostatic density, thus is a function of height and can account for temperature stratifications. The deep Boussinesq model is discussed in more detail in a following chapter and therefore only the equations are given above.

## **5.4. Turbulence Modelling**

The different available turbulence models and the description of the standard k- $\epsilon$  model is given in appendix C. In order to make the model amenable to atmospheric turbulence it is necessary to make certain modifications in the form of source terms in the differential equations and altering the standard equation constants. These modifications are described in the following section.

### ***Modifications on the k- $\epsilon$ model***

The standard k- $\epsilon$  model, with  $C_{\epsilon 3}$  set equal to zero, cannot account accurately for buoyancy effects, Davidson (1990). Several modifications have been suggested by numerous authors to account for the anisotropic effects of buoyancy. Plumb and Kennedy

(1977) tested different model constants for applications of buoyancy near a vertical wall, Davidson (1990) incorporates elements of both the k-ε model and the Reynolds stress model to the buoyancy problem and Bottema (1997) suggests modification due to “inactive turbulence” thought to be generated by gravity waves or low frequency contributions such as “thermals”.

Duynkerke (1988) has solved for the following constants in applications of the k-ε model for neutral and stable boundary layers. Apart from modified model constants, Duynkerke also introduces a transport term in the ε equation modelled using the gradient assumption as:

$$D = \frac{\partial}{\partial x_i} \left[ \mu_T \frac{\partial k}{\partial x_i} \right] \quad (5-19)$$

The introduction of this additional source term in the ε equation is only active in the equation when positive, Montavon (1998), and is an indication of the stability of the atmosphere. The modified model constant proposed by Duynkerke(1988) are tabulated below:

Table 5-1: Modified k-ε model constants

Model constant	$C_\mu$	$C_{\varepsilon 1}$	$C_{\varepsilon 2}$	$C_{\varepsilon 3}$	$\sigma_k$	$\sigma_\varepsilon$
Modified k-ε	0.033	1.46	1.83	0.0	1.0	2.38
Standard k-ε	0.09	1.44	1.92	0.0	1.0	1.3

$C_\mu$  is determined from the assumption that in the neutral surface layer  $C_\mu = (u_*^2/k)^2$ , using measurements for  $u_*$  and  $k$  close to the ground.  $C_{\varepsilon 2}$  is experimentally derived from grid turbulence and  $C_{\varepsilon 1}$  is obtained experimentally in shear-dominated flows. Values for  $C_{\varepsilon 1}$  and  $C_{\varepsilon 2}$  are related to the critical Richardson number through the following relationship, Duynkerke (1988):

$$C_{\varepsilon 1} = C_{\varepsilon 2}(1 - Ri_c) \quad (5-20)$$

which gives a value for the critical Richardson number of  $Ri_c \approx 2.0$ .

As can be seen above, in the standard k- $\varepsilon$  model the value of  $C_{\varepsilon 3}$  is set equal to zero. There has been much controversy about the effect of buoyancy on the production and dissipation of turbulence, Rodi (1980), and specifically in the value of this constant. In using the standard buoyancy modified k- $\varepsilon$  model, a value of 1 has been used in the  $\varepsilon$  equation, where the source terms for the  $\varepsilon$  equation are slightly modified in CFX 4-4 (2001) as:

$$\begin{aligned} \frac{\partial}{\partial t}(\rho\varepsilon) + \frac{\partial(\rho\bar{u}_j\varepsilon)}{\partial x_j} = \\ \frac{\partial}{\partial x_j} \left( \frac{\mu_T}{\sigma_\varepsilon} \frac{\partial \varepsilon}{\partial x_j} \right) + C_{\varepsilon 1} \rho \frac{\varepsilon}{k} (P + C_{\varepsilon 3} \max(G, 0)) - C_{\varepsilon 2} \rho \frac{\varepsilon^2}{k} \end{aligned} \quad (5-21)$$

$$G = -\beta \left( \frac{\nu_T}{\sigma_T} \right) \left( \frac{\partial \bar{T}}{\partial x_i} \right) g \quad (5-22)$$

The value of G, the buoyancy source term, is only applied to the  $\varepsilon$  equation when positive, for unstable flows and acts as a sink for turbulent kinetic energy for stable flows,  $\partial T / \partial z > 0$ . P is a term for the shear production of turbulence kinetic energy as defined in appendix C.

### ***Boundary conditions for atmospheric turbulence***

As with the governing equations of momentum and energy, the differential equations of k and  $\varepsilon$  are transport equations whereby the variable is transported by processes of diffusion and convection. For this reason it is necessary to specify correct values for the turbulence kinetic energy, k, and turbulence dissipation rate,  $\varepsilon$ , at the boundaries of the flow domain. In modelling of atmospheric flow with a cross wind, the inlet turbulence values can be related to mean flow properties, Hernández et al. (1995) and Huser et al. (1997).

In the case of the buoyancy driven flow of the solar chimney, the inlet velocity profile is not known *a priori*. Thiart (2002) and König and Mokhtarzadeh-Dehgahn (2002) both use constant values for inlet turbulence kinetic energy,  $k$ , and turbulence dissipation rate,  $\varepsilon$ . The default for a pressure boundary in CFX 4-4 is a Neumann, zero gradient, condition. These values are tabulated below.

Table 5-2: Boundary conditions for turbulence

	$k$	$\varepsilon$
Thiart (2002)	0.001	0.00001
König and Mokhtarzadeh-Dehgahn (2001)	1.19	0.00266
CFX 4-4 Default	$\frac{\partial k}{\partial x_n} = 0$	$\frac{\partial \varepsilon}{\partial x_n} = 0$

As can be noticed there is a large variation in turbulent kinetic energy,  $k$ , and the turbulence dissipation rate. This author is not suggesting that these are the upper and lower limits, but that there is in the literature, large discrepancies as to what values to be used. The choice of turbulent boundary values has an impact on the stability of the solution to the flow field in the calculation of turbulent viscosity at the inlet:

$$\mu_T = \rho C_\mu \frac{k^2}{\varepsilon} \quad (5-23)$$

Using the above-tabulated values for  $k$ ,  $\varepsilon$  and  $C_\mu$ , the following values for the turbulent viscosity are calculated:  $0.003696 \text{ kg m}^{-1} \text{ s}^{-1}$  and  $19.676 \text{ kg m}^{-1} \text{ s}^{-1}$  respectively. As mentioned before, there is no way of knowing before hand what the optimal value for the turbulence should be. In the following chapter the modelling of the solar chimney, three different results have been obtained for the above cases in order to notice what, if any, effect the inlet viscosity has on the flow field.

The term “optimal” is used rather than the term “correct” to describe the turbulence constants since the underlying eddy viscosity assumption of the  $k$ - $\varepsilon$  model is being

optimised as opposed to the modelling of turbulence, which as Ferziger et al. (2002) suggests for atmospheric flows, would be better modelled with a large eddy simulation.

## 5.5. Discussions and Conclusions

This chapter has quantified the various aspects of atmospheric modelling introduced in chapter 4. The important aspects of compressibility, buoyancy and turbulence have been investigated in terms of the application of different models used in CFX 4-4. It has been shown that of the two compressibility options offered, the weakly compressible model theoretically fails to correctly model the temperature profile, for an adiabatic derivation, or the density profile, for a fully compressible adiabatic temperature profile and is therefore unsuited to this model unless the equation of state is modified such that the density is a function of the potential temperature.

The available buoyancy models have been described and also shown to be lacking in correctly modelling a stratified density based on a real temperature profile. This is due to the buoyancy source term being derived in terms of a constant reference temperature in terms of the Boussinesq assumption and a constant reference density in the case of the compressible buoyancy option. Any variation in temperature or density from the constant reference value will result in sources in the momentum equations, which do not reflect the true nature of the flow.

In order for the buoyancy model not to have an effect on the flow field, the temperature at the boundary conditions must be set such that the buoyancy source term is zero for an initially stable and stationary field. This means that a constant ambient condition must be specified for both free boundaries, in the case of the model and that this temperature must be the temperature of the ground surrounding the collector in the chimney model. Another option is to use the deep Boussinesq model to define the buoyancy source term and stratified temperature in terms of the potential temperature, while setting the density as a function of height.

Modifications to the  $k$ - $\varepsilon$  model for applications in atmospheric flows have been described and the question of correct values for the turbulence properties at boundary conditions has been posed.

## CHAPTER 6. SOLAR CHIMNEY NUMERICAL MODEL

---

### 6.1. Introduction

Chapter 3 described the boundary conditions and assumptions for the numerical model of the solar chimney power plant. This chapter details the development of the two-dimensional axisymmetric model. As mentioned in chapter 3, a two-dimensional model is possible for modelling the flow field above the collector under the two assumptions of zero cross wind and ignoring the effects of Coriolis forces on the field. This model makes use of the geometric symmetry around the axis of the chimney of the plant.

Standard operating values for the wall temperatures and the chimney outlet temperature and velocity have been defined in chapter 3. The Dirichlet values for these boundaries are repeated here for continuity. The free atmospheric boundary is specified as a pressure boundary with a Dirichlet condition on the pressure and temperature at the inlet condition and Neumann boundaries for all flow variables at an outlet condition, details of this boundary are given in appendix B. Values for turbulence kinetic energy,  $k$  and turbulence dissipation rate,  $\epsilon$ , are however treated differently and will be further extrapolated on in this chapter. In this regard three different conditions for turbulence have been used to obtain results for comparison on the pressure boundaries.

In order to test for grid independence of the solutions, four separate models have been specified. Firstly three successively refined grids were used, the refinement being in the order of 2 so that Richardson extrapolation can be used to find a grid independent solution. To check for errors due to false diffusion of the solution because of upwind differencing, the fourth model is run with second order accurate central differencing on the velocities and QUICK differencing on the enthalpy equation, on the medium grid. Two convergence criteria have been defined to show that the solution for each of the models has in fact converged. The first relates to the absolute value of the residuals and the second to the absolute value of the change of variable for successive iterations.



The results obtained offer comparison of the temperature field and velocity flow field. For the case of variable turbulence boundary conditions a comparison is made of the velocity field and contours of the turbulence kinetic energy,  $k$ , and turbulence dissipation rate,  $\epsilon$ .

## 6.2. Axisymmetric Geometry

Figure 6-1 shows the axisymmetric cut out used for the model. A wedge shaped model is used in the solution of the flow field, with decreasing control volume size towards the centre of the chimney, the axis of symmetry.

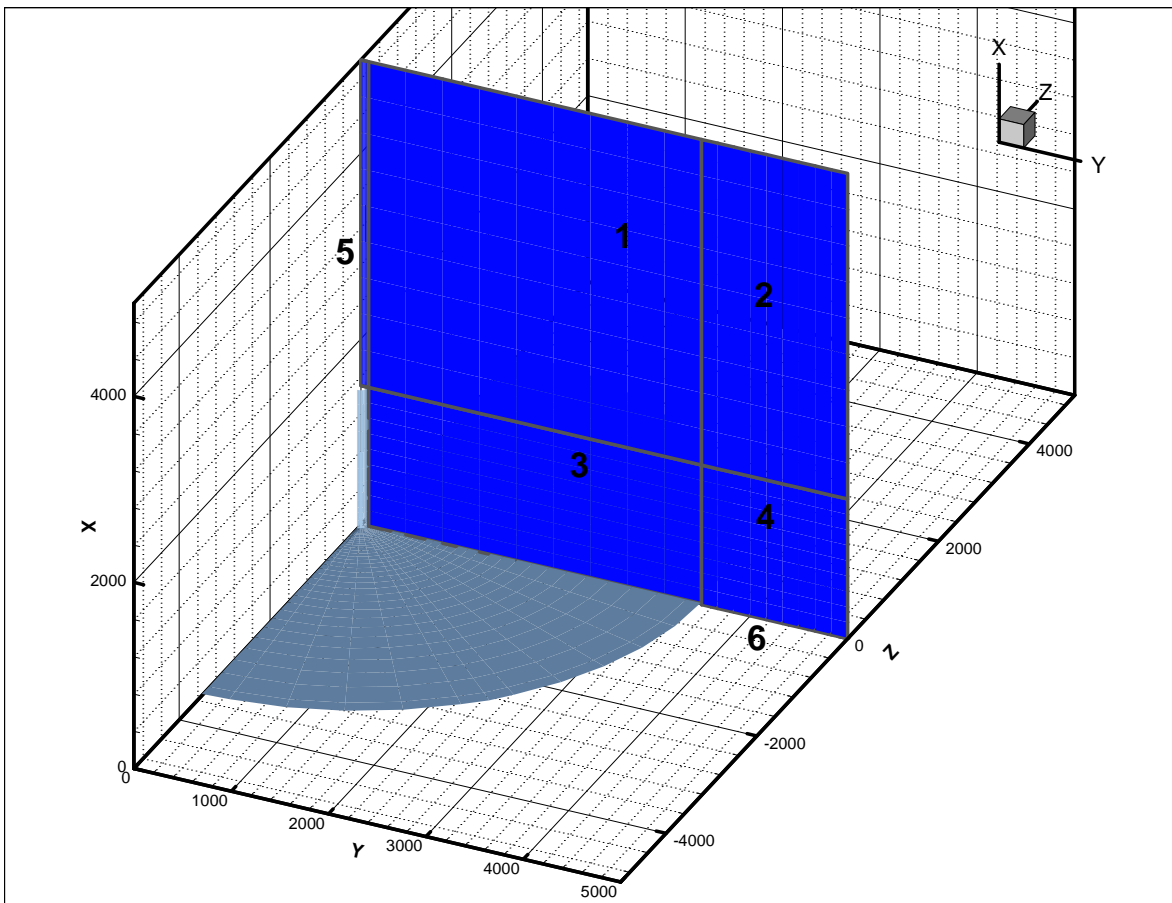


Figure 6-1: Axisymmetric section of the solar chimney

The geometry is created in CFX-Build, the pre-processing module of CFX 4.4. For an axisymmetric model CFX-Build gives the option of creating a rectangular two-dimensional model and specifying in the program that the numerical model resembles a wedge. This

option was used in the modelling of the chimney in order to satisfy the condition of decreasing control volumes towards the axis.

The default direction for the axis of symmetry in an axisymmetric model is the x-direction in a Cartesian co-ordinate system. This convention has been adopted in the creation of the geometry, once again seen in figure 6-1.

### **6.2.1. Grid**

CFX 4-4 provides a block structured solution procedure, in that simple geometries can be constructed by creating regular rectangular blocks. In the figure above one can see the individual blocks for the model. The node seeds are then matched at each of the block interfaces. It can be seen that apart from the four large blocks above the ground and the collector, two smaller blocks exist above the chimney and to the right of the inlet to the collector, blocks 5 and 6. The size of the numerical mesh associated with the small blocks must match that of the larger blocks, so that volumetric source terms for the discretized equations do not vary substantially between interfaces, as this could cause convergence difficulties.

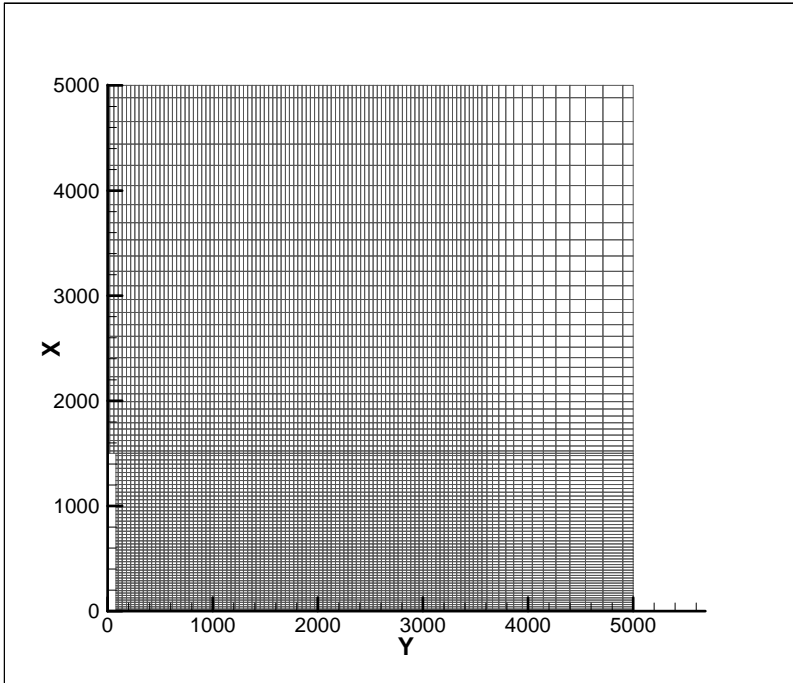


Figure 6-2: Course grid

The grid above the collector is uniform in both the x and y directions, with the size of the control volumes matched to the control volumes above the exit to the chimney in the y-direction. This is done so that the control volumes are matched at the edge of the chimney. This matching is shown in figure 6-3 below. It is also important that the expansion of the control volumes does not exceed a value of 4, as this might cause problems with the large differences in source terms between cells.

This imposes severe restriction on grid generation for the solar chimney due to the large differences in the physical geometry and dimensions of the problem. In order to realise the flow field at the collector inlet at least one control volume of 10 m is needed. Larger control volumes are required at the outer region, specifically blocks 1,2 and 4, so that less computational resources are used on these regions where the information for the flow field is not critical. For this reason the size of the control volumes for each of the refined grids is derived from the size at the collector inlet and chimney outlet.

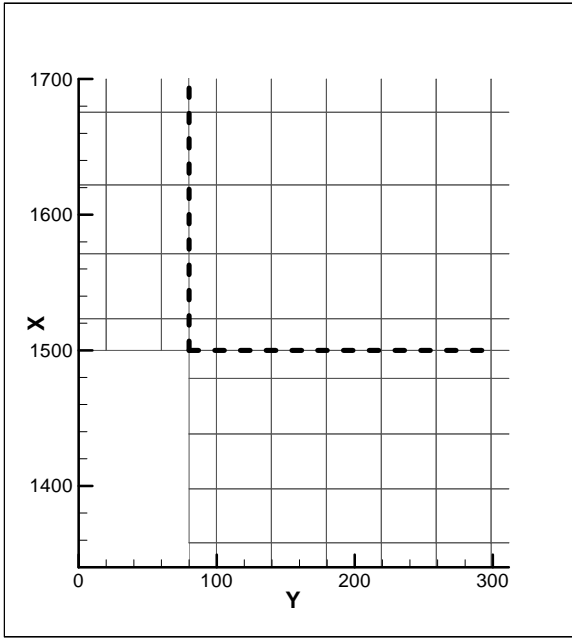


Figure 6-3: Grid at chimney exit

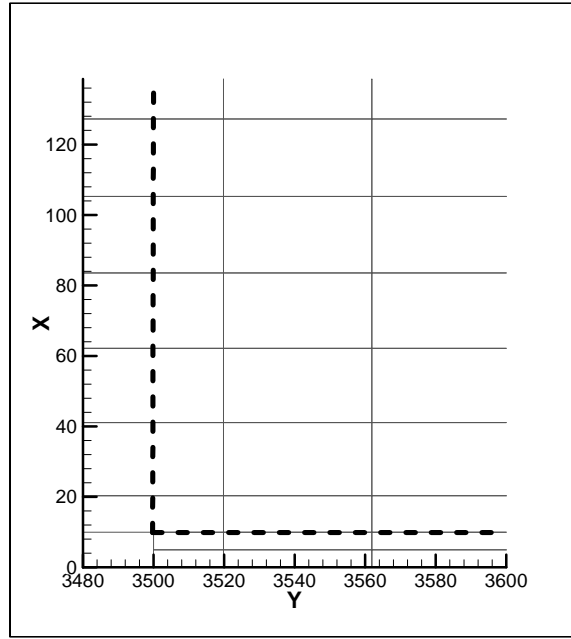


Figure 6-4: Grid at collector inlet

The details of the refinement are shown in the table below, while the matching at the collector inlet and chimney outlet is demonstrated in the figures above.

Table 6-1: Grid refinement

		Coarse		Medium		Fine	
Block, Direction	Refined	L <sub>1</sub>	L <sub>2</sub>	L <sub>1</sub>	L <sub>2</sub>	L <sub>1</sub>	L <sub>2</sub>
2, x	One-way	40	240	20	120	10	60
2, y	Uniform	40	40	20	20	10	10
5, x	Uniform	40	40	20	20	10	10
5, y	Uniform	40	40	20	20	10	10
6, y	One-way	40	200	20	100	10	50

As can be seen, one way biasing is used to increase the control volume size towards the upper right section of the model. This is done in order to minimize computational resources where small gradients are expected. In order to utilise Richardson extrapolation, the ratio of grid expansion must be kept consistent for each refinement of the grid. In order to ensure that the ratio of the grid expansion is the same for each finer grid, the values of

$L_1$  and  $L_2$  are both decreased by a factor of 2. This is achieved by specifying the initial,  $L_1$ , and final,  $L_2$ , control volume lengths in the two-dimensions. Where  $L_2$  is the length of the larger dimension and  $L_1$  is the length of the smaller dimension. This is shown below for a one-dimensional expansion. CFX 4-4 automatically generates a grid with an expansion ratio of approximately 1.4 by changing the number of nodes in the direction of the expansion.

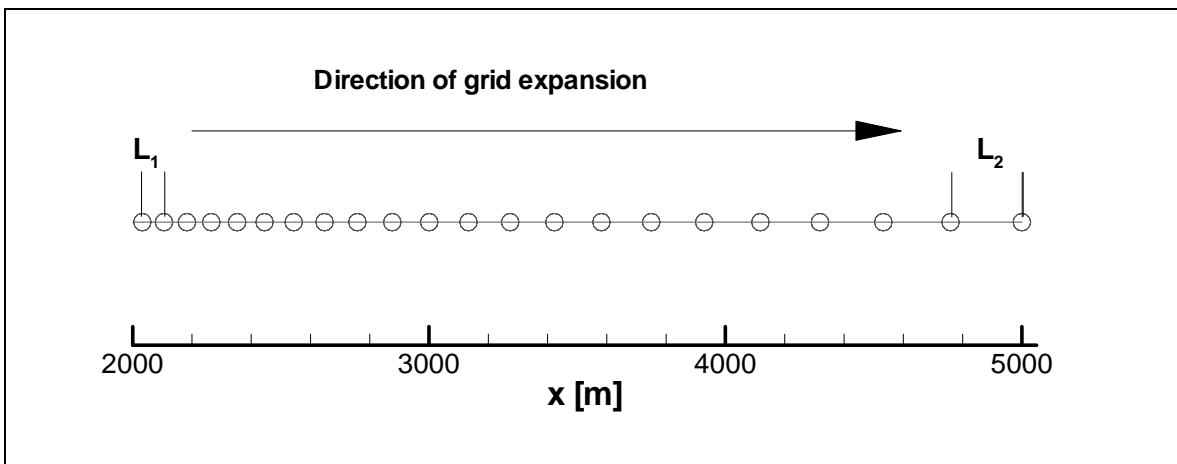


Figure 6-5: Grid expansion in the x-direction above the chimney

Using these values to generate the grids for the three cases gives the following number of control volumes for each refined grid.

Table 6-2: Number of control volumes

Grid	Coarse	Medium	Fine
Number of control volumes	6 945	27 815	111 208

## 6.3. Boundary Conditions

### 6.3.1. Wall boundaries

- All walls considered smooth
- Dirichlet values specified on the ground and collector walls

- Neumann condition on chimney wall
- Constant ground temperature of 300 K
- Constant collector temperature of 320 K
- Zero heat flux from chimney wall to surrounding

### 6.3.2. Mass flow boundaries

#### *Chimney inlet*

- Normal average velocity 15 m s<sup>-1</sup>
- Outlet temperature 320 K
- Turbulence kinetic energy  $k$  is described in terms of the average velocity at the chimney outlet, König and Mokhtarzadeh-Dehghan (2002):

$$k \cong 0.002 \bar{u}^2 \quad (6-1)$$

- Dissipation of turbulence,  $\varepsilon$ , defined in terms of  $k$  and a characteristic length scale of the chimney.

$$\varepsilon \cong \frac{k^{3/2}}{l} \quad (6-2)$$

$$l = 0.1d_{ch} \quad (6-3)$$

#### *Collector Outlet*

- Mass is locally conserved between chimney outlet and inlet to the collector.
- Mass fraction is specified in the command file, for a value of unity the above condition for mass conservation is realised.
- The outlet temperature is specified for the case of re-circulating flow at an outlet boundary condition.
- Real temperature set at 300 K

### 6.3.3. Pressure boundaries

#### *Pressure*

The pressure specified, is the pressure solved in CFX 4-4, which is a change in pressure from a hydrostatic condition. Further details of the pressure used in calculations is given in appendix B

$$p = p_{total} - p_h \quad (6-4)$$

For an incompressible model the total pressure,  $p_{total}$ , is simply equal to the hydrostatic pressure calculated for a constant reference density,  $\rho_{ref}$ , which is the same as the  $p_h$  in the above equation.

$$p_{total} = p_h = -\rho_{ref} g z. \quad (6-5)$$

Therefore the value of the pressure at the boundary is set equal to zero Pascal.

#### *Temperature*

The pressure boundary temperature is specified as a constant value equal to the ground temperature surrounding the collector. This is done so that buoyancy forces are ignored everywhere except where the collector and chimney outlet temperature have an effect on the flow.

- $T = 300 \text{ K}$

#### *Turbulence*

The default condition for turbulence at a pressure boundary is a zero gradient Neumann condition. Dirichlet values can be set at pressure boundaries. There is however some question as to which values to use for the model of the chimney.

Turbulence values can be related to the planetary boundary layer velocity profile, Guyot (1998) and consequently to the stability of the atmosphere. For a neutrally stable atmosphere, König and Mokhtarzadeh-Dehghan (2002), give the following uniform turbulence profiles:

$$k = 1.19 \text{ m}^2 \text{ s}^{-2} \quad \varepsilon = 0.00266 \text{ m}^2 \text{ s}^{-3} \quad (6-6)$$

Thiart (2002) uses relatively smaller values at the atmospheric boundary in modelling the flow above the solar collector. The assumption is that the average velocity of air sufficiently far from the solar chimney will be very small and that little or no turbulence will be convected into the flow domain.

$$k = 0.001 \text{ m}^2 \text{ s}^{-2} \quad \varepsilon = 0.00001 \text{ m}^2 \text{ s}^{-3} \quad (6-7)$$

The values specified have an effect in the stability of the flow field through the convection of turbulent viscosity,  $\mu_T$ , into the flow domain.

$$\mu_T = \frac{\rho C_\mu k^2}{\varepsilon} \quad (6-8)$$

This gives values of  $20.7 \text{ kg m}^{-1} \text{ s}^{-1}$  and  $0.003894 \text{ kg m}^{-1} \text{ s}^{-1}$  respectively. It can be seen that these values differ by several orders of magnitude and should be investigated.

Three separate models using each of the boundary conditions for turbulence were solved. The results for the Neumann condition and the higher turbulence values are shown in the results. Turbulence values as suggested by Thiart (2002), see equation 6-7, were also attempted in one of the above-mentioned models. The low viscosity, however, caused instability in the flow field and satisfactory convergence could not be obtained, even for very small under relaxation factors.



### 6.3.4. Symmetry boundaries

The two-dimensional model makes use of the symmetric geometry of the collector and chimney. For this reason, a symmetry boundary is specified at the axis of the chimney. For a two-dimensional model automatic symmetry boundaries are imposed in the symmetry direction. These faces are the positive and negative z faces seen in figure 6-1.

### 6.3.5. Initial conditions

Initial conditions for the flow field are set up so that a first iteration value can be used for the solution process. An initial zero flow field is specified for velocities and a constant temperature of 300 K is specified as the initial temperature. The initial pressure field is also specified as zero. Initial values for turbulence parameters of k and  $\epsilon$  are the same as the pressure boundary values for these variables defined above.

## 6.4. Model Assumptions

Apart from the assumptions mentioned in defining the boundary conditions. The following assumptions regarding the flow field have been made.

- Constant thermal properties throughout the flow field.
- Steady state solution
- Turbulence modelled with the k- $\epsilon$  buoyancy modified model
- Model constant uses are those suggested by Duynkerke (1988) and are tabulated below

Table 6-3: Turbulence constants

Model constant	$C_\mu$	$C_{\epsilon 1}$	$C_{\epsilon 2}$	$\sigma_k$	$\sigma_\epsilon$
Modified k- $\epsilon$	0.033	1.46	1.83	1.0	2.38

## 6.5. Numerical Control

As seen in appendix B, numerical control of a particular solution is obtained by specifying the number of iterations for a solution and the minimum allowable value of the mass residual. Further control of the solution is obtained in the specification of discretization schemes and under-relaxation factors for the discretized equations.

In order to be sure of a converged solution, it is also necessary to specify convergence criteria for a particular solution. This convergence criterion is usually related to the particular problem under investigation in that the required level of accuracy must be obtained, Cook and Lomas (1997).

### 6.5.1. Discretization schemes

In the solution of the successively refined grids the default hybrid discretization schemes were used, except in the mass conservation equation where central difference is always used. For the medium grid solution with higher order differencing it was noticed that the solution is highly unstable when central differencing is used for all the equations. It was necessary to specify different differencing for each of the individual equations. These are tabulated below.

Table 6-4: Differencing schemes

Variable	u	v	p	$\rho$	k	$\varepsilon$	h
Differencing	central	central	hybrid	upwind	hybrid	hybrid	QUICK

### 6.5.2. Under-relaxation factors

The under-relaxation factors, URFs, relate to the change of the value of a particular variable from the previous iteration. If the URFs are too small then the solution will take more computational time to reach a sufficiently converged solution, if the URFs are too

large then instability may result and convergence may not be achieved. In the models of solar chimney, similar URFs to those suggested by Thiart (2002) have been used. For the refined grids it is necessary to relax the equations further for stability. The only difference in the URFs is with the solution of the energy equation. For buoyancy driven flows, Cook and Lomas (1997) suggest that the energy equation is relaxed less than the momentum and turbulence equations. Under-relaxation factors for all the equations are tabulated below.

Table 6-5: Under-relaxation factors

Variable	Coarse grid	Medium grid	Fine grid	Higher order
u	0.2	0.2	0.05	0.02
v	0.2	0.2	0.05	0.02
p	0.8	0.8	0.4	0.4
h	0.8	0.8	0.4	0.4
k	0.2	0.2	0.05	0.02
$\varepsilon$	0.2	0.2	0.05	0.02

### 6.5.3. Convergence criteria

Two convergence criteria were used to ascertain if the solution was in fact converged. The first is related to the change of the values between successive iterations and the second is based on the value of the residual, the sum of the errors between the source terms and the convection/diffusion terms, in the discretized equations is small compared to the magnitude of the absolute values of the variables.

Results shown and calculated are for the medium grid in the case of a Neumann condition on the pressure boundaries for k and  $\varepsilon$ . In appendix B, it is shown that the residuals are the sum of the errors over the entire flow domain; the average residual can then be calculated as:

$$R_{ave} = \frac{R}{N} \quad (6-9)$$

where R is the value of the residuals obtained in the line-graph output and N is the number of control volumes for the particular model. The test for convergence is based on the mass residual and the enthalpy residuals. In the figure below the convergence history for the mass and the enthalpy is shown.

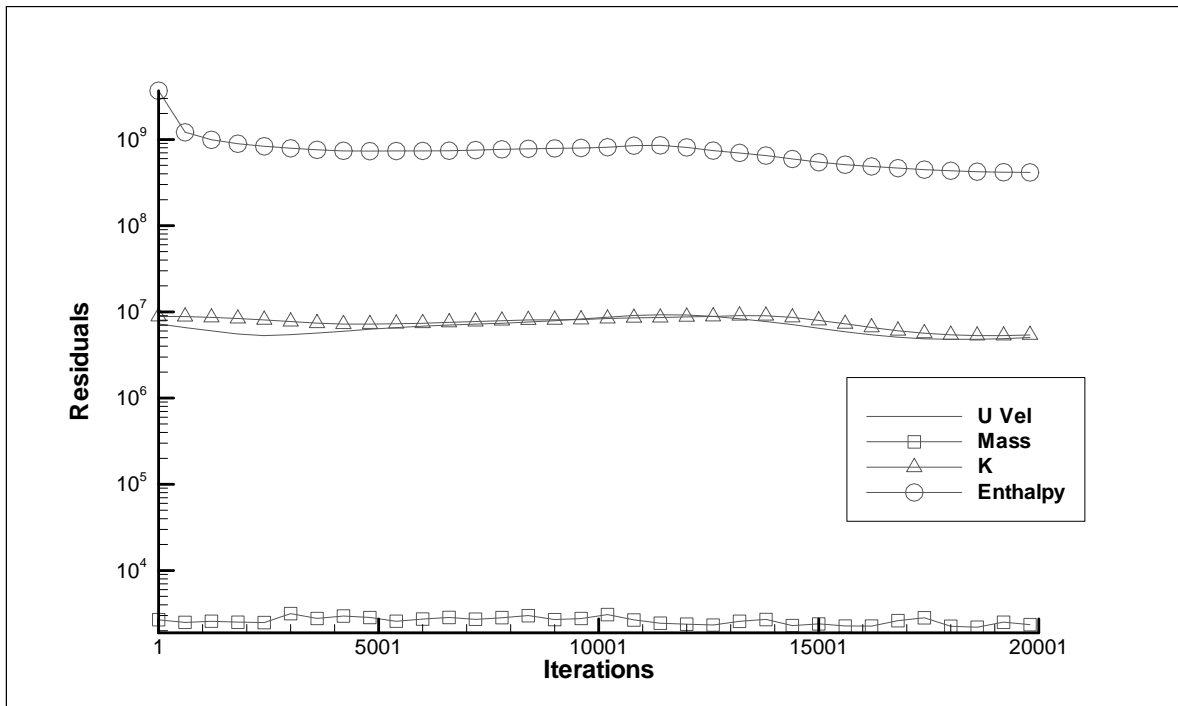


Figure 6-6: Convergence history

For the medium grid, convergence history shown above, the residual on the energy equation is approximately  $4.2 \times 10^8$  W and on the mass continuity approximately  $2 \times 10^3$  kg. The number of control volumes for the medium grid is around 30 000. This means that the average residual for mass is around 0.05 kg.

For the enthalpy, the value of the residual is compared to the total enthalpy in watts entering the flow domain from the hot wall and the chimney outlet. The value for the total enthalpy entering the domain is available from the CFX output file and is approximately  $8.8 \times 10^{10}$  W. This gives an error of approximately 1% on the energy equation for the medium grid. Similar results were obtained for the coarse and fine grids. The change per iteration for all variables is less than 0.01%.

## 6.6. Results

### 6.6.1. Grid convergence study

Richardson extrapolation, described in appendix D, is used in order to get a grid independent solution at two areas in the flow field where the gradients of the variables are the most extreme. In the first case, line information from the chimney wall to approximately 1000 m, in the horizontal direction was extracted from the converged solutions of the three refined grids and the higher order discretization solution. The vertical height above the collector was 500 m. In figure 6-7, the velocities in the vertical direction are compared.

As can be seen in figure 6-7, the values for the u velocity, for all three successively refined grids and the higher order solution, compare well with the grid convergence answer obtained.

Figure 6-8 shows the comparison of temperature at the same location above the collector. Once again the three solutions converge onto the grid independent solution. It is interesting to note the similarity in the profiles between temperature and velocity in the figures. This can be expected as the flow above the collector is primarily buoyancy driven.

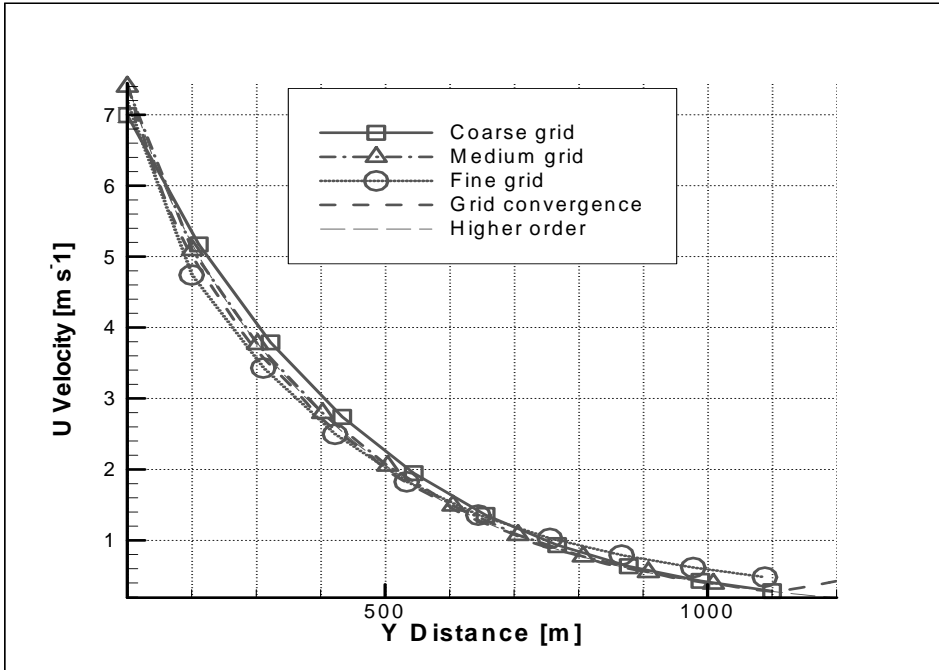


Figure 6-7: u Velocity comparison above collector

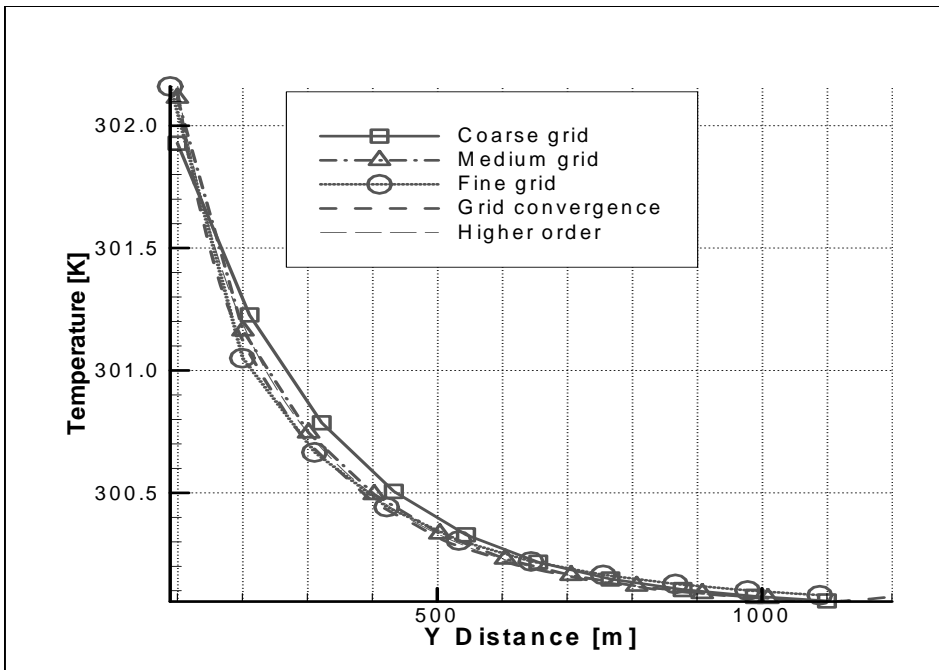


Figure 6-8: Temperature comparison above collector

In the second set of results horizontal line information was extracted from a height above the chimney outlet of 500 m. Once again the horizontal distance was 1000 m. Figure 6-9

shows a comparison of vertical velocities around the chimney normalised with respect to the centreline velocity at the outlet of the chimney,  $15 \text{ m s}^{-1}$ .

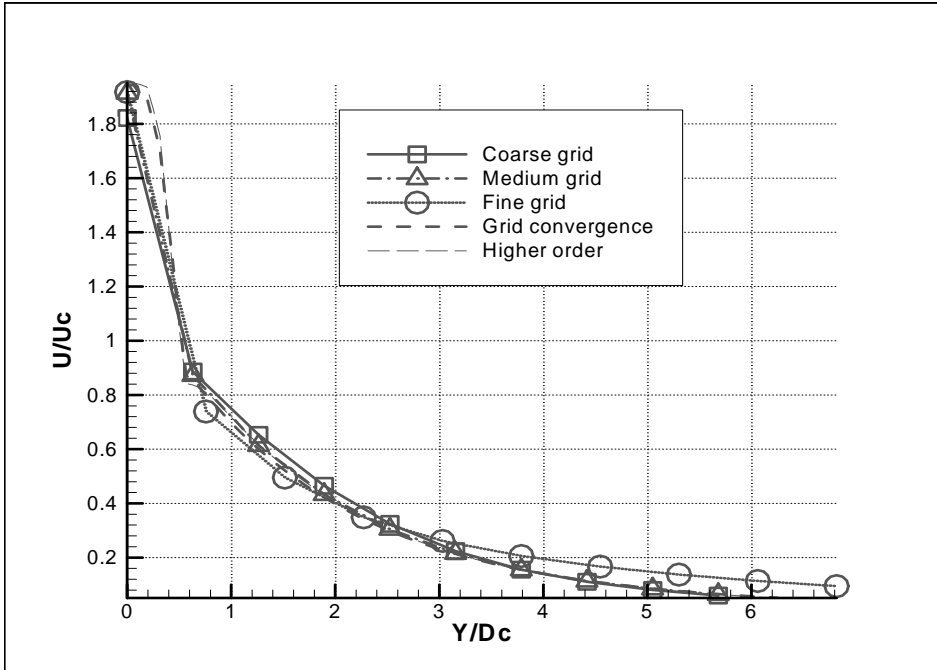


Figure 6-9: Normalised u-velocity above the outlet of the chimney

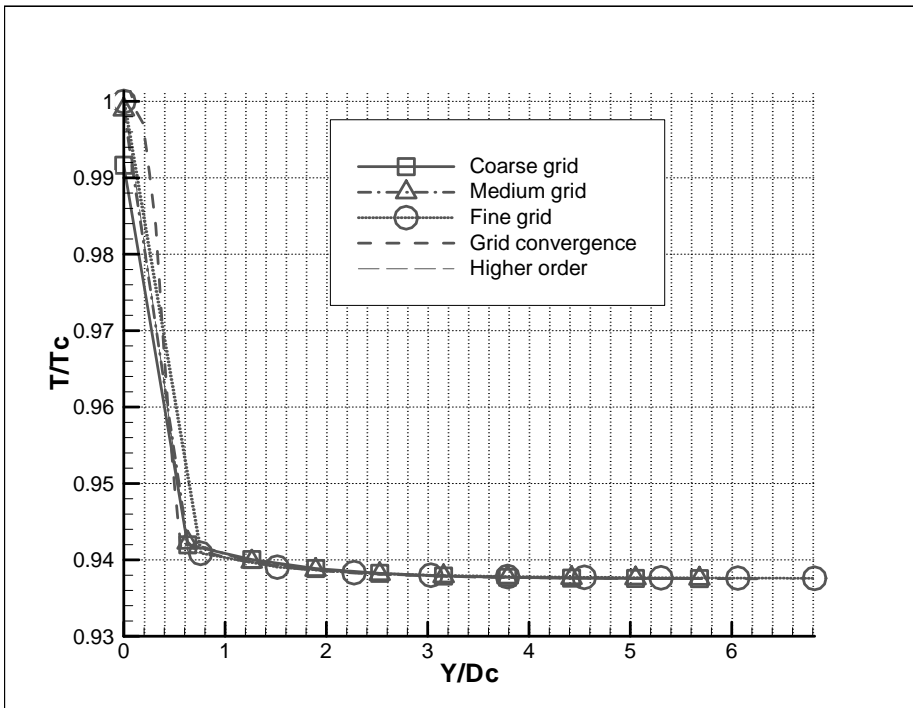


Figure 6-10: Normalised temperature above the outlet of the chimney

The y-abscissa describes the distance from the axis of symmetry. In this case the values are normalised with respect to the chimney diameter. In 6-10, temperature values are extrapolated to find a zero grid solution above the chimney. The y-axis values indicate the air temperature normalised with respect to the chimney outlet temperature, 320 K.

### 6.6.2. Flow Field

The flow field results for the medium grid with a Neumann condition for turbulence on the pressure boundaries is shown in the following figures. The first figure shows the temperature field above the collector.

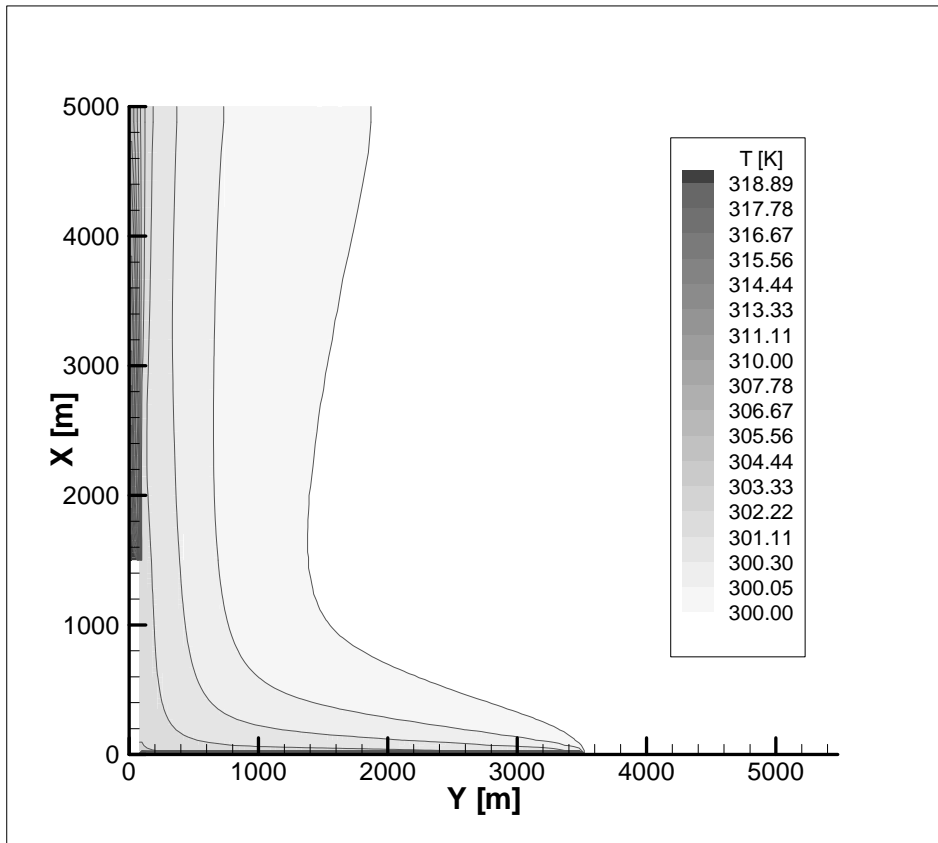


Figure 6-11: Temperature contours

One can see that the air above the collector does not heat up much due to the temperature of the collector. It would seem that the hot air is limited to a thin layer just above the



collector with the flow field above the collector being dominated by the induced velocity along the surface and convecting the heat downstream towards the chimney wall.

The following figure shows the modified pressure for the flow field and the velocity flow field, where a uniform vector plot is superimposed on a contour plot of speed in order to show the magnitude of the vectors.

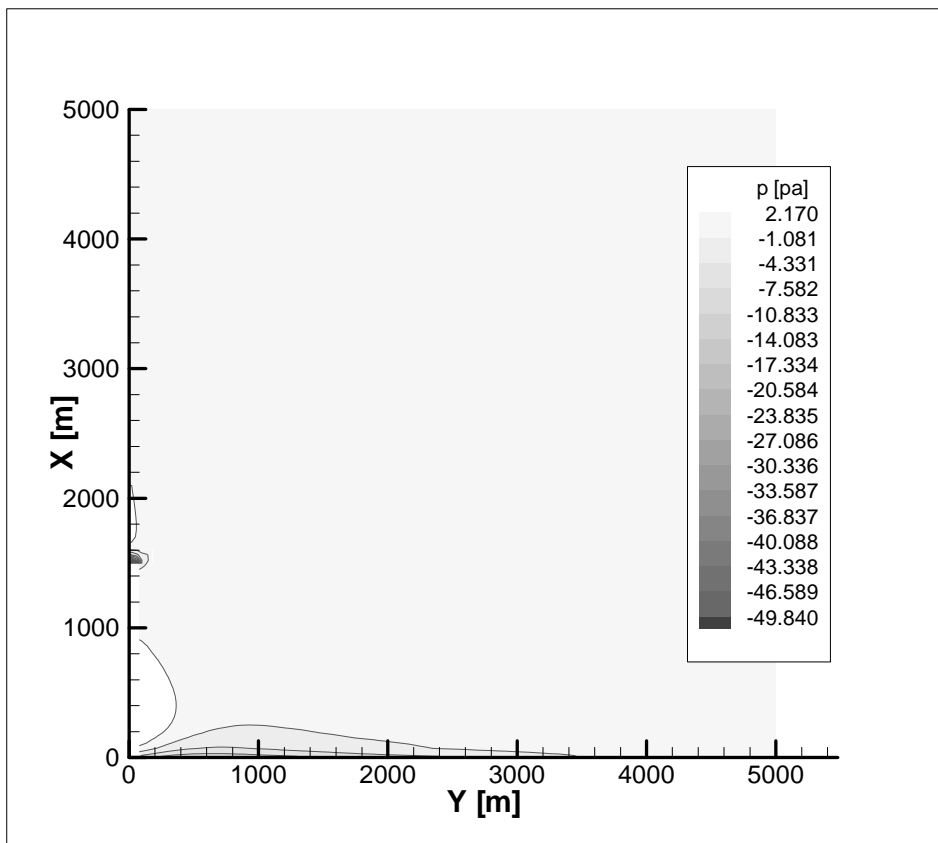


Figure 6-12: Pressure contours

A low pressure is observed along the top of the collector. This is due to the buoyancy from the hot collector surface forcing cooler air to be drawn into the flow field. A similar effect is noticed at the chimney outlet whereby mass conservation is enforced by drawing air into the region above and around exit of the chimney. The induced flow field can be observed in figure 6-13.

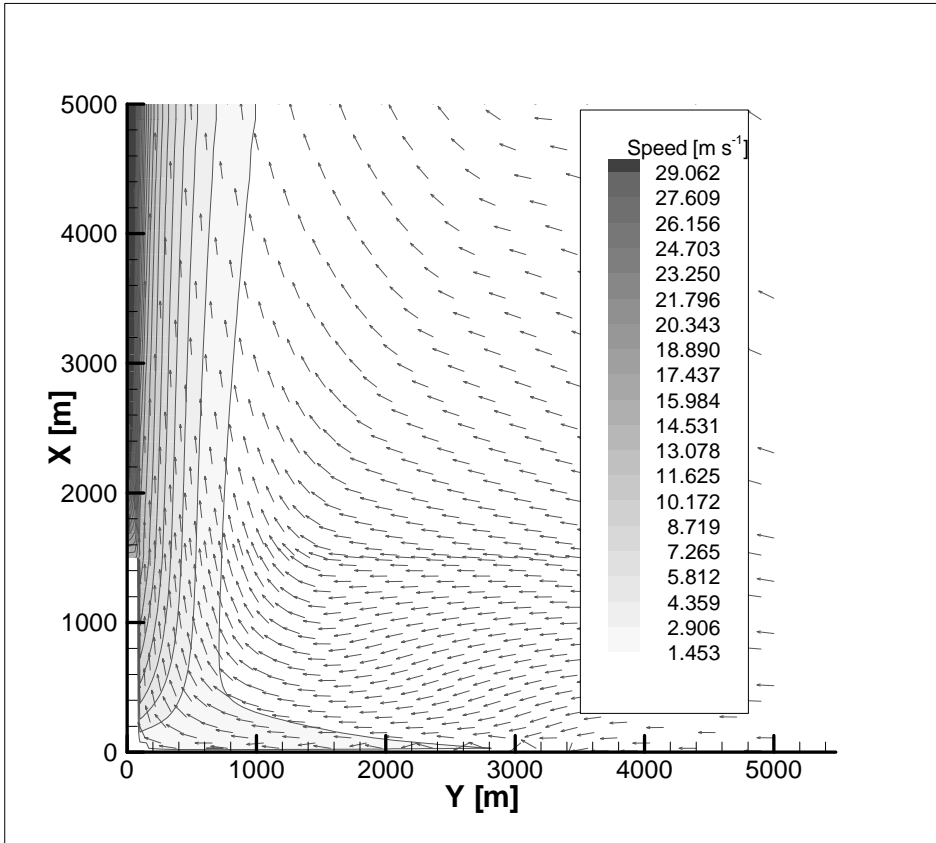


Figure 6-13: Velocity vectors and speed contours

The effect of the entrainment of the air due to the high velocity air from the chimney can clearly be seen in the figure above. The maximum velocity of the air above the chimney demonstrates the influence of buoyancy and the higher temperature of the air, with a magnitude almost double that of the specified chimney outlet velocity.

### 6.6.3. Streamlines

Figure 6-14 shows the streamlines for the velocity field above the collector. The general flow pattern is similar to that obtained by Thiart (2002), the difference can be seen in the height at which air is drawn into the collector

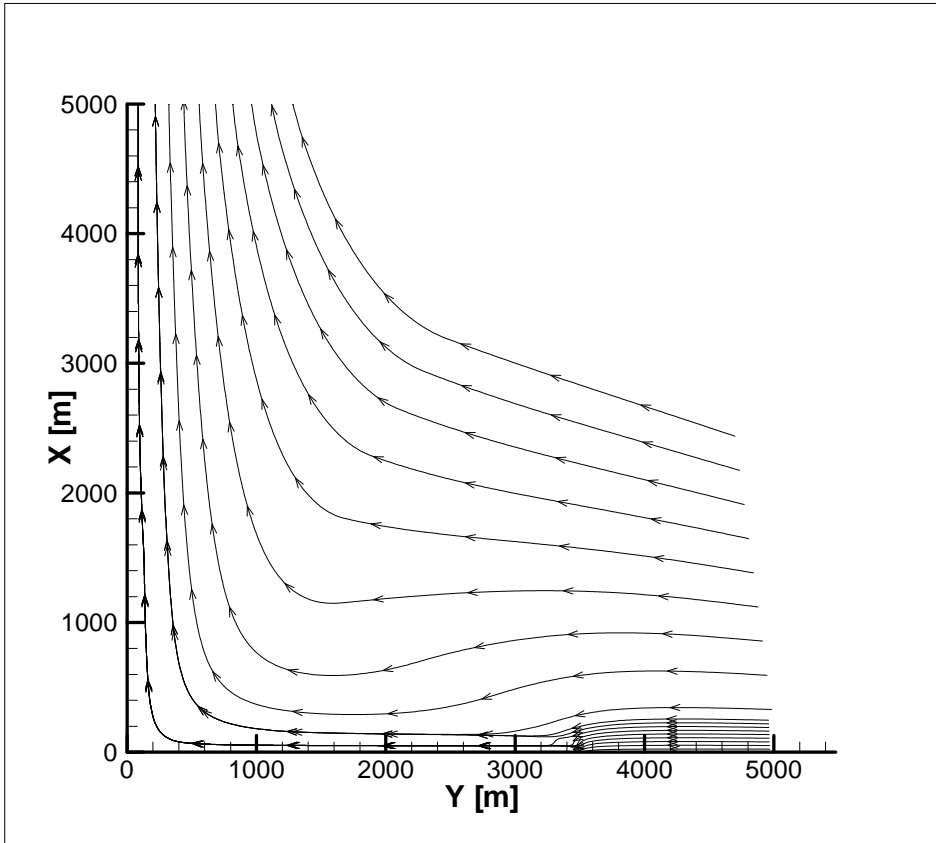


Figure 6-14: Streamlines

In the model solved by Thiart (2002) the air was drawn from a height of approximately 240 m at a distance of 1 km. This is significantly higher than the observed height at which air is drawn into the collector in the present model of approximately 40 m. This could be due to the values for  $k$  and  $\epsilon$  input in this model. As mentioned above in section 6.3.3, the values used here are substantially higher than those used by Thiart (2002). Another reason for the difference in height at which air is drawn into the collector could be the difference in boundary application between the numerical solver utilised by Thiart (2002) and CFX 4-4.

#### 6.6.4. Comparison of Turbulence Values

Figure 6-15 demonstrates the turbulent viscosity contours for the condition of a Neumann, zero gradient, at the inlet pressure boundary. Shear production of turbulence kinetic energy is seen to dominate at the region around the chimney plume.

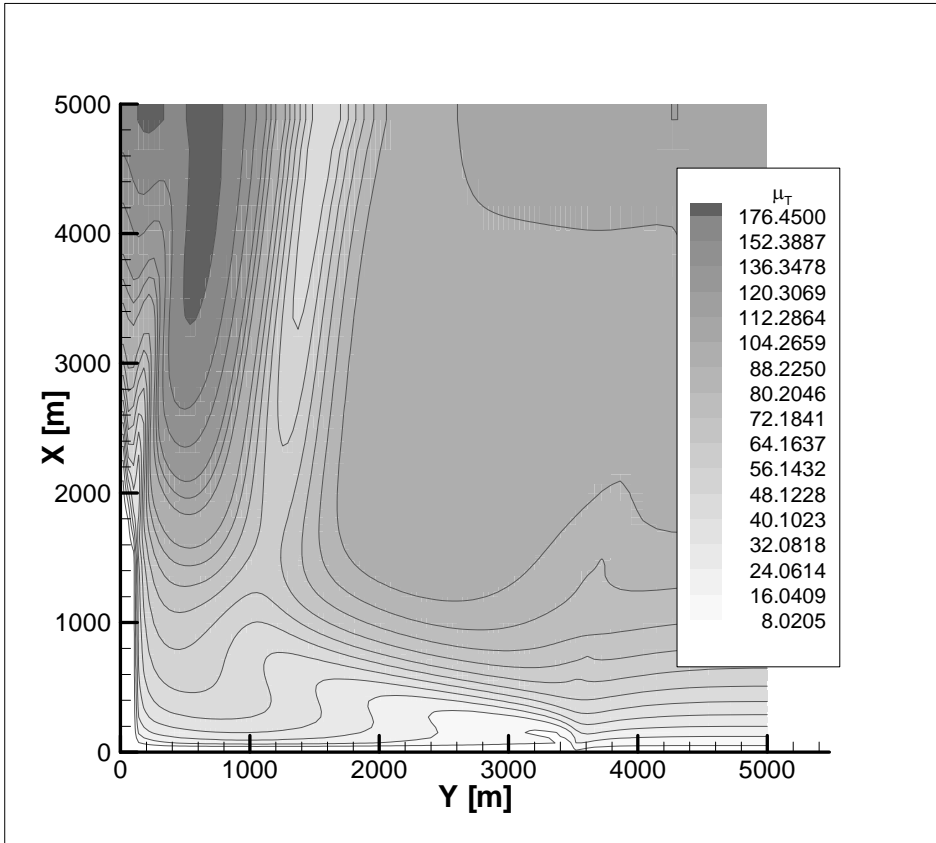


Figure 6-15: Turbulent viscosity contours - Neumann boundary

Figure 6-16 shows the turbulent viscosity for inlet Dirichlet  $k$  and  $\epsilon$  values as suggested by König and Mokhtarzadeh-Dehghan (2002) shown above in section 6.3.3. Once again the effect of the chimney plume on the production of turbulence kinetic energy by shear can be seen.

The values obtained for the turbulent viscosity  $\mu_T$  for the different boundary conditions of input turbulence vary significantly. The production of turbulence due to shear from the chimney outlet is seen to predominate in that the maximum values for both boundary conditions seem to occur in approximately the same region. It is obvious that the specification of the boundary values for turbulence will have a significant effect on the final solution of the flow field, in the solution of the temperature field in the form of the eddy diffusivity.

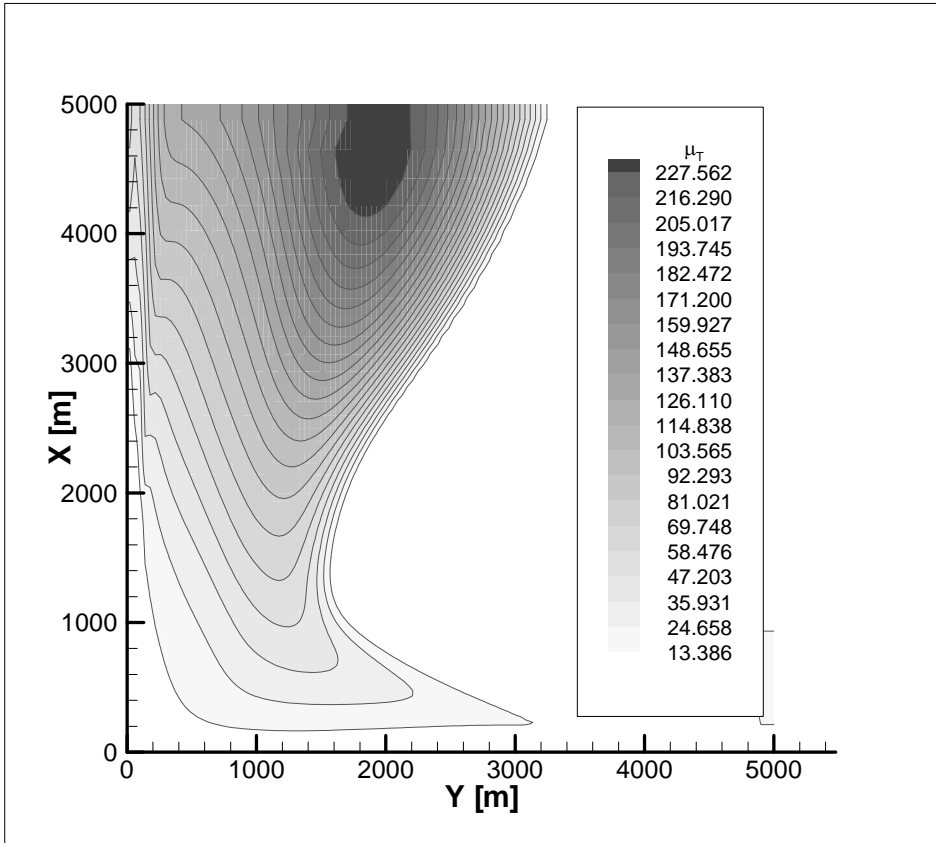


Figure 6-16: Turbulent viscosity - Dirichlet boundary

## 6.7. Conclusion

A two-dimensional axis-symmetrical, rectangular grid, model of the field above the solar chimney power plant has been generated and solved in CFX 4-4. The grid independence of the model has been demonstrated using Richardson extrapolation to obtain a zero grid solution for areas with large gradients in velocity and temperature and it has been shown that the final solution is relatively independent of the grid used.

Results have shown that the specification of turbulence variables for  $k$  and  $\epsilon$  have a significant impact on the solution of the flow field in terms of the turbulent viscosity production. The question of which method or values to use is open to debate and further research should definitely be conducted in the correct values for these variables at the inlet boundary.

The general flow field compares relatively well with results obtained by Thiart (2002). It has been noticed that the height from which air is drawn into the collector is significantly lower than that observed by Thiart (2002), however. This might be due to the values of  $k$  and  $\varepsilon$  used by Thiart (2002) at the pressure boundary being significantly lower than either that specified or calculated in this model. This cannot be verified as a converged solution for the turbulence boundary values specified by Thiart (2002) could not be realised in this study.

## CHAPTER 7. DEEP BOUSSINESQ MODEL

---

### 7.1. Introduction

The deep Boussinesq model is based on the assumption that the solution to the flow field does not deviate substantially from a reference hydrostatic condition. The density is specified only as a function of height, and is thus decoupled from the solution for pressure and temperature. There is no equation of state. The momentum due to buoyancy in the vertical direction is modelled by a difference in the potential temperature solved in a control volume from a reference hydrostatic potential temperature specified as a function of height. For an adiabatic process the potential temperature is constant.

Duynkerke (1987) shows the existence of additional source terms for turbulence kinetic energy,  $k$ , and turbulence dissipation rate,  $\varepsilon$ . The addition of a source term in the dissipation equation is also specified. This term accounts for stability of the atmospheric processes in the  $k$ - $\varepsilon$  model.

Implementation of this model in CFX 4-4 involves a number of additional FORTRAN routines. These are: Specification of a density field which is constant as a function of the vertical co-ordinate direction, addition of a source term in the vertical momentum equation in order to model buoyancy effects and additional source terms in the  $k$  and  $\varepsilon$  equations for the production and dissipation of kinetic energy. Each of these routines are discussed below and results for a simple test case are given. The solution for the deep Boussinesq model is compared to the solution for the Boussinesq assumption for the same wall boundary values. It can be seen in the equation for the potential temperature, that potential temperature and real temperature are the same at ground level.

## 7.2. Theoretical Considerations

### 7.2.1. Hydrostatic density profile

Given a real temperature profile, a hydrostatic atmospheric pressure profile is solved by integrating the pressure gradient equation.

$$dp_h = -\rho_h g dz \quad (7-1)$$

With the density given as a function of the vertical hydrostatic pressure profile and of the real vertical temperature profile as:

$$\rho_h = \frac{p_h}{RT_h(z)} \quad (7-2)$$

For a neutrally stable atmosphere the temperature profile follows the dry adiabatic lapse rate. The hydrostatic pressure profile, solved in appendix A, is then used to calculate a hydrostatic density profile from the above equation using the DALR temperature profile.

### 7.2.2. Energy equation

It can be shown, using the first law of thermodynamics and the assumption of small deviations of properties, that the energy equation can be solved in terms of the potential temperature. The final solution of which is a standard transport equation for the potential temperature. The details of this derivation are given in appendix E.

$$\frac{\partial}{\partial t}(\rho\theta) + \bar{\nabla}(\vec{v}\rho\theta) = \rho \frac{d\theta}{dt} = \rho \frac{1}{c_p} \frac{\theta}{T} \frac{dh}{dt} \quad (7-3)$$



According to Montavon (1998), for purely adiabatic processes, the energy conservation equation is therefore a simple advection-diffusion equation for the potential temperature, with a vanishing diffusion term. Hence for processes without radiative heat flux or latent heat release ( $dh/dt = 0$ ), the potential temperature is conserved along flow trajectories, which makes it a very convenient variable to simulate atmospheric processes. In general, a diffusion term is introduced into the above equation to account for turbulent mixing.

### 7.2.3. Buoyancy source term

For the specified temperature and pressure profiles a hydrostatic potential temperature profile is solved based on the following equation:

$$\theta_h(z) = T_h(z) \left( \frac{P_0}{p_h(z)} \right)^{R/C_p} \quad (7-4)$$

The derivation of the buoyancy term is based on the assumption that the deviation of properties from the hydrostatic state is small. Taking derivatives of the ideal gas law, for small changes in properties, gives the following relationship.

$$\frac{dp}{p} = \frac{dT}{T} + \frac{d\rho}{\rho} \quad (7-5)$$

Taking the derivative of the potential temperature equation, as in the derivation of the energy equation, one obtains equation 7-6, below.

$$\frac{d\theta}{\theta} = \frac{dT}{T} - \frac{R}{C_p} \frac{dp}{p} \quad (7-6)$$

Substitution of equation 7-5 into 7-6, gives the following relationship between density changes and potential temperature changes.

$$\frac{d\rho}{\rho} = -\frac{d\theta}{\theta} + \left(1 + \frac{R}{C_p}\right) \cdot \frac{dp}{p} \quad (7-7)$$

Providing that the Mach number of the flow is much smaller than unity, and that the change in pressure is small with respect to the absolute pressure, which is expected for atmospheric processes, the second term in the above equation can be neglected. This leads to the approximation.

$$\frac{d\rho}{\rho} = -\frac{d\theta}{\theta} \quad (7-8)$$

Or alternatively, relating changes from the hydrostatic state, the following equation is derived. This equation couples the energy conservation equation with the vertical momentum equation.

$$(\rho_h - \rho) = \frac{\rho_h}{\theta_h} (\theta - \theta_h) \quad (7-9)$$

#### 7.2.4. Modifications to the k-ε model

It was previously mentioned in chapter 4, that the standard k-ε model is modified to take into account the anisentropic effects of buoyancy. Duynkerke (1998) describes the modification in terms of the potential temperature, and this source term is added to both the k equation as well as the ε equation, as mentioned in chapter 5.

$$G = -\frac{\mu_{eff}}{\sigma_H} \frac{g}{\theta_h} \frac{\partial \theta}{\partial z} \quad (7-10)$$

The addition of this extra term acts as a sink for turbulence for a stably stratified atmosphere, when  $\partial\theta/\partial z > 0$ , and is only active in the ε equation for unstable

atmospheres,  $\partial\theta/\partial z < 0$ , Montavon (1998). The other addition to the k- $\epsilon$  equation is the source term in the  $\epsilon$  equation. This addition is also only active for unstable atmospheres.

$$D = \frac{\partial}{\partial x_i} \left[ \mu_T \frac{\partial k}{\partial x_i} \right] \quad (7-11)$$

### 7.3. CFX 4-4 Application

#### 7.3.1. USRDEN

The user FORTRAN routine USRDEN is used to modify the equation of state for compressible flow options or to specify an equation for variable density in incompressible flow situations. In order to specify the hydrostatic density profile derived previously in this chapter it is first necessary to define the real temperature profile and pressure profile as functions of the vertical co-ordinate. In the axis-symmetric case, the default condition for the vertical co-ordinate is the x variable.

In the FORTRAN routine, supplied in appendix F, the hydrostatic pressure and real DALR temperature profile are described as user functions of the height, x. The gas constant for air is defined and the density is then altered so that it is only a function of position, with changes in the x-direction.

#### 7.3.2. User scalar transport equation

CFX 4-4 allows for the solution of transport equations for up to five additional user scalar variables, CFX user manual. These transport equations take the form:

$$\frac{\partial(\rho \theta)}{\partial t} + \frac{\partial(\rho \theta u_i)}{\partial x_i} = \frac{\partial}{\partial x_i} \left( \Gamma \frac{\partial \theta}{\partial x_i} \right) + S \quad (7-12)$$

where  $S$  represents source terms and  $\Gamma$  represents the diffusion of the scalar. For steady state, turbulent flow the transport equation for potential temperature is expressed thus:

$$\frac{\partial(\rho\theta u_i)}{\partial x_i} = \frac{\partial}{\partial x_i} \left( \frac{\mu_T}{\sigma_\theta} \frac{\partial}{\partial x_i} \theta \right) \quad (7-13)$$

The sources represent the latent heat flux that appears for non-adiabatic processes such as evaporation and condensation. For dry, adiabatic air the sources are zero. The diffusion of potential temperature is related to the turbulent viscosity and the turbulent Prandtl number.

The solution of the potential temperature equation is determined, as with all transport equation, by the values of the scalar at the boundary conditions.

### 7.3.3. USRDIFF

The user FORTRAN routine USRDIFF is used to modify diffusivities of any variable in CFX and also for any user scalar. In order to achieve this the turbulent Prandtl number for the potential temperature is called using the function GETADD, and the viscosity VIS, is obtained using the routine GETVAR, which locates the address for flow variables. It is then a simple matter of setting the new diffusivity, GAMMA, as defined in section 7.3.2 above for the user scalar POTTEMP, the potential temperature.

### 7.3.4. USRSRC

Alterations of the equations, particularly for the addition of sinks and sources in the momentum equations, are done using the FORTRAN routine USRSRC. The routine is called after the equations have been linearised in the form:

$$\text{Convection} - \text{Diffusion} = \text{Sources} \quad (7-14)$$

Due to the fact that the equations have been obtained by integration over the control volume, the source term must have the form of the product of the source term and the control volume.

There are two options for the source terms,  $S_u$  and  $S_p\phi_p$ . Where  $\phi$  represents the variable of the equation to which the source term must be added.  $S_u$  is for the addition of independent source terms, while  $S_p$  is used when source terms are functions of the variable. It is very important to linearise the equations for the source terms correctly, CFX 4-4 (2001), and to correctly specify the additions to  $S_u$  or  $S_p$ . If the term for  $S_p$  is positive, diagonal dominance of the solution matrix will be violated. This can be overcome by adding the contribution to  $S_u$ , using old values of the variable.

### ***Momentum***

The dimensions of the source terms for the momentum equations are  $\text{kg m s}^{-2}$ . The above density difference approximation is multiplied by the value for gravitational acceleration,  $g$ , and by the volume of the control volume. This momentum source term is added using the user FORTRAN routine, USRSRC. See Appendix F for the source code. The source term is only activated if there is a deviation of the potential temperature from the hydrostatic potential temperature. For this reason a hot and a cold wall are used in the following test model in order to implement a potential temperature difference and activate the buoyancy source term for potential temperature.

### ***k- $\epsilon$ Sources***

The addition of extra source terms in the k- $\epsilon$  model has been described previously. As in the addition of sources in the momentum equation, this is achieved with the USRSRC routine. It is important to linearise the source terms in the k- $\epsilon$  equation in order to maintain diagonal dominance of the co-efficients in the linearised equations. Appendix C has further details on the solution to the discretized equations.

## 7.4. Sample Test Case

In order to test the solution of the deep Boussinesq model, a sample model was set up. The test model is a two dimensional rectangular domain, comprised of two blocks. Two blocks are necessary in order to define the two walls; differences in temperature from the two walls will dictate the onset of a flow field due to buoyancy and the final flow field solution.

### 7.4.1. Model geometry

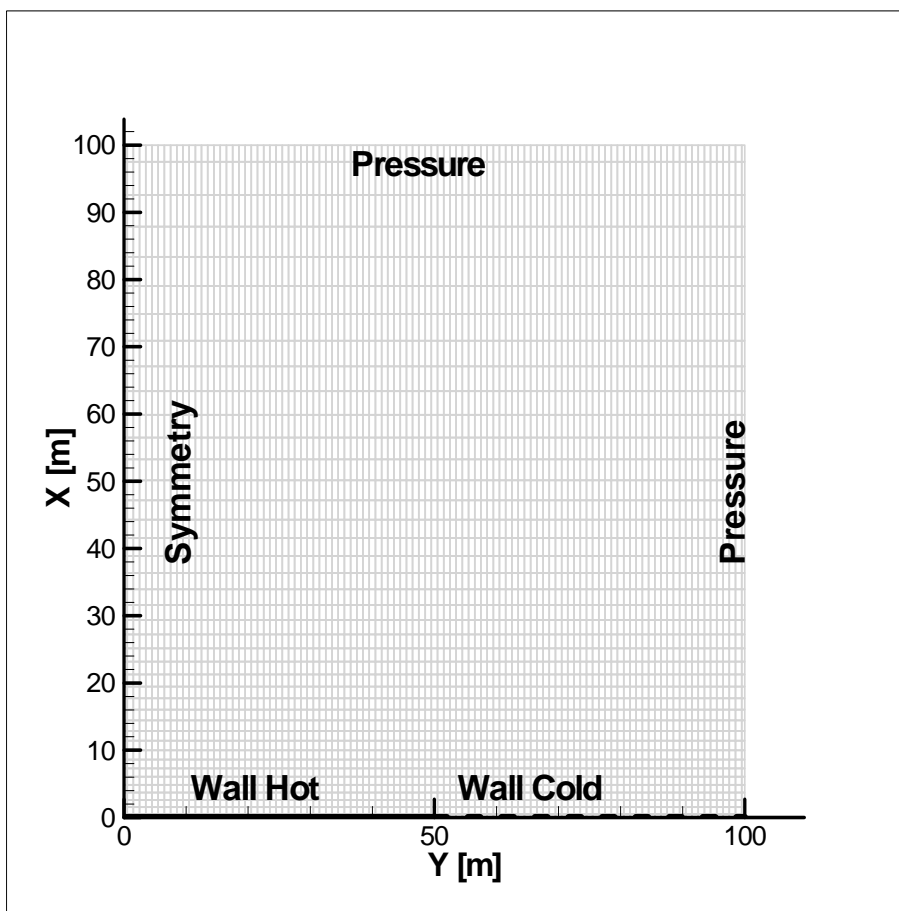


Figure 7-1: Test model boundary conditions

The total length and height of both block is 100 m by 100 m. The grid is refined such that finer control volumes occur near the walls. Boundary conditions for the block have been chosen to be similar to boundary conditions for the final model of the solar chimney. These boundary conditions are described below.

### **7.4.2. Boundary conditions**

The two wall boundaries, one hot and one cold, are indicated. A symmetry boundary is prescribed for the left side atmospheric boundary; this is similar to the assumption of an axis of symmetry at that boundary. The upper and right side pressure boundaries need further explanation.

#### ***Pressure***

Due to the fact that CFX 4-4 solves for a modified pressure, and that the basic assumption of a hydrostatic pressure is utilised in the development of this model, the pressure specified is a deviation from the hydrostatic assumption. For both pressure boundaries the pressure is specified in the command file as zero, i.e. hydrostatic pressure value. The temperature at the pressure boundaries is also assumed to be an adiabatic temperature profile for dry air, and for this reason a constant value of 300 K for the potential temperature is specified. This is also the temperature of the cold floor, as this is the reference temperature for the DALR. A zero flux, Neumann condition is specified on  $k$  and  $\epsilon$ .

#### ***Walls***

The walls are specified on the lower surface of the blocks, as shown in figure 7.1. The temperature of the cold wall is specified at the same potential temperature, 300 K, as that of the right pressure boundary so that there is no buoyant force on the incoming air. The temperature of the hot wall is varied such that the effect on the flow field can be observed for different boundary values.

#### ***Symmetry***

A symmetry boundary is specified on the left boundary. This is done so that the model is a simplification of the solar chimney model geometry.

### **7.4.3. Model assumptions**

#### ***Compressibility***

The model is run as an incompressible model as the variation in density is accounted for the specification of density as a function of height, the hydrostatic density function.

#### ***Physical properties***

Due to the solution of the energy equation in terms of the potential temperature, the model is specified as isothermal, in that the energy equation is solved for potential temperature and the real temperature is not used in obtaining a solution. The specific heat and viscosity are therefore constant for the entire flow domain. Initially the diffusivity of the potential temperature scalar equation is set as a constant in the command file. This is done to decouple the potential temperature transport equation from the turbulence equation in order to assist in convergence of the solution.

#### ***Time dependence***

A steady-state assumption is made for the flow field.

### **7.4.4. Numerical considerations**

#### ***Discretization***

Discretization of the partial differential equations of momentum conservation, mass conservation and the modified energy equation in terms of potential temperature is achieved by the default hybrid scheme, as described in appendix B.



### *Under relaxation factors*

Initially the relaxation factors as used by Thiart (2002) were used in the solutions, except for the URF for  $\theta$ , which is the same order of magnitude as the pressure URF so that the solution for the energy conservation in terms of potential temperature is enforced more aggressively than the momentum. As will be seen the relaxation factors had to be altered in order to stabilise the solution for the correct solution of the energy equation in terms of  $\theta$  and for the coupling of the diffusion term to the turbulent viscosity,  $\mu_T$ . The most utilised under-relaxation factors for these models are tabulated below.

Table 7-1: Under-relaxation factors

u	v	k	$\epsilon$	$\theta$	p
0.02	0.02	0.02	0.02	0.4	0.8

## **7.5. Results**

Each of the modifications for the deep Boussinesq model were introduced independently so that the effects of the different components could be observed. The diffusivity specified in the models for the testing of the buoyancy source term was initially set as the maximum value of the turbulent viscosity  $\mu_T$  obtained from the Boussinesq approximation.

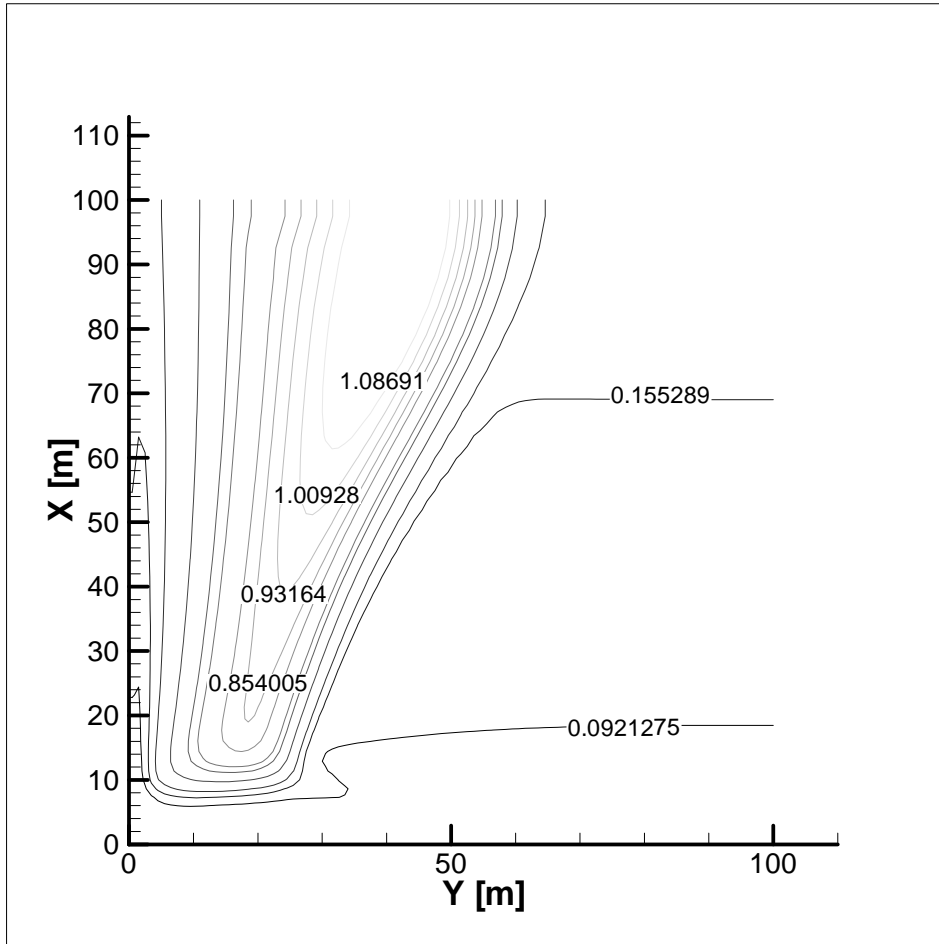


Figure 7-2: Turbulent viscosity - Boussinesq approximation

### 7.5.1. Boussinesq approximation

The figure above shows the solution for the turbulent viscosity for the Boussinesq approximation with a temperature on the hot plate of 320 K. As can be seen in the figure above, the maximum value is approximately  $1 \text{ kg m}^{-1} \text{ s}^{-1}$ . Solutions for the temperature and velocity fields are given later in the chapter when comparing with the final solutions of the deep Boussinesq model.

### 7.5.2. Hydrostatic density profile

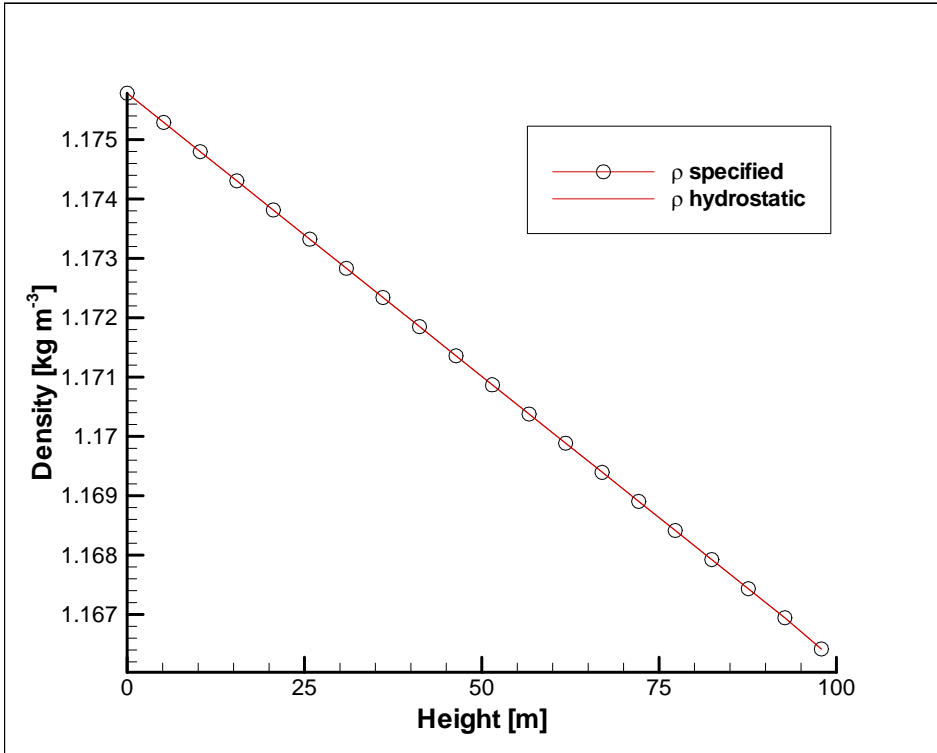


Figure 7-3: Comparison of density

The profile of density obtained for USRDEN is displayed in Figure 7-3 above, as well as a hydrostatic density profile based on the DALR. The excellent correlation is understandable due to the fact that the density is calculated from the hydrostatic pressure and real temperature field for an adiabatic process and is displayed here to demonstrate that the density is specified correctly as a function of height.

### 7.5.3. Addition of buoyancy

It is important to observe that there is in fact a zero flow field for the stable condition, when no potential temperature gradients exist in the flow field. This entails the addition of a buoyancy source term in the momentum equation, without specifying a driving potential temperature difference on the hot wall. Results from this test are displayed below.

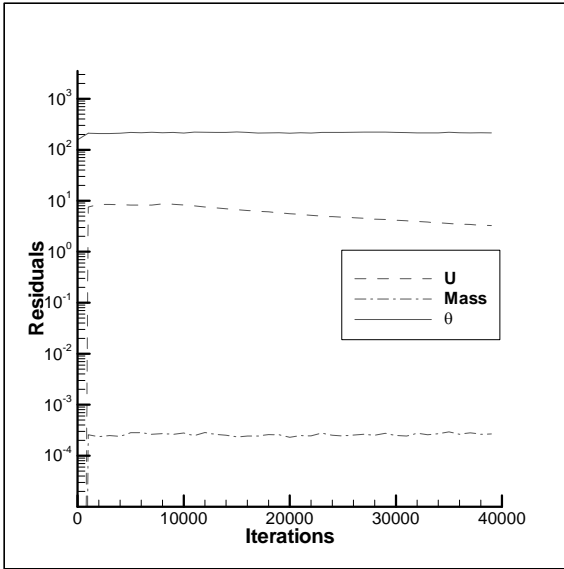


Figure 7-4: Residual plot for "zero" flow test

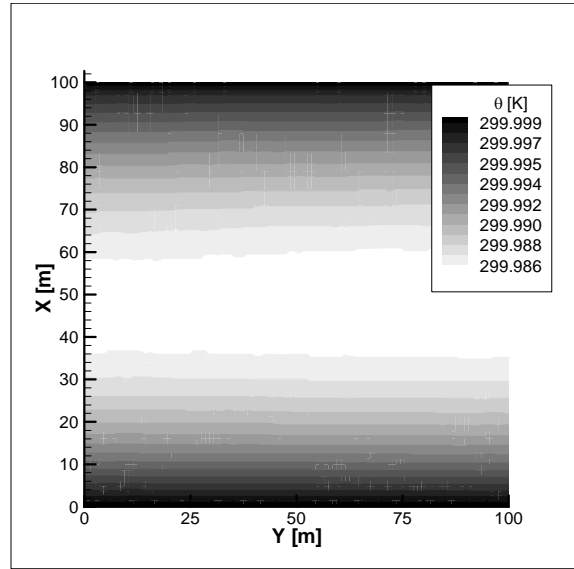


Figure 7-5: Potential temperature contour plot

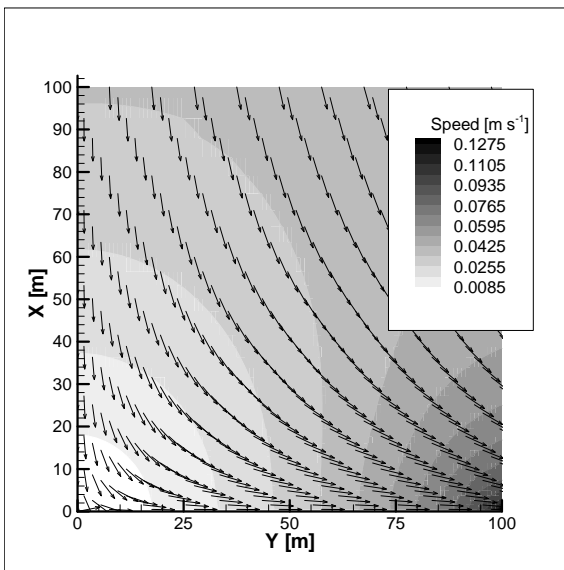


Figure 7-6: Speed contours and vector plot

It can be seen above that the residuals do not change significantly from the first iteration to the last iteration. A possible reason for this is the value of the initial field chosen. For potential temperature,  $\theta$ , the initial value is 300 K, the expected final value of the solution. A zero flow field for velocity and pressure was also specified.

Another criteria for convergence of the solution, is that the values of the variables do not change appreciably from iteration to iteration. For the potential temperature the value change is in the order of  $10^{-4}$  K per iteration.

The flow field seems to be very dependent on the correct solution to the transport equation of the potential temperature. For a very small error in potential temperature a large error in the flow field is induced. In order to test this dependence of the velocity field on the potential temperature solution, a second test case for the buoyancy source is investigated. The following results demonstrate the flow field for a potential temperature difference between the hot plate and the cold plate of 1 K.

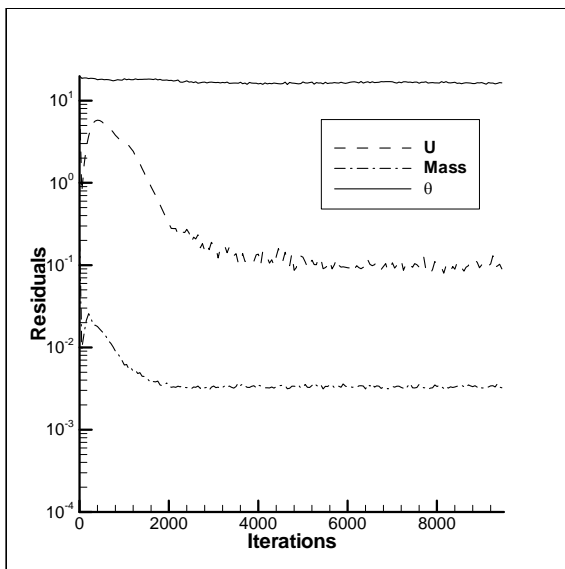


Figure 7-7: Residual plot -  $\Delta\theta = 1$ K

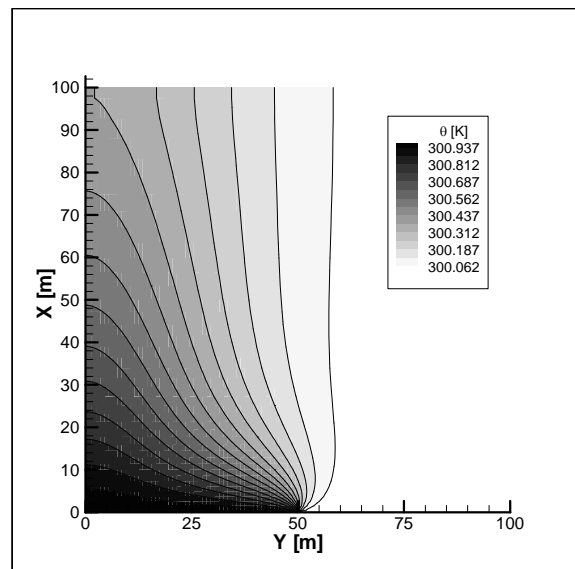


Figure 7-8: Potential temperature contour plot

In the above model, the diffusion,  $\Gamma$ , in the potential temperature transport equation is set at a constant value. It was noticed that for a decreasing  $\Gamma$  the solution becomes increasingly more unstable. The value of  $\Gamma$  for the present results is set at  $1 \text{ kg m}^{-1} \text{ s}^{-1}$ . In the next section the dependence of the solution on the scalar diffusivity is investigated.

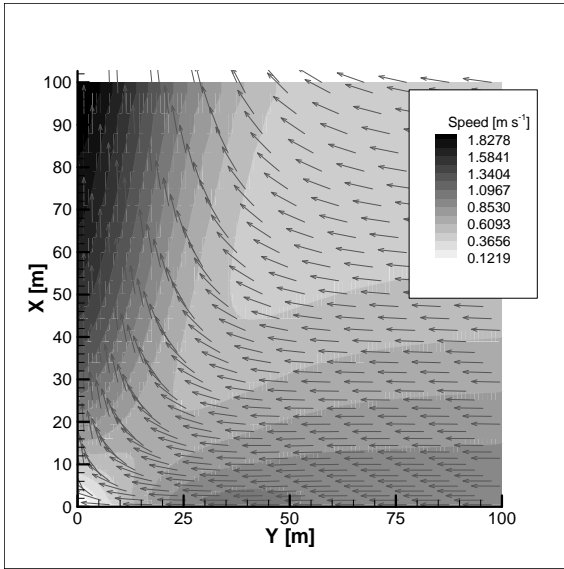


Figure 7-9: Speed contours

As can be seen in the figures above, imposing a temperature difference between the hot plate and the cold plate has the effect of stabilising the flow and creating the expected field.

The following plots show the potential temperature and speed contours for the condition of a 20 K temperature difference between the hot and cold plates

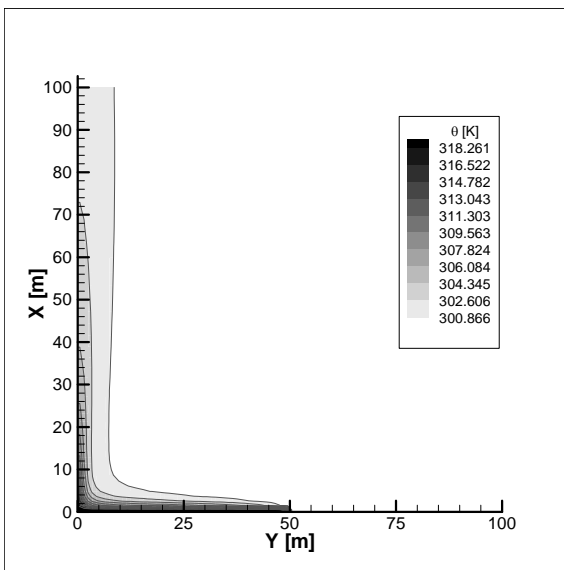


Figure 7-10: Potential temperature contours

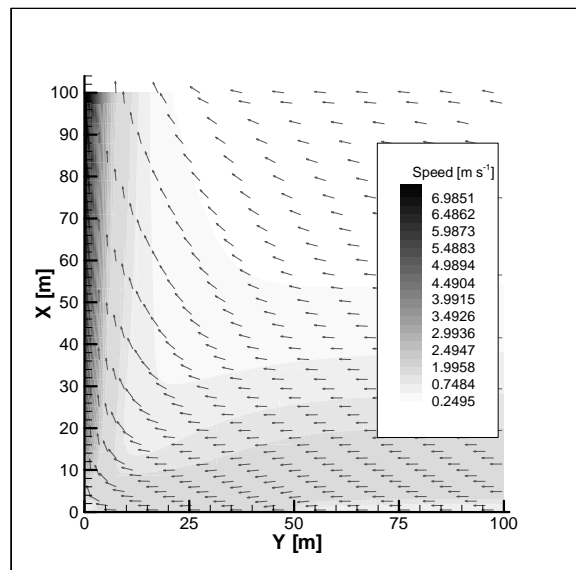


Figure 7-11: Speed contours

### 7.5.4. Addition of k-ε source terms

The results shown in the figures below show the difference in values for k and ε due to the implementation of the source terms in the k-ε equations. In both cases the diffusivity has been retained as  $1 \text{ kg m}^{-1} \text{ s}^{-1}$ .

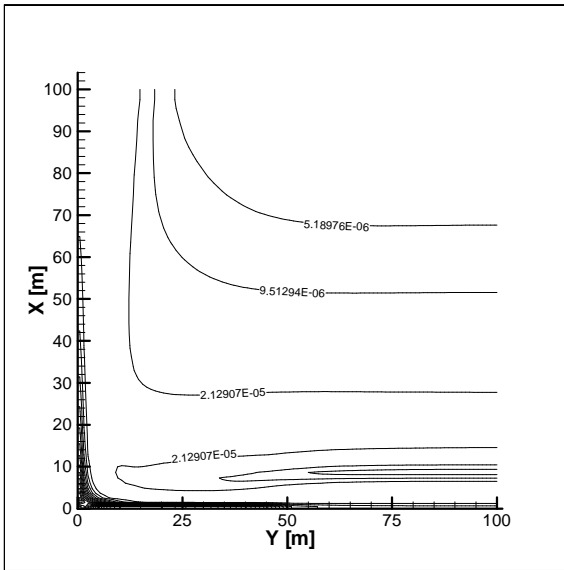


Figure 7-12: k - no additional source terms

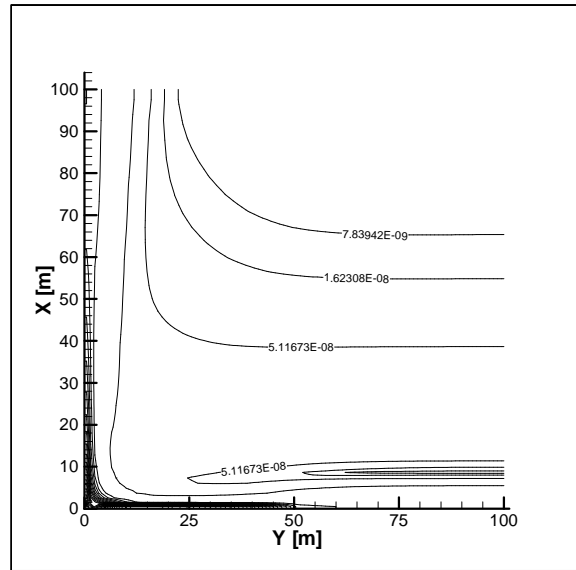


Figure 7-13: ε - no additional source terms

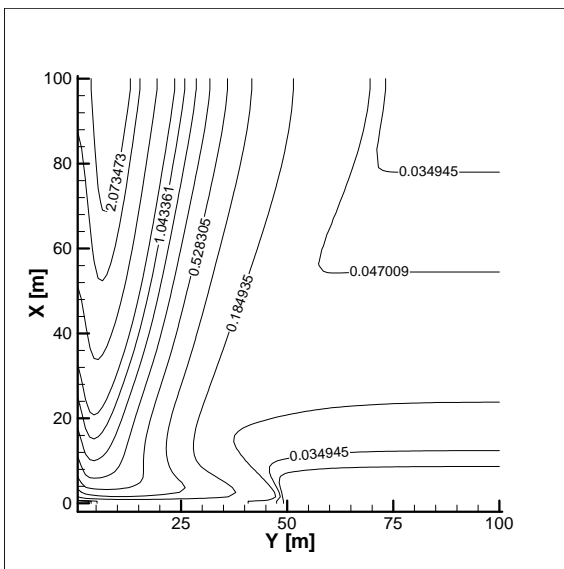


Figure 7-14: k buoyancy and dissipation source terms

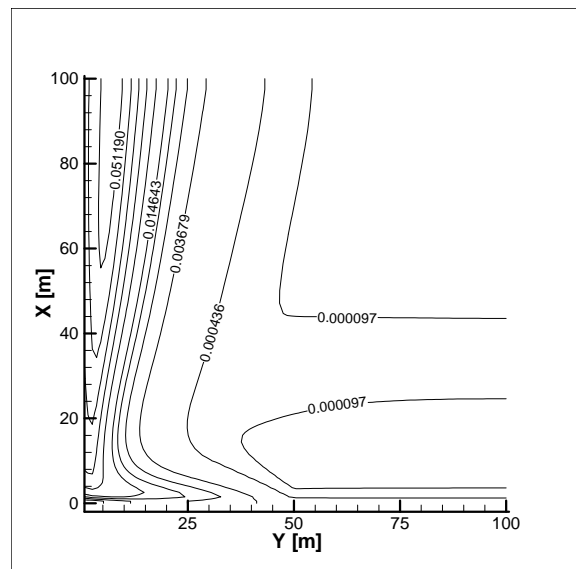


Figure 7-15: ε buoyancy and dissipation source terms

It can be seen above that the addition of buoyancy into the k-ε equation greatly affects the production of turbulence in the flow.

### 7.5.5. Diffusion coupling

The diffusion coupling links the diffusivity of the potential temperature to the solution of k and ε through the equation for the turbulent viscosity,  $\mu_T$ . Values of turbulent viscosity, and therefore diffusivity, will vary from orders of the molecular viscosity to approximately the same maximum value as observed in the Boussinesq approximation. It was noticed that the solution for the flow field becomes unstable for low constant diffusivities, and initial results for the diffusion coupling.

In order to stabilise the solution, a viscosity of  $50 \text{ kg m}^{-1} \text{ s}^{-1}$ , was specified as an initial field, and the URF for viscosity was set at  $10^{-4}$ . This had the effect of allowing a pseudo-laminar solution for the potential equation at each iteration. This relaxation factor was also increased after every ten thousand iterations.

The figures below show the results for the turbulent viscosity and potential temperature contours for the diffusion coupled solution.

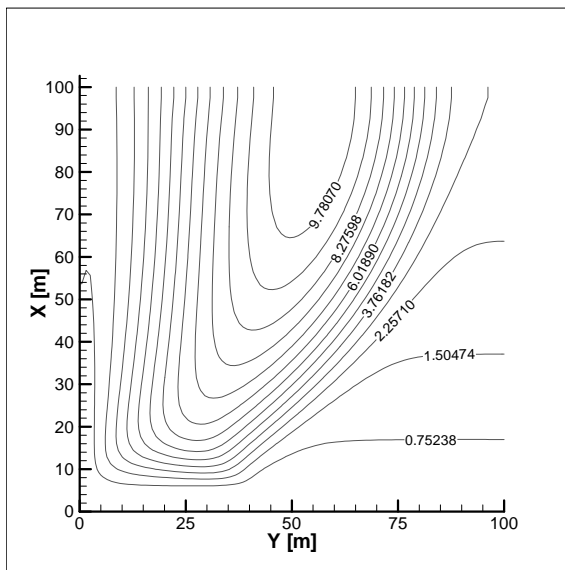


Figure 7-16: Complete model -  $\mu_{\text{eff}}$

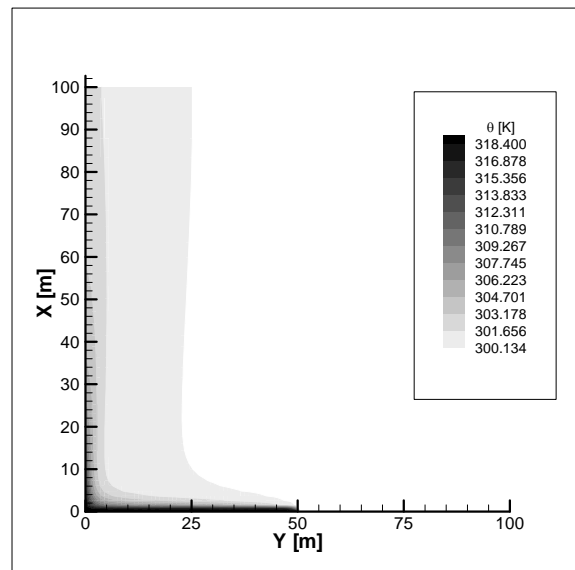


Figure 7-17: Complete model - Potential temperature



### 7.5.6. Comparison with Boussinesq Approximation

The final results for the deep Boussinesq model are now compared to the flow field for the Boussinesq approximation.

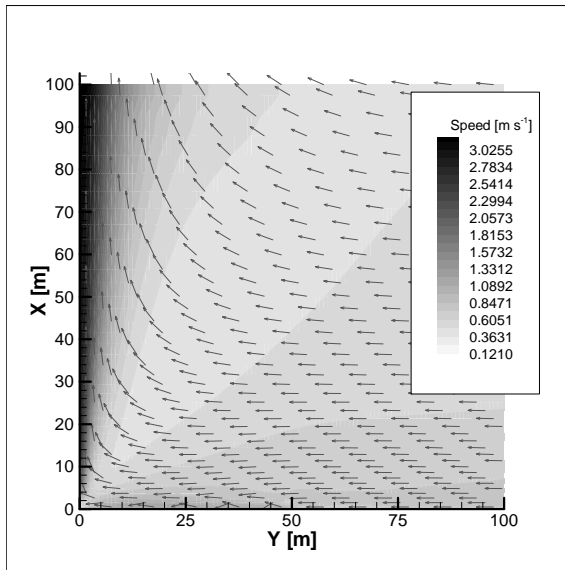


Figure 7-18: Complete model – Speed contours

The results above show that the maximum velocity induced by the buoyancy in terms of the potential temperature is significantly greater than that for the Boussinesq model, at least three times as much. Looking at the source terms for the momentum equation for both shows the magnitude of the differences.

$$(\rho_h - \rho) = \frac{\rho_h}{\theta_h}(\theta - \theta_h) \quad \text{Potential temperature momentum source} \quad (7-15)$$

$$(\rho_h - \rho) = \rho_0\beta(T - T_{ref}) \quad \text{Real temperature momentum source} \quad (7-16)$$

For incompressible flow,  $\beta$ , is approximately equal the inverse of  $T_{ref}$ . For an adiabatic process the potential temperature is constant, and in this case equal to  $T_{ref}$ . The difference

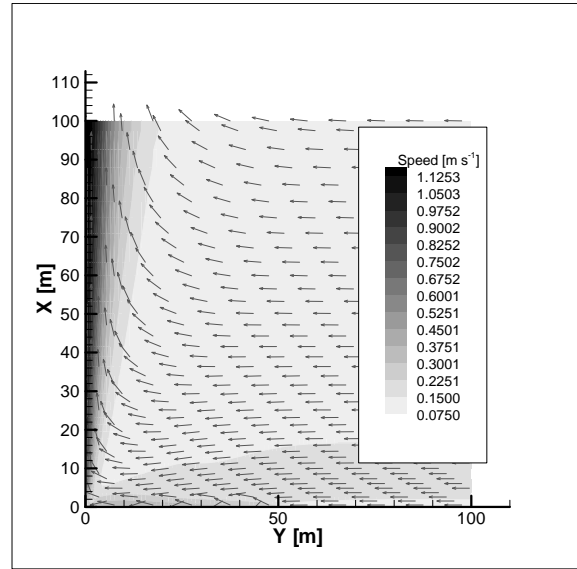


Figure 7-19: Boussinesq approximation – Speed contour

in the momentum sources can then only be accounted for in the difference between the constant reference density in the Boussinesq approximation and the hydrostatic density for the deep Boussinesq model, or the solution of the temperature and potential temperature respectively.

The hydrostatic density, however, varies only by a maximum of 2% from the reference density. It would appear then that the differences are caused by the diffusion terms in the respective energy equations. In the deep Boussinesq model the potential temperature is diffusing more than the enthalpy in the standard energy equation. It has been shown in the previous sections that the diffusion coefficient,  $\Gamma$ , strongly determines the final solution of the potential temperature field. The potential temperature gradient also has an effect on the production of turbulence through the introduced buoyancy production term.

Using the potential temperature definition, equation 7.4 above, and calculating the hydrostatic pressure for a constant density it is possible to calculate the equivalent potential temperature for the Boussinesq approximation.

$$p_h(x) = p_0 - \rho_0 g x \quad (7-17)$$

The following contour plot is obtained.

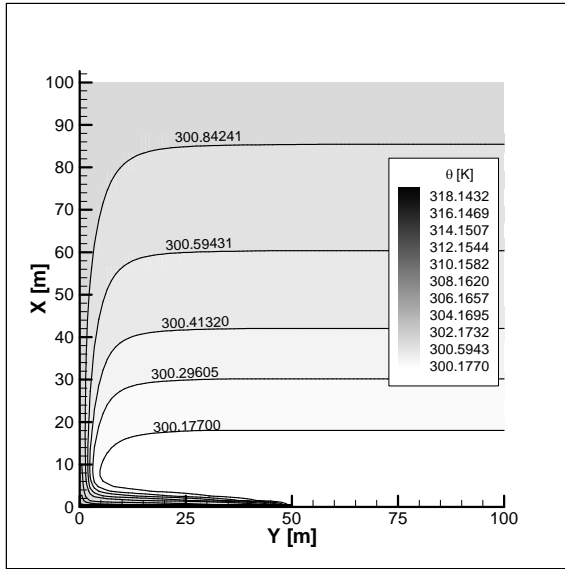


Figure 7-20: Boussinesq Approximation –  
Potential temperature contours

The effect of setting a constant ambient temperature, as in the Boussinesq approximation, can be seen in the figure as a positive potential temperature gradient. A positive potential temperature gradient is indicative of a stable atmosphere, which tends to inhibit vertical motion. Specifying an increasing hydrostatic potential temperature gradient in the buoyancy source term would arguably also decrease the momentum source terms in the deep Boussinesq model.

## 7.6. Discussion and Conclusions

The application of a deep Boussinesq model and the solution of the energy equation in terms of the potential temperature have been shown in this chapter. It can be seen that an accurate solution of the potential temperature equation is important in resolving the flow field due to the instability of the buoyancy equation resulting from a very small deviation of the potential temperature from a hydrostatic reference state. For this reason the transport equation for the potential temperature needs to be more under-relaxed than the other transport equations for momentum,  $k$  and  $\epsilon$ .

Additions to the  $k$ - $\epsilon$  model to account for buoyancy in the flow are seen to have a very large effect on the final solution of the viscosity field. The effect of the source term in the

diffusion equation to account for atmospheric stability,  $D$ , has however not been demonstrated.

In the comparison between the Boussinesq approximation and the deep Boussinesq model it was noted that the magnitude of the induced velocities is approximately three times larger for the deep Boussinesq than the normal Boussinesq. It appears that this is due to the fact that specifying a constant temperature field numerically has the same effect as a constant temperature field in the physical reality of the problem. The stability of the atmosphere has been demonstrated to have a large impact on the final solution.

In effect then, the standard Boussinesq approximation approximates a highly stable atmosphere. It would be interesting to see what the effect of solving the deep Boussinesq model with a non-adiabatic hydrostatic potential temperature profile would be. This would involve the addition of additional source terms in the potential temperature transport equation and the solution of a hydrostatic density profile and a subsequent real temperature profile.

# CHAPTER 8. FURTHER WORK

## 8.1. Three-dimensional Model

In reality, the assumption of a zero cross flow over the solar chimney is seldom realised. It is necessary then to create a three-dimensional model so that inlet velocity profiles can be specified on the boundaries. A two dimensional model, used previously, can not work due to the fact that the field will naturally follow the flow field solved for the two-dimensional model, without being indicative of the actual solution. Keeping the assumption of negligible Coriolis simplifies the three-dimensional model in the plane of symmetry can still be assumed either parallel to or perpendicular to the wind direction. A model for the former was constructed and is demonstrated in the figure below.

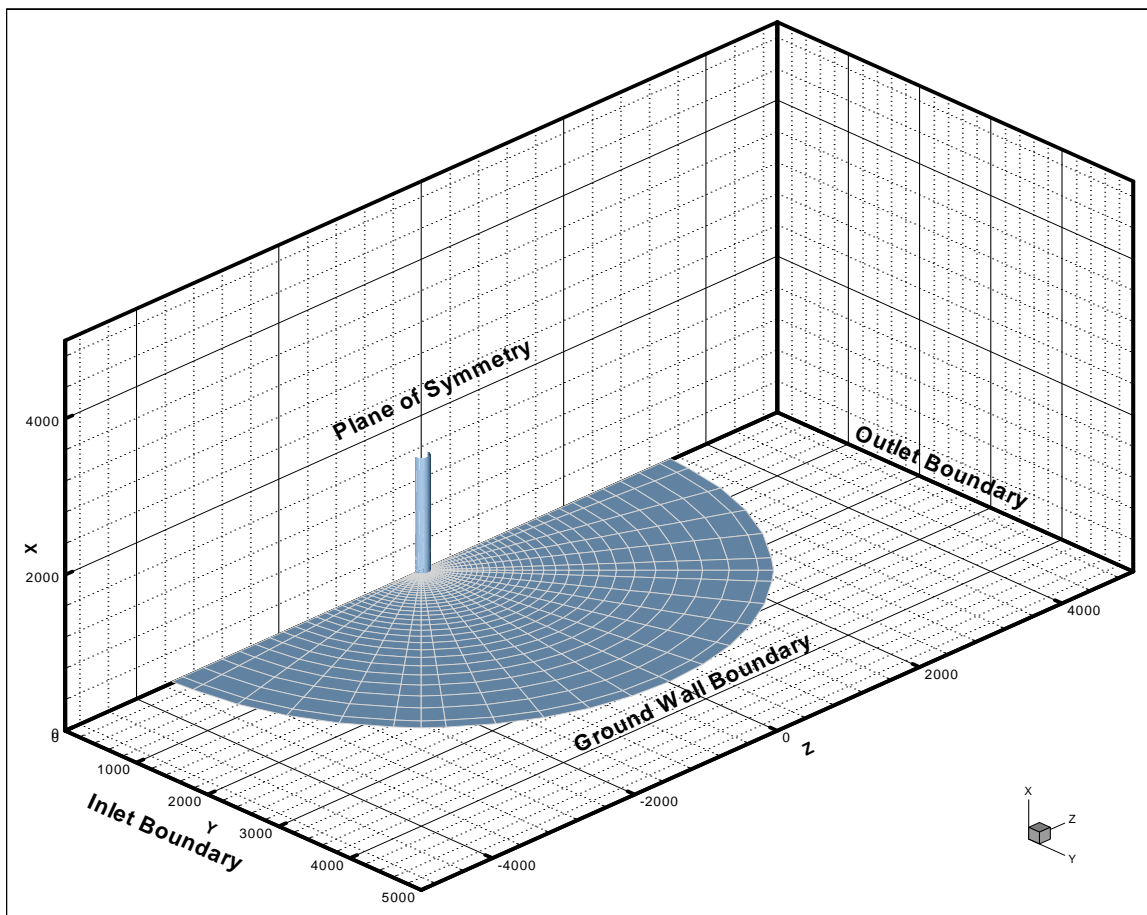


Figure 8-1: Model geometry and boundaries

### 8.1.1. Grid

Due to the circular nature of the chimney and collector, it is necessary to have a combination of cylindrical and rectangular grids to accurately describe the geometry.

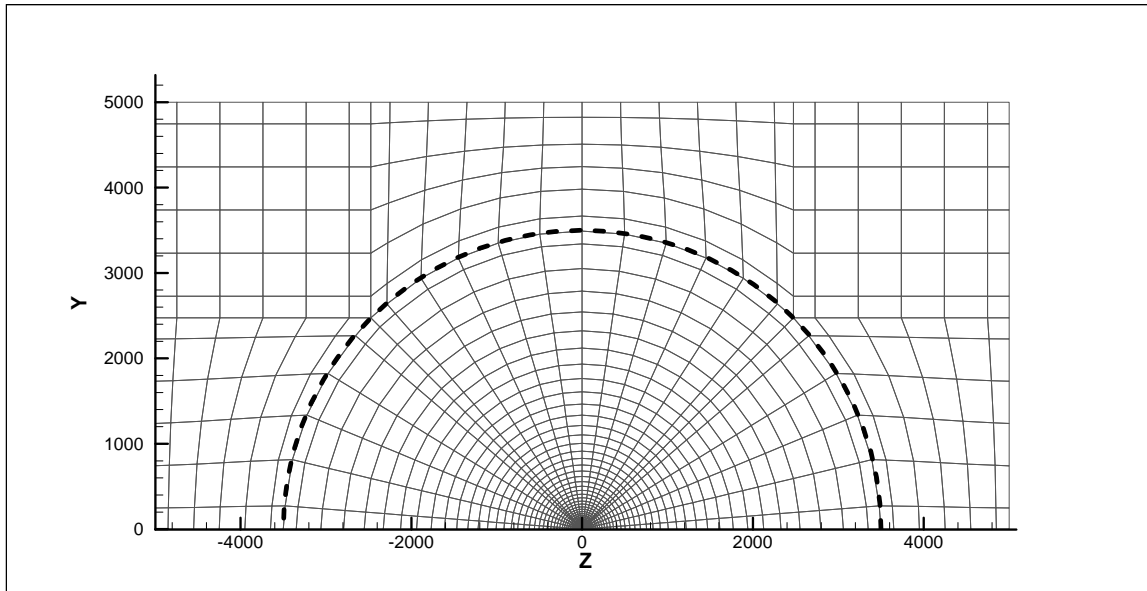


Figure 8-2: Top view of model

The collector of the chimney is modelled with a c-grid. An interface exists between the c-grid and an h-grid at the outer perimeter of the collector, where the cylindrical co-ordinates of the collector meet the rectangular blocks. The interface can be seen in the above figure. The bold dashed line demarcates the collector boundary.

An h-grid is patched onto a c-grid for the control volumes above the chimney. This can be seen on the right hand side of figure 8-3. The dashed half circle indicates the position of the chimney. This leads to a number of small control volumes above the chimney. These redundant nodes are necessary so that the number of control volume on the patches between the blocks can be matched and sufficient control volumes can be created on the outer boundary blocks, this can be seen in the above figure where the radial lines from the collector match the rectangular grid lines. Unmatched grids are possible in CFX 4-4, but these may lead to continuity errors and convergence problems and were not used.

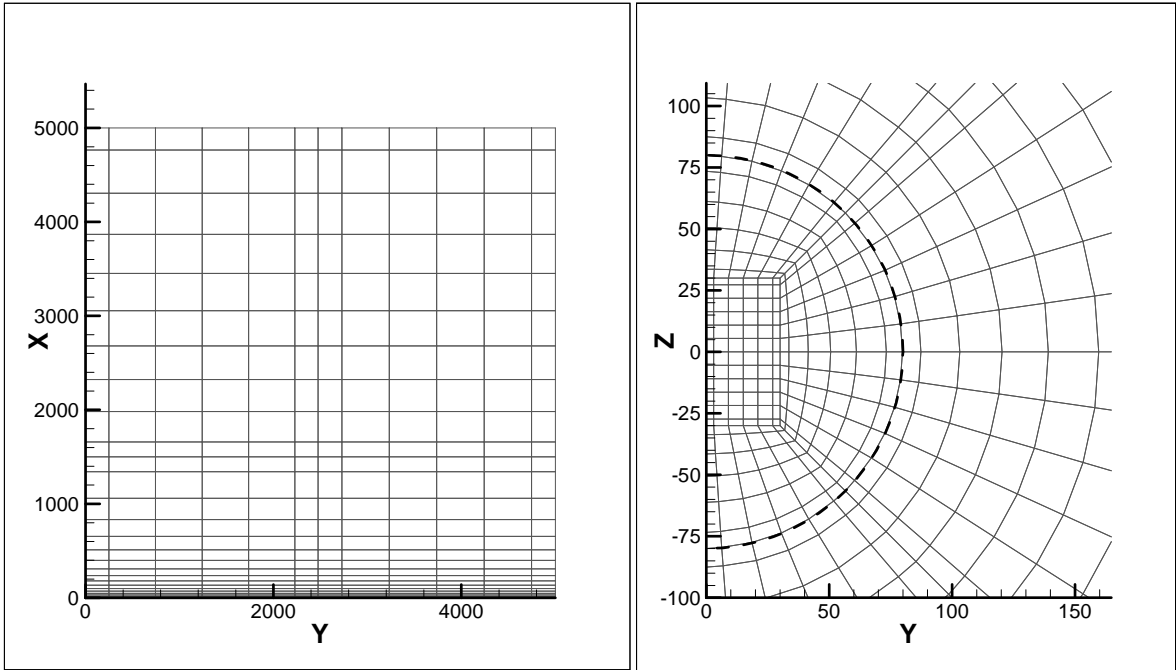


Figure 8-3: Front view and chimney detail

To the left of the above diagram the front view of the model can be seen. This is the view of the atmospheric inlet plane. Linear one way-biased grid refinement was done above the collector in order to minimise grid expansion in this region. Grid refinement was also achieved with one way biasing on the radial control volumes from the chimney.

## 8.2. Large Eddy Simulation Turbulence Model

According to Kim and Boysan (1999), the fidelity of CFD solutions for turbulent flows is dictated by turbulence modelling and the models used. The modelling of the flow for the solar chimney, and any environmental flow, is shown to be highly dependent on the modelling of turbulence. Many authors have demonstrated the inability of the  $k-\epsilon$  model in accurately predicting turbulence for these types of flows. Even though there are a number of modifications to the model to account for the atmospheric turbulence the fundamental principles of isotropic and wall governed turbulence are questionable. The large eddy simulation solves the laminar governing equations for the large eddies in the flow and uses simple models of turbulence for the smaller eddies, which are more amenable to the isotropic assumption. LES is believed to be the only option available for accurate

modelling of atmospheric turbulence, Ferziger et al. (2002). Coupled with this is the increase in computing resource available, which make LES of atmospheric flows less timely and more accessible for use in atmospheric flows.

### **8.3. Variable Density**

For atmospheric processes above approximately 1000 m, the variation in density becomes significant in the modelling of the momentum and energy equations. It is necessary to investigate the use and stability of a fully compressible solution before an accurate model of the solar chimney can be realised.



## CHAPTER 9. CONCLUSION

---

In this project an attempt has been made to numerically model the flow field above the collector of the solar chimney power plant, due to the outlet velocity and temperature of the chimney and the buoyancy driven flow above the collector.

In order to achieve this it is necessary to first specify certain operating conditions of the plant so that appropriate numerical boundary conditions may be formulated. In chapter 3, results obtained from a numerical study of the flow below the collector by Hedderwick (2001), have been used to formulate a set of standard operating values. This chapter also highlighted the difficulties inherent in the modelling of “free” boundaries. The numerical boundaries needed to approximate atmospheric processes far from the actual field being investigated. It was shown that there are three methods of modelling these boundaries. Of these three only two were appropriate for the modelling of the field above the collector without a cross wind, and both of these methods require knowledge of, among other variables, the pressure at these boundaries.

Due to the fact that the chimney exit is well within the atmospheric boundary layer, and the numerical model must account for variation in properties therein, it is necessary to investigate the variation of properties and the predominant processes in this region. In chapter 4, a detail of the properties of the atmospheric boundary layer and the variation of these properties was described, in particular temperature and density. Atmospheric air can be approximated as an ideal gas and can be modelled as being “dry”, without water vapour. Under this approximation it is possible to formulate equations for the pressure and temperature for an adiabatic process. This dry adiabatic lapse rate is a common approximation for atmospheric processes and is used here.

The local gradients in temperature are not always adiabatic. This leads to the definition of stability in the atmosphere. For local temperature gradients less than the DALR, the atmosphere is unstable and the reverse is true for gradients greater than the DALR.

Atmospheric stability has the effect of accelerating flow in unstable conditions and decelerating flow for stable conditions. From the definition, the adiabatic condition is known as neutrally stable. The local temperature also has an effect on buoyant processes occurring in the atmosphere, in that the forces due to buoyancy relate the density of a parcel of air to the density of the surrounding air. Coupled with this is the idea that buoyancy has an effect of increasing local atmospheric turbulence. These three processes were found to be important in atmospheric flow modelling: Compressibility of atmospheric air due to variation in density, buoyancy in the atmosphere related to atmospheric stability and the generation or destruction of turbulence in the atmosphere. In order to obtain a realistic model of the flow field above the collector and the chimney it is important that correct modelling of the above factors is realised.

Correctly modelling these processes is however dependent on the commercial CFD package utilised, because of differing assumptions made in specifying flow variables and boundary conditions. An example of this is the solution for a modified pressure in CFX 4-4. In chapter 5, the modelling of density variation, buoyancy and turbulence were investigated in the context of the available models in the package, CFX 4-4 by AEA Technology, plc. It was found that, for the default models, severe simplifications of the flow field were necessary. Due to the fact that buoyancy is modelled as a difference between the density and a *constant* reference density, in the case of compressible flows, and a constant reference temperature, in the incompressible Boussinesq approximation, it is not possible, without modification to the program, to model any kind of atmospheric stratification. The only options available, such that the flow field is solely determined by a buoyancy force caused by the temperature of the collector, are using a weakly compressible approximation with a constant ambient temperature, or an incompressible option using the Boussinesq approximation. A literature and internet study revealed a modification to the incompressible assumption, the deep Boussinesq model, which can be used to model density and temperature stratification by assuming that the flow field deviates slightly from a hydrostatic condition. In the hope of later utilising this model, the Boussinesq approximation was initially applied to a two-dimensional axisymmetric representation of the flow field. Two further assumptions were used in the development

of the two-dimensional model: Coriolis forces are negligible and a steady state is achievable.

Chapter 6 details the construction of a two-dimensional block structured, rectangular grid for the numerical solution of the flow field above the collector and the chimney of the solar chimney power plant. The standard operating conditions, as described in chapter 3, were used as input values. Variable turbulence boundary conditions were tested to see what the effect of the input turbulence has on the final solution of the field.

In order to insure that the solution is independent of the grid size for the model, a grid convergence study was undertaken. Using three successively refined grids and Richardson's extrapolation in order to find the theoretical zero grid solution, it was found that the solutions for all three refined grids could be used to obtain a correct solution. The refined grids were also compared to a solution obtained for higher order discretization schemes and good correlation was observed.

The results for the different turbulence inputs show that the turbulent viscosity obtained differs significantly between models. These results indicate that the correct specification of turbulence values is vital in the realisation of the correct flow field.

General field results for temperature indicate that the effects of the hot collector are limited to a thin region just above the glass. It would appear that the induced flow is sufficient to create a forced convection zone, whereby the hot air is convected to the chimney wall without allowing for diffusion into the atmosphere. The velocity field and streamlines are also shown in chapter 6. The flow field generally follows that obtained by Thiart (2000), in a solution obtained with the Boussinesq approximation on a body fitted grid and the incompressible assumption. The differences occur in the height at which air is drawn into the collector. Results obtained by Thiart indicate a height of approximately 240 m, while the results in the present study show a height of only 40 m. It is believed that the differences in this height are due to the different specification of turbulence on the pressure boundary.

In chapter 7, an alternate approach to the modelling of buoyancy is described. The deep Boussinesq model assumes that the flow variables of pressure, temperature and density, do not vary significantly from a hydrostatic state. This allows for the specification of a hydrostatic density profile as a function of height. Buoyancy is modelled as a deviation in the potential temperature calculated, to the potential temperature of the hydrostatic condition for a real temperature profile. In order to test the application of the deep Boussinesq model a simple 100 m by 100 m block was created with two wall boundaries whereby the temperature could be varied, in effect, placing a thermal step in the flow field. The hydrostatic profile used is that obtained for the dry adiabatic temperature profile detailed in chapter 4. Test input values used were similar to that used for the model of the solar chimney. The results obtained were compared to results from the Boussinesq approximation for that same boundary conditions. In addition to these alterations to the standard model, a buoyancy source term as a function of potential temperature is introduced as well as a diffusion term dependent on the stability of the atmosphere.

It was seen that the general flow field for both models is very similar. However, the maximum velocities for the Boussinesq approximation were three times less than those obtained for the deep Boussinesq model.

The solution of the energy equation also showed differences between the models. Diffusion of potential temperature into the flow field is much greater than for the equivalent diffusion of temperature for the standard model. For a 100 m model, the difference between specifying a constant density and a variable density is approximately 1%, and it seems unlikely that this would cause such a large difference in the velocity fields. The diffusion of both potential temperature, in the deep Boussinesq model, and temperature in the standard model are both determined by the turbulent viscosity. It was seen that the addition of the extra source terms in the  $k-\varepsilon$  model have a significant effect on the final solution for the viscosity. As mentioned in chapter 7, the source term in the  $\varepsilon$  equation, is a function of the stability of the atmosphere. A possible reason for the difference in the flow field is that the Boussinesq approximation is in fact modelling a very stable atmosphere with a temperature gradient much larger than the adiabatic, neutrally

stable, temperature profile used in the deep Boussinesq model. This would explain the difference in flow velocity. This however has not been conclusively determined.

This thesis has shown that before a reliable numerical model of the flow field around solar chimney is obtained, many questions still need to be answered. An important concept is that of the correct model to use for turbulence. It was shown that different turbulent boundary conditions for the k- $\epsilon$  model significantly change the solution for the turbulent viscosity for an atmospheric process of these proportions. What then of a completely different turbulence model?

Apsley (2003) puts things into perspective with this quote from Charles Babbage<sup>1</sup>.

“On two occasion I have been asked, ‘Pray, Mr Babbage, if you put into the machine wrong figures, will the right answers come out’. I am not able to rightly apprehend the confusion of ideas that could provoke such a question.”

---

<sup>1</sup> Charles Babbage (1791 – 1871) was an English Mathematician who is credited for inventing the first successful automatic calculator, known as the Difference Engine #1. He is also known as the grandfather of modern computing.

## REFERENCES

---

Apsley, DD (2003) Internet Resource:

<http://personalpages.umist.ac.uk/staff/david.d.apsley/lectures/comphydr/index.html>.

Batchelor, GK (1954) Heat convection and buoyancy effects in fluids, Symons memorial lecture, Source unknown, 339 – 358.

Blackadar, AK (1998) Turbulence and Diffusion in the Atmosphere, Springer Press, Corrected 2<sup>nd</sup> Printing.

Bornoff, RB and Mokhtarzadeh-Dehgahn, MR (2001) A numerical study of interacting buoyant cooling-tower plumes, Atmospheric Environment, Vol. 35, 589 – 598.

Bottema, M (1997) Turbulence closure model “constants” and the problems of “inactive” atmospheric turbulence, Journal of Wind Engineering and Industrial Aerodynamics, Vol. 67, 897 – 908.

CFX 4-4 (2001), Users manual, AEA Technology plc.

Cook, MJ and Lomas, KJ (1997) Guidance on the use of computational fluid dynamics for modelling buoyancy driven flows, Internet Resource:

<http://www.hvac.okstate.edu/pdfs/bs97/papers/P140.PDF>.

Davidson, L (1990) Second-order corrections of the k- $\epsilon$  model to account for non-isotropic effects due to buoyancy, International Journal of Heat Mass Transfer, Vol. 33, No. 12, 2599 – 2608.

Duynkerke, PG (1988) Application of the E- $\epsilon$  turbulence closure model to the neutral and stable boundary Layer, Journal of the Atmospheric Sciences, Vol. 45, No. 5, 865 –

880.

Ferziger, J H and Perić, M (2002) Computational Methods for Fluid Dynamics, 3<sup>rd</sup> Edition, Springer Publishers.

Ferziger, JH, Koseff, JR and Monismith, SG (2002) Numerical simulation of geophysical turbulence, Computers and Fluids, Vol. 31, 557 – 568.

Gannon, AJ and von Backstöm, TW (2000) Solar chimney analysis with system loss and solar collector performance, ASME Journal of Solar Energy Engineering, Vol. 122, 133 - 137.

Guyot, G (1998) Physics of the Environment and Climate, English Language Edition, John Wiley and Sons Ltd.

Hedderwick, RA (2000) Performance Evaluation of a Solar Chimney Power Plant, MSc Thesis, Department of Mechanical Engineering, University of Stellenbosch.

Hernández, J, Crespo, A and Duijm, NJ (1995) Numerical modelling of turbulent jet diffusion flames in the atmospheric surface layer, Combustion and Flame, Vol. 101, 113 – 131.

Hoffman, JE (1997) The Influence of Temperature Stratification in the Lower Atmospheric Boundary Layer on the Operating Point of a Natural Draft Dry – Cooling Tower, Department of Mechanical Engineering, University of Stellenbosch.

Houghton, EL and Carpenter, PW (1993) Aerodynamics for Engineering Students, 4<sup>th</sup> Edition, Edward Arnold, a division of Hodder Headline PLC.

Huser, A, Nilsen, PJ, and Skåtun, H (1997) Application of k- $\epsilon$  model to the stable ABL: Pollution in complex terrain, Journal of Wind Engineering and Industrial Aerodynamics,

Vol. 67&68, 425 – 436.

Jaluria, Y (1980) Natural Convection Heat and Mass Transfer, Pergamon Press.

Kays, WM and Crawford, ME (1993) Convective Heat and Mass Transfer, 3<sup>rd</sup> Edition, McGraw-Hill International.

Kim, S and Boysan, F (1999) Application of CFD to environmental flows, Journal of Wind Engineering and Industrial Aerodynamics, Vol. 81, 145 – 158.

König, CS and Mokhtarzadeh-Dehgahn, MR (2002) Numerical study of buoyant plumes from a multi-flue chimney released into an atmospheric boundary layer, Atmospheric Environment, Vol. 36, 3951 – 3962.

Kröger, DG (1998) Air-Cooled Heat Exchangers and Cooling Towers, Department of Mechanical Engineering, University of Stellenbosch.

Launder, BE (1975) On the effects of a gravitational field on the turbulent transport of heat and momentum, Journal of Fluid Mechanics, Vol. 67, part 3, 569 – 581.

Launder, BE and Spalding, DB (1972) Mathematical Models of Turbulence, Academic Press.

Lumley, JL and Panofsky, HA (1964) The Structure of Atmospheric Turbulence, John Wiley and Sons.

Mills, AF (1995) Heat and Mass Transfer, Richard D Irwin Inc, Irwin Heat Transfer Series.

Montavon, C (1998) Validation of a non-hydrostatic numerical model to simulate stratified wind fields over complex topography, Journal of Wind Engineering and Industrial Aerodynamics, Vol. 74 – 76, 273 – 282.



Nieuwstadt, FTM (1985) A model for the stationary, stable boundary layer, Turbulence and Diffusion in Stable Environments, Ed. JCR. Hunt, Clarendon Press, Oxford.

NPARC (2003) Internet Resource:

<http://www.grc.nasa.gov/WWW/wind/valid/tutorial/tutorial.html>.

Plumb, OA and Kennedy, LA (1977) Application of a k- $\epsilon$  turbulence model to natural convection from a vertical isothermal surface, Journal of Heat Transfer, February, 79 – 85.

Poreh, M (1996) Investigation of heat islands using small scale models, Atmospheric Environment, Vol. 3, No. 3, 467 – 474.

Rodi, W (1980) Turbulence Models and Their Application in Hydraulics, International Association for Hydraulic Research.

Sagaut, P (2000) Large Eddy Simulation for Incompressible Flows, An Introduction, 1<sup>st</sup> Edition, Springer Publishers, 2000.

Schlaich, J (1995) The Solar Chimney – Electricity from the sun, Edition Axel Menges, Stuttgart.

Schreüder, WA (1986) Numerical Prediction of Air Flow About and Air-Cooled Heat Exchanger, Department of Mechanical Engineering, University of Stellenbosch.

Shabbir, A and Taulbee, DB (1990) Evaluation of turbulence models for predicting buoyant flows, Journal of heat transfer, Vol.112, 945 – 951.

Sinai, YL (2000) Exploratory CFD modelling of pool fire instabilities without cross-wind, Fire Safety Journal, Vol. 35, 51 – 61.

Tecplot 7-5 (1998) Tecplot User's Manual, Amtec Engineering, Inc.

Thiart, GD (2000) Course notes for Numerical Fluid Dynamics 844, Department of Mechanical Engineering, University of Stellenbosch.

Thiart, GD (2002) Preliminary CFD analysis of a solar chimney, HEFAT 2002, 1<sup>st</sup> International Conference on Heat Transfer, Fluid Mechanics and Thermodynamics, April 8 – 10, Kruger Park, South Africa.

Van Stijn, TL and Nieuwstadt, FTM (1986) Large eddy simulation of atmospheric turbulence, Notes on Numerical Methods in Fluid Dynamics, Ed. D Rues and W Kordulla, Vieweg Publishers.

White, FM (1991) Viscous Fluid Flow, 2<sup>nd</sup> Edition, McGraw-Hill International Editions.

White, FM (1994) Fluid Mechanics, 4<sup>th</sup> Edition, McGraw-Hill International Editions.

Wilcox, DC (1994) Turbulence Modeling for CFD, DCW Industries, Inc.

Wilks, N (2001) Global Warming will be Greater, Says UN, Professional Engineering, Vol.14, No. 2, January.

Witt, P (1995) Notes on post-processing CFDS-Flow3D results and the use of FL3D2TEC, Version 1, Swinburne University of Technology.

Yan, Z and Holmstedt, G (1999) A two-equation turbulence model and its application to a buoyant diffusion flame, International Journal of Heat and Mass Transfer, Vol. 42, 1305 – 1315.



## APPENDIX A. ADIABATIC LAPSE RATE

---

## A.1. Fully Compressible DALR

Kröger (1998). Considering a small parcel of air moving in an atmospheric pressure field, in an adiabatic process.

The pressure gradient in a gravity field is given by:

$$\frac{dp}{dz} = -\rho g \quad (\text{A-1})$$

For an isentropic process, i.e. adiabatic and reversible, the relationship below holds.

$$\frac{p}{\rho^\gamma} = \text{const.} \quad (\text{A-2})$$

Air may be assumed to behave as a ideal gas at atmospheric temperatures and pressure; the ideal gas law gives the relationship between temperature, density and pressure.

$$\rho = \frac{p}{RT} \quad (\text{A-3})$$

Substituting equation A-3 into A-2 and differentiating with respect to altitude gives the following.

$$\frac{(1-\gamma)}{\gamma} \frac{dp}{p} + \frac{1}{T} \frac{dT}{dz} = 0 \quad (\text{A-4})$$

Replacing  $dp/dz$  with  $-\rho g$ , and substituting the ideal gas relationship for the pressure term in A-4 one can find as a temperature gradient:

$$\frac{dT}{dz} = \frac{-g(\gamma-1)}{\gamma R} \quad (\text{A-5})$$

Acceleration due to gravity,  $g$ , can be considered constant due to negligible changes with respect to altitude and latitude.

For dry air, with constant  $c_p$ , and  $c_v$  values.

$$\gamma = \frac{c_p}{c_v} = 1.4 \text{ And } R = 287.08 \text{ J kg K}^{-1}, \text{ for } g = 9.80 \text{ m s}^{-2}$$

$$\frac{dT}{dz} = -0.00975 \text{ Km}^{-1} \quad (\text{A-6})$$

This temperature gradient is known as the dry adiabatic lapse rate, DALR.

In order to find a temperature profile as a function of height it is necessary to integrate A-6 with respect to height, to find.

$$T = T_1 - \frac{g(\gamma - 1).z}{(\gamma R)} \quad (\text{A-7})$$

For dry air, A-7 reduces to:

$$T = T_1 - 0.00975z \quad (\text{A-8})$$

In order to find an adiabatic pressure profile for an isentropic atmosphere it is necessary to integrate A-1 with respect to height after making the ideal gas substitution for the density term, A-3

$$\frac{dp}{p} = \frac{-gdz}{RT} \quad (\text{A-9})$$

Substituting A-7 into A-9 and integrating gives:

$$p = p_1 \left[ 1 - \frac{g(\gamma - 1)z}{(\gamma RT_1)} \right]^{\gamma/(\gamma-1)} \quad (\text{A-10})$$

For dry air, A-10 reduces to:

$$p = p_1 \left( 1 - \frac{0.00975z}{T_1} \right)^{3.5} \quad (\text{A-11})$$

The equations for the temperature and pressure profiles can then be used to calculate air density at any altitude.

## A.2. Weakly Compressible Adiabatic Temperature Profile

Weakly compressible equation of state:

$$\rho = \frac{P_{ref}}{RT} \quad (\text{A-12})$$

Pressure gradient in a gravitational field:

$$\frac{dp}{dz} = -\rho g \quad (\text{A-13})$$

For an isentropic process:

$$\frac{p}{\rho^\gamma} = Const \quad (\text{A-14})$$

Substituting the equation of state into the above equation gives:

$$\frac{pT^\gamma}{p_{REF}^\gamma} R^\gamma = Const \quad (A-15)$$

Applying the chain rule and differentiating with respect to z, height, gives:

$$\frac{p\gamma T^{\gamma-1} R^\gamma}{p_{REF}^\gamma} \frac{dT}{dz} + \frac{T^\gamma R^\gamma}{p_{REF}^\gamma} \frac{dp}{dz} = 0 \quad (A-16)$$

Dividing by the constant,  $\frac{T^\gamma R^\gamma}{p_{REF}^\gamma}$ , gives the following equation:

$$\frac{\gamma}{T} \frac{dT}{dz} + \frac{1}{p} \frac{dp}{dz} = 0 \quad (A-17)$$

Combining like terms:

$$\frac{1}{p} \frac{dp}{dz} = -\gamma \frac{1}{T} \frac{dT}{dz} \quad (A-18)$$

And integrating both sides with respect to z, gives the following relationship between temperature and pressure:

$$T = T_o \left( \frac{p_o}{p} \right)^{1/\gamma} \quad (A-19)$$

In order to find the correct pressure term, substitute the equation of state into the pressure gradient equation and the above temperature profile into the resulting equation to give:

$$\frac{dp}{dz} = C_1 p^{1/\gamma} \quad (A-20)$$



where  $C_1$  is:

$$C_1 = -\frac{P_{REF} g}{RT_o p_o^{1/\gamma}} \quad (A-21)$$

Collecting like terms and integrating with respect to height gives:

$$p = \left[ \left( 1 - \frac{1}{\gamma} \right) C_1 z + p_o^{(1-1/\gamma)} \right]^{\gamma/(\gamma-1)} \quad (A-22)$$

## APPENDIX B. CFD BASICS

---

## B.1. Introduction

Computational Fluid Dynamics (CFD) is the field of engineering and science, which deals with the numerical solution of discretized equations for the governing partial differential equations of fluid dynamics. These are known as the Navier-Stokes equations. In complete form, the Navier-Stokes equations are non-linear partial differential equations, which are very difficult to solve analytically. The governing equations, as well as the initial and boundary conditions, are approximated by means of a discretization method. There are a number of discretization techniques that have been developed in order to solve the N-S equations. Finite difference methods (FDM), finite element methods (FEM) and finite volume methods (FVM) are the most widely used. CFX 4-4 (2001) solves the basic conservation equations of mass, momentum and energy using the finite volume method. Descriptions of these methods are available in most textbooks on the subject and only the FVM will be discussed here.

## B.2. Governing Equations

Fluid flows are governed by three basic physical principles, namely that mass is conserved, momentum is conserved and that energy is conserved. The resulting governing equations are mathematical descriptions of these three principles. The system includes five equations, namely three momentum equations, the energy equation and the continuity equation, and seven variables,  $\rho$ ,  $p$ ,  $u$ ,  $v$ ,  $w$ ,  $T$ ,  $h$ . In order to close the system two additional equations are necessary, an equation of state, which relates density to pressure and temperature, and an equation relating the static enthalpy to temperature and pressure.

$$\rho = \rho(p, T) \tag{B-1}$$

$$h = h(p, T) \tag{B-2}$$

The derivations of the laminar governing equations of motion are described in numerous textbooks on the subject and only the relevant derived partial differential equations are

displayed here, with a description of the terms. These are the compressible continuity, momentum and energy equations, known as the Navier-Stokes equations. Due to the complex nature of turbulent flows, turbulence models must be used to describe these flows. The equations given below are in index notation, CFX 4-4 (2001).

$$\frac{\partial \rho}{\partial t} + \frac{\partial}{\partial x^i} (\rho U^i) = 0 \quad \text{Continuity} \quad (\text{B-3})$$

$$\frac{\partial}{\partial t} \rho U^k + \frac{\partial}{\partial x^i} (\rho U^i U^k) = -B^k + \frac{\partial \sigma^{ik}}{\partial x^i} \quad \text{Momentum} \quad (\text{B-4})$$

The terms on the left hand side of the momentum equation represent the transient component and the transport of momentum across a control volume respectively. The first term on the right hand side comprises of the external body forces acting on a control volume, these are typically forces due to gravity, rotational forces and porous resistances. Divergence of the stress tensor is represented by the last term on the right hand side of the momentum equation, where:

$$\sigma^{ij} = -p \delta^{ij} + \left( \zeta - \frac{2}{3} \mu \right) \frac{\partial U^k}{\partial x^k} \delta^{ij} + \mu \left( \frac{\partial U^j}{\partial x^i} + \frac{\partial U^i}{\partial x^j} \right) \quad (\text{B-5})$$

This is a combination of normal forces and shear stresses on the control volume.

$$\frac{\partial}{\partial t} \rho H + \frac{\partial}{\partial x^i} \left( \rho U^i H - \lambda \frac{\partial T}{\partial x^i} \right) = \frac{\partial p}{\partial t} \quad \text{Energy} \quad (\text{B-6})$$

### B.2.1. Scalar advection-diffusion equation

All the above equations can be written as scalar advection – diffusion equations.  $\Gamma$  is a diffusion co-efficient and  $S$  is a source term representing the generation or destruction of  $\Phi$ .

$$\frac{\partial}{\partial t} \rho \Phi + \frac{\partial}{\partial x^i} \left( \rho U^i \Phi - \Gamma \frac{\partial \Phi}{\partial x^i} \right) = S \quad (\text{B-7})$$

### B.3. Discretization of differential equations

In order to make the governing equations amenable to a numerical solution the transport equations are discretized. It is these discrete equations, which are solved for the final flow field. Gradient diffusion is almost always discretized using central differencing. There are many schemes available for discretization of the advection terms; some of these are discussed below. The naming convention for a one dimensional control volume is demonstrated in the figure below.

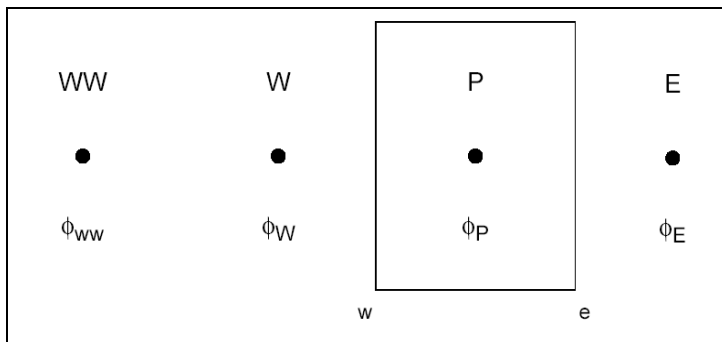


Figure B-1: One-dimensional control volume - CFX 4-4(2001)

#### B.3.1. Advection schemes

##### *Central difference*

Central differencing amounts the using a linear approximation between nodal values for the face value of  $\phi_i$ .

$$\phi_w = \frac{1}{2}(\phi_W + \phi_P) \quad (\text{B-8})$$

Central differencing is second order accurate, CFX 4-4 (2001), but is rarely used because it often requires very small under-relaxation factors and sometimes gives non-physical solutions.

### ***Upwind difference***

The value of  $\phi_i$  at the interface,  $\phi_w$ , is taken as the value of  $\phi$  at the upwind node, for flow from left to right of the control volume, this value would be  $\phi_w$ .

### ***Hybrid difference***

The hybrid differencing scheme is based on piecewise linear approximation to the exponential scheme. Central differencing is used if the Péclet number, convection coefficient divided by the diffusion co-efficient, is less than 2 and upwind differencing is the Péclet number is greater than 2.

$$Pe = \frac{\rho u \Delta x}{\Gamma} \approx \frac{\text{advection}}{\text{diffusion}} \quad (\text{B-9})$$

### ***Quadratic interpolation for convective kinematics (QUICK)***

The QUICK advection scheme fits a quadratic polynomial through three control volume nodes in order to extrapolate values of the variables at the downstream face. The nodes on either side of the interface are used, as well as a further upwind node. For  $u > 0$ , the values at the interfaces are calculated as, Apsley (2002):

$$\phi_e = -\frac{1}{8}\phi_w + \frac{3}{4}\phi_P + \frac{3}{8}\phi_E \quad (\text{B-10})$$

$$\phi_w = -\frac{1}{8}\phi_{WW} + \frac{3}{4}\phi_W + \frac{3}{8}\phi_P \quad (\text{B-11})$$

The scheme is third order accurate and conservative.

### **B.3.2. Under Relaxation Factors**

Under relaxation factors are used for a number of reasons in the solution process. The amount, by which a variable changes for each iteration, can be reduced. The equation for the solution with under-relaxation factors is given below:

$$\phi = \phi_{old} + \lambda \Delta\phi \quad (\text{B-12})$$

This allows for a reduction of instabilities associated with the non-linearity of the governing equations, CFX 4-4 (2001). Another convenience of employing under-relaxation factors is that the linear algebraic solver is presented with an easier problem to solve.

### **B.4. Pressure Velocity Coupling**

It can be seen in the governing equations described above that a source term in the momentum equations is described in terms of a pressure gradient term. However the static pressure field is unknown before hand and no differential equation has been defined to allow for the solution of the pressure field. The default method, in CFX 4-4 and in many CFD applications, for calculating the pressure field from a variation in the velocity field is the SIMPLE method, or the Semi-Implicit Method for Pressure-Linked Equations. This involves guessing an approximate pressure and velocity field, and then solving the momentum equations based on the guessed pressure field. A pressure correction equation based on corrections needed to the approximate field is solved and these corrections are then added to the guessed solution for the flow field. The corrected pressure field is then used to once again solve the momentum equation in order to obtain correct values for the velocity field. Thiart (2000).

The derivation of the SIMPLE algorithm is described in detail in most books on CFD, for example Ferziger and Perić (2002), and is only briefly described above for the sake of completeness.

## **B.5. Components of a CFD Code**

All CFD codes comprise of at least 3 elements; the pre-processor, the solver and the post-processor. In the pre-processor model information in the form of geometric information and modelling assumptions, such as initial and boundary conditions, and fluid properties are stated. The solver contains the algorithms needed to solve the governing equations, while the post-processor allows for the graphic representation of the results from the solver. In CFX 4-4 the elements are CFX -Build and CFX -Setup, CFX -Solver and CFX -Post respectively. Other programs may be used to represent the data from the solver. In most of the cases in this thesis Tecplot, by Amtec, has been used.

### **B.5.1. CFX -Build and CFX -Setup**

The pre-processor of CFX 4-4 consists of two main elements, CFX -Build and CFX -Setup. CFX -Build is used to input the specific geometric information of the problem and CFX -Setup constitutes the front end Solver interface. The products of these two programs are a geometry file from Build and a command file from Setup.

CFX -Build is based on the MSC/PATRAN product, which has been specifically adapted for use with the CFX 4-4 solver. Build is an interactive geometric modeller and allows for the creation of multi-block geometries for input into the CFX -Solver.

Apart from the creation of geometric information, the specification of boundary conditions and domain discretization in the form of nodal seeding is also achieved in Build. Most geometries can be created in Build, for very complex geometries it is also possible to import geometry files created by most CAD packages including IGES, CATIA and Pro Engineer files.



### **B.5.2. Model Geometry**

CFX 4-4 uses a local co-ordinate system to permit the use of multi-block grid structures. Model geometries are made up of several blocks that are “glued together” in such a way that neighbouring cells meet on whole faces. Node seeds are placed on individual blocks. The code allows for uniform and non-uniform grid, this is beneficial for grid refinement in areas where large gradients in the flow variables are expected.

#### ***Grid Generation***

CFX 4-4 offers two options for grid generation. Simple models can be achieved through the use of rectangular grids, or more complex models may be achieved through body fitting. The Rhie and Chow algorithm is used in the application of body fitting to arbitrary two or three-dimensional geometries, CFX 4-4 (2001). This allows for the transformation of a complex physical geometry into a simple rectangular flow domain in computational space. Details can be found in CFX 4-4 (2001) and other texts on CFD.

#### ***Mesh Quality***

Mesh quality describes the deviation of individual control volumes of a particular model from idealised cubic control volumes. CFX – Build is able to calculate values for a particular geometry of: orthogonality, grid expansion, cell volume, skew, twist and taper.

### **B.5.3. Boundary Conditions**

#### ***Inlet***

CFX 4-4 *INLET boundaries* allow for a Dirichlet condition to be specified for the required inlet variables of the flow. It is possible to specify multiple inlets into the computational domain. The necessary inlet variables may either be specified using the command file, or by means of the user FORTRAN sub-routine USRBCS. The command file is used for real number magnitudes of the appropriate variables. In this respect only block velocity profiles

can be used, if specified in this way. The same applied for turbulence values and temperature profiles. In order for specific velocity profiles to be input, the USRBCS routine is used.

### ***Outlet***

In order to specify mass exiting the flow domain, two options are available. These are *OUTLET* boundaries and *PRESSURE* boundaries. At the outlet, the mass flow is specified explicitly in  $\text{kg s}^{-1}$  or in terms of the percentage of the sum of the mass calculated from the inlets. This is relevant when there are multiple outlet boundaries, as in the case of this model. For incompressible flow it is necessary that the mass flow be specified to machine accuracy if the actual mass flow is specified and that the sum of the percentages for the latter case is equal to one. For compressible flow, this is not necessary. This allows for explicit specification of a mass percentage from pressure boundaries.

It is possible that mass will return into the flow domain from an outlet boundary. This necessitates the specification of inflow values for all parameters. If these values are not specified, default ambient value properties will be used. These may or may not be valid for a particular model and must thus be specified.

### ***Pressure***

For outlet conditions where the velocity profile or mass flow rate is unknown, a pressure boundary can be used if the pressure at that outlet is known. CFX – Solver uses a modified pressure in calculating the flow field. This is the pressure based on the total pressure with modifications based on the reference pressure; the hydrostatic pressure formulated from the reference density and pressure changes due to turbulence quantities. The pressure, which is specified at the boundary condition, is equal to the modified pressure. Other variables, temperature and turbulent kinetic energy and dissipation, are specified explicitly.

For all models, the first modification to the pressure is the removal of a reference pressure value. The default reference pressure is 101300 Pa. This is done in order to reduce errors resulting from subtracting large numbers.

$$P = P_{abs} - P_{ref} \quad (\text{B-13})$$

The second modification is to obtain the mechanical pressure, see White (1991). This subtracts the sum of the bulk viscosity and the 2/3 of the molecular viscosity. This modification is only valid for compressible flows.

$$p' = p + \left(\frac{2}{3}\mu - \zeta\right)\nabla U \quad (\text{B-14})$$

The third modification to the pressure is the removal of the hydrostatic component. This is only applicable when buoyant flows are being modelled.

$$p'' = p' - \rho_o(\vec{g}x) \quad (\text{B-15})$$

The final modification to the pressure field is to account for turbulence.

$$p''' = p'' + \frac{2}{3}\rho k \quad (\text{B-16})$$

As in *OUTLET* boundaries, re-circulation of the flow through pressure boundaries is possible. In the case of flow into the domain, discrete values for pressure and temperature are used. For flow out of the domain, the final value for pressure and temperature at the boundary nodes are extrapolated from values at the nodes, one control volume from the wall.

### ***Wall***

Walls occur on the domain boundary adjacent to fluid cells where no other boundaries have been specified. They are used to set boundary conditions on velocity, temperature and other scalars. The default is to have zero velocity, zero heat flux and zero flux of other

transported values. Wall boundaries are also used to implement special treatments for the near wall boundary layer.

### ***Symmetry***

The boundary conditions of symmetry planes are simply that all variables are mathematically symmetrical. This means that there is zero diffusion across the boundary, except the component of velocity normal to the boundary and the components of the Reynolds shear stress and Reynolds flux involving the normal velocity, which are all anti-symmetric.

### ***Command File***

CFX – Setup is an interactive program used to generate and edit CFX 4-4 command files. All of the problem specifications are generated in the command file including, fluid properties, modelling assumptions, discretization schemes and solver data. Varying levels of complexity of the problem are allowed for. In the event of any absence of user specified information default values are used.

The addition of USER FORTRAN sub-routines and additional scalars is also specified using the command file.

### **B.5.4. CFX – Solver**

CFX – Solver solves the discretized representation of the particular problem, based on the input parameters from CFX – Setup and the geometry information contained in the output files from CFX – Build. Only a few output facilities for the solver are available, these include an error file if an error occurs due to incorrect problem specifications for the command file or programming errors associated with the FORTRAN sub-routines. The main output file is the dump file, which contains the final values of the variables for the converged solution and geometric information. It is also possible to obtain information for line plots of residuals.

### ***Residual Line Graph Information***

The residuals of a transport equation are the differences between the source terms and the diffusion-advection terms in the transport equation. CFX 4-4 offers continuous information on the state of the residuals during the solution of any flow problem. These values are output to the linegraph module of CFX 4-4. The residuals, in the case of the linegraph values, represent the sum of all the absolute values of the errors for the flow field, summed over all the control volumes. An average residual value can be obtained by dividing the residual value by the number of control volumes in order to investigate the magnitude of a particular error on a variable.

$$R_{ave} = \frac{R}{N} \quad (B-17)$$

### **B.5.5. CFX -Analyse**

Post processing creates a graphical representation of the solutions of the discretized Navier-Stokes equations. Post-processing programs utilise the output files from the solver. In some cases it is necessary to alter the format of the information in order to be read by a selected post-processor. A number of post-processors are available in the CFX 4-4 package.

CFX – Analyse is a software tool for post-processing of CFX 4-4 results. It is based on the CFX – Tascflow post-processor. As with most post-processors it allows for specification of planes or solids where necessary information is required. A wide range of plotting options are available, including contour plots of specified variables, animations for transient flow problems and vector plots.

### **B.5.6. Tecplot**

Tecplot 7-5 is a commercially available post-processing and data visualisation program by AMTEC, Tecplot 7-5 (1998). The input format for data files can be either binary or ASCII files. Tecplot 7-5 demands a particular format for the representation of the data files, for this reason it is necessary to manipulate CFX 4-4 dump files. The application program, flow3d2tec, was used. This program, written as part of a PhD by Peter Witt, was obtained through private communication, Witt (1995)

## APPENDIX C. TURBULENCE MODELLING

---

## C.1. Turbulence Models

White (1991) has separated the different turbulence treatments into 6 main categories.

- *Zero-equation models*: The eddy viscosity is directly applied to the momentum equation in the form of a mixing-length, analogous to the eddy-viscosity.
- *One equation*: Usually involves modelling of the eddy-viscosity in terms of the turbulent kinetic energy term.
- *Two equations*: Where both the turbulence kinetic energy ( $k$ ) and a model of turbulence dissipation ( $\epsilon$ ), some turbulence length scale ( $L$ ), or a scale of vorticity fluctuations ( $\omega$ ).
- *Reynolds stress models*: Involves the modelling of a differential equation of the tensor, which represents the turbulent stresses, Wilcox (1994).
- *Almost model free*: Large eddy simulation models.
- *Model Free*: Direct numerical simulation of turbulence.

The above models vary in complexity, with varying degrees of accuracy and applicability for each of them. Zero-equation, also known as algebraic, models are the simplest models for turbulent flows. They do, however, only work well for the flows for which the model has been “fine tuned”, Wilcox (1994). Similarly, one-equation models require new length scales for each different application. The only advantage of using a one-equation model over a two-equation model would be a numerical consideration based on the added stability of solving for only a single parameter when describing turbulence.

Two-equation models are the most popular and most widely used models, specifically the  $k$ - $\epsilon$  model. Despite its robustness, the  $k$ - $\epsilon$  model has inherent disadvantages due to the underlying principle of isotropy, and has been found to give inaccurate results for flows dominated by strong anisotropy and non-equilibrium effects. The  $k$ - $\epsilon$  model also predicts poorly for bluff body and re-circulation zones and tends to over predict  $k$ , and in this way the turbulent viscosity at these zones, Kim and Boysen (1999). This overproduction of the turbulent kinetic energy is then convected downstream where further errors result.



Similar to the zero and one-equation models, fine tuning of the model constants for different applications is also necessary, but to a lesser extent. In the modelling of turbulence with respect to the solar chimney power plant, a modified, buoyancy extended,  $k$ - $\epsilon$  model has been used. The standard buoyancy model is widely used due to its simplicity, however it tends to seriously under-predict the spreading rate of vertical buoyancy jets and over-predict the entrainment of horizontal stably-stratified flow, Yan and Holmstedt (1999). A brief description of the model as well as the determination of the model constant for atmospheric flow phenomena is given in the following sections.

Before continuing on to a description of the  $k$ - $\epsilon$  model, an introduction to Large Eddy Simulation, LES, is given. LES models for turbulence are believed to be the best for modelling high Reynolds number atmospheric phenomena, Sagaut (2000).

In a LES simulation the large eddies are numerically computed using the complete Navier-Stokes equations and the conservation of energy equations, without simplifications. The underlying premise of this is that the larger eddies are directly influenced by the boundary conditions and must therefore be computed. In contrast, the smaller eddies are nearly isotropic and are more amenable to modelling. Initially a filtering approach is used in order to decompose the flow into large-scale motions and sub-grid scales, the complexity of the specific filter depends on the nature and complexity of the problem at hand.

According to Sagaut (2000), there are three different sub-grid viscosity model types.

- Models based on resolved scales evaluate the viscosity using global quantities of the resolved scales.
- Models based on the energy at the cut-off calculate the sub-grid viscosity from the highest resolved frequency.
- Models based on the sub-grid scales directly model sub-grid viscosity from information directly related to the size of the grid.

Large Eddy Simulation requires far more computational resources than Reynolds averaged Navier-Stokes equations (RANS), and thus is beyond the scope of this project. It has

however been found to accurately predict turbulence quantities in atmospheric flows and is believed to be the optimal model for such flow processes, Ferziger et al (2002).

## C.2. Reynolds averaged Navier-Stokes Equations

### *Time averaging*

The starting point for all turbulence models is the decomposition of flow parameters into a mean value and a fluctuating component. An averaging procedure is then used in order to average out the high frequency unsteadiness associated with the turbulent processes. For statistically steady process, Thiart (2000), time averaging can be used such that:

$$\phi(\mathbf{x}, t) = \bar{\phi}(\mathbf{x}) + \phi'(\mathbf{x}, t) \quad (\text{C-1})$$

$$\bar{\phi}(\mathbf{x}) = \lim_{\Delta t \rightarrow \infty} \frac{1}{\Delta t} \int_0^{\Delta t} \phi(\mathbf{x}, t) dt \quad (\text{C-2})$$

The limit of  $\Delta t$  tends to a value larger than any turbulent fluctuations. The averaging of properties of flow processes is known as Reynolds averaging.

### *Reynolds stresses and turbulent scalar fluxes*

Reynolds averaging of the Navier-Stokes equation, RANSE, leads to the existence of two terms, which cannot be uniquely represented in terms of the mean quantities. Thiart (2000). These are:

$$\begin{aligned} - \overline{\rho u'_i u'_j} & \quad \text{Reynolds stress tensor} \\ - \overline{\rho u'_i \phi'} & \quad \text{Turbulent scalar flux} \end{aligned}$$

The existence of these terms in the governing equations means that modelling is needed in order to obtain closure, the number of variables must be matched by the number of

equations. Different turbulence models obtain closure of the RANS equations following different flow assumptions. Wilcox (1994).

### ***Eddy viscosity***

The Boussinesq eddy-viscosity concept assumes that turbulent stresses are proportional to the mean velocity gradients of the flow and that the turbulent diffusion mimics the molecular diffusion-gradient process. Rodi (1980) gives the following expression:

$$-\overline{\rho u'_i u'_j} = \mu_T \left( \frac{\partial U_i}{\partial x_j} + \frac{\partial U_j}{\partial x_i} \right) - \frac{2}{3} \rho k \delta_{ij} \quad (\text{C-3})$$

Where  $\mu_T$  is the turbulent viscosity. The second term on the right hand side of the equation makes the equation relevant to normal stresses, where  $\delta$  is the Kronecker delta and is zero unless  $i = j$ . Wilcox (1994) offers comments on the validity of assuming the analogy between molecular diffusion and turbulent diffusion. Most turbulence models are however based on the eddy-viscosity concept. It is important to note that the turbulent viscosity is not a fluid property but rather a property of the flow. The implication of a scalar eddy-viscosity is consistent with the assumption of isotropic turbulence, Schreüder (1986).

### ***Eddy diffusivity***

Analogous to the eddy-viscosity, turbulent heat or mass transport is assumed to relate to gradients of the property, Rodi (1980).

$$-\overline{\rho u'_i \phi'} = \Gamma_T \frac{\partial \Phi}{\partial x_i} \quad (\text{C-4})$$

The  $\Gamma_T$  term is known as the turbulent diffusivity of heat or mass; this is, similar to eddy-viscosity, a property of the flow rather than a property of the fluid. The relationship

between eddy-viscosity and eddy-diffusivity can be shown through the turbulent Prandtl number:

$$\sigma_T = \frac{\mu_T}{\Gamma_T} \quad (C-5)$$

This value varies little across any flow and from flow to flow, Rodi (1980), buoyancy and streamline curvature however can affect the value of  $\sigma_T$ .

### C.3. k- $\epsilon$ Turbulence model

The k- $\epsilon$  model is known as a *turbulence energy equation* model, Wilcox (1994), in that the model is based on the equation for turbulence kinetic energy per unit mass k, where:

$$k = \frac{1}{2}(\overline{u'u'} + \overline{v'v'} + \overline{w'w'}) \quad (C-6)$$

The model retains the eddy-viscosity approximation while providing an equation for the turbulent length scale in order to obtain closure. This is done by formulating an equation for  $\epsilon$ , the dissipation of k per unit mass, Wilcox (1994). Derivation of the model, see Thiart (2000), Wilcox (1994), leads to the following equations for the standard k- $\epsilon$  model::

$$\mu_T = \rho C_\mu k^2 / \epsilon \quad \text{Eddy Viscosity} \quad (C-7)$$

$$\mu_{\text{eff}} = \mu_T + \mu \quad \text{Effective Viscosity} \quad (C-8)$$

Partial differential equations are derived in order to solve for the generation of k, the turbulence kinetic energy and  $\epsilon$ , the dissipation rate of turbulence, these are given below, Rodi (1980):

$$\frac{\partial}{\partial t}(\rho k) + \frac{\partial(\rho \bar{u}_j k)}{\partial x_j} = \frac{\partial}{\partial x_j} \left( \frac{\mu_T}{\sigma_k} \frac{\partial k}{\partial x_j} \right) + \rho(P + G - \varepsilon) \quad (\text{C-9})$$

$$\begin{aligned} \frac{\partial}{\partial t}(\rho \varepsilon) + \frac{\partial(\rho \bar{u}_j \varepsilon)}{\partial x_j} = \\ \frac{\partial}{\partial x_j} \left( \frac{\mu_T}{\sigma_\varepsilon} \frac{\partial \varepsilon}{\partial x_j} \right) + C_{\varepsilon 1} \rho \frac{\varepsilon}{k} (P + G) (1 + C_{\varepsilon 3} R_f') - C_{\varepsilon 2} \rho \frac{\varepsilon^2}{k} \end{aligned} \quad (\text{C-10})$$

Where P is the shear production modelled as:

$$P = \nu_T \left( \frac{\partial \bar{u}_i}{\partial x_j} + \frac{\partial \bar{u}_j}{\partial x_i} \right) \frac{\partial \bar{u}_i}{\partial x_j} \quad (\text{C-11})$$

And G is production due to body forces, for buoyant production, this becomes:

$$G = -\beta \left( \frac{\nu_T}{\sigma_T} \right) \left( \frac{\partial \bar{T}}{\partial x_i} \right) g \quad (\text{C-12})$$

$\beta$  is thermal expansion co-efficient defined as:

$$\beta = - \left( \frac{1}{\rho} \right) \left( \frac{\partial \rho}{\partial T} \right) \quad (\text{C-13})$$

And g is the acceleration due to gravity.

### ***Evaluation of model constants***

It can be seen that a number of empirical constants occur in the differential equations for k and  $\varepsilon$ . For the calculation of  $C_{\varepsilon 2}$  the fact that for grid turbulence the diffusion and

production terms, P+G, tend to zero, Rodi (1980), is calculated from measured rates of decay of k and found to lie in the range of 1.8 to 2.0. Measurements in local shear layers have been used to determine the value of  $C_\mu$  to be approximately 0.09. Similarly  $C_{\varepsilon 1}$  has been calculated from the assumption that in the near wall region P is approximately equal to  $\varepsilon$ . The values suggested by Rodi (1980) are tabulated below:

Table C-1: Standard k- $\varepsilon$  model constants

$C_\mu$	$C_{\varepsilon 1}$	$C_{\varepsilon 2}$	$\sigma_k$	$\sigma_\varepsilon$
0.09	1.44	1.92	1.0	1.3

The constants should not be considered universally applicable to all flow situations, Rodi (1980), and even for relatively simple flows these constants might require different values or be specified as functions of other flow variables.

### ***Relating length scales and intensity to k- $\varepsilon$***

The specification of turbulence values for a particular problem is based on the assumption for the amount of turbulence in a particular configuration, the turbulence intensity, and an assumption as the dissipation of that turbulence as a characteristic length. These can be related to k and  $\varepsilon$  values using the following equations, CFX 4-4 (2001)

$$k_{inl} = 1.5(i.u_{inl})^2 \quad (C-14)$$

$$\varepsilon_{inl} = \frac{k_{inl}^{3/2}}{0.3D} \quad (C-15)$$

### ***Wall treatment***

Boundary conditions for turbulence are very important to specify correctly, as it is near the wall that the effects of turbulence are usually the greatest, Schreüder (1986). There are two general methods of approaching wall boundary conditions in the k- $\varepsilon$  model. The first is the

used in the low Reynolds number k-ε model where a fine numerical grid is used at the boundaries. The second method is to specify wall functions for turbulence quantities near the wall. This is done in order to avoid the need for a fine mesh near the wall, Montavon (1998). The initial assumption is that the velocity in the control volume adjacent to the ground; is parallel to the ground. For a fully developed boundary layer, the velocity profile in the boundary layer can be approximated by the following functions, White (1991):

$$u^+ = z^+ \quad \text{When } z^+ < z_0^+ \quad \text{The viscous sub-layer.} \quad (\text{C-16})$$

$$u^+ = \frac{1}{\kappa} \ln(Ez^+) \quad \text{When } z^+ > z_0^+ \quad \text{Logarithmic region} \quad (\text{C-17})$$

Above,  $z^+$  and  $u^+$ , are dimensionless length and velocity functions, defined below:

$$z^+ = \frac{z u_*}{\nu} \quad (\text{C-18})$$

$$u^+ = \frac{u}{u_*} \quad (\text{C-19})$$

The friction velocity,  $u_*$ , is the friction velocity defined as:

$$u_* = \sqrt{\frac{\tau_0}{\rho}} \quad (\text{C-20})$$

In order for the velocity profiles to be continuous at the interface between the viscous sub-layer and the logarithmic layer, it is necessary that the dimensionless length at the interface be defined as:

$$z_0^+ = \frac{1}{\kappa} \ln(Ez_0^+) \quad (\text{C-21})$$

The default values for E and  $z_0^+$  are 9.793 and 11.225 respectively.

The second assumption is that the production and dissipation for k are equal close to the wall. In this assumption of equilibrium close to the wall the following equation is obtained for  $\varepsilon$ , Montavon (1998):

$$\rho\varepsilon = \mu \left( \frac{\partial \bar{u}}{\partial z} \right)^2 \quad (\text{C-22})$$

The shear stress at the wall can then be found from the turbulent viscosity equation and the shear stress relationship:

$$\mu_T = \rho C_\mu \frac{k^2}{\varepsilon} \quad (\text{C-23})$$

$$|\tau| = \mu \left( \frac{\partial u}{\partial z} \right) \quad (\text{C-24})$$

Using the above relationships, the wall shear stress is calculated using the following equation:

$$\tau_w = \rho C_\mu^{1/2} k \quad (\text{C-25})$$

Whereby the diffusion at the wall node can be calculated as:

$$\varepsilon = C_\mu^{3/4} k^{3/2} \frac{1}{\kappa z} \quad (\text{C-26})$$

With the above parameterisation of  $\varepsilon$  the turbulent kinetic energy equation is solved for k at the node adjacent to the wall, using flow variables from the interior of the flow to solve



for the source terms in the equation. From the solution for  $k$ , the wall shear stress can be calculated.

In the first node adjacent to the wall, within the wall function approximation, the perpendicular component of the velocity is taken as zero and the parallel component of the velocity is proportional to the wall stress,  $\tau_w$ , for the two-dimensional case:

$$u = \frac{\tau_w}{T_M} \quad (C-27)$$

Where  $T_M$  is the turbulent wall multiplier given by the following functions:

$$T_M = \frac{\mu}{z} \quad \text{For } z^+ < z_0^+ \quad (C-28)$$

$$T_M = \frac{\rho^{1/2} \tau^{1/2} \kappa}{\ln(Ez^+)} \quad \text{For } z^+ > z_0^+ \quad (C-29)$$

A similar approach is used to model the behaviour of the temperature profiles and additional scalars, such as the potential temperature, CFX Users manual.

$$\phi^+ = \text{Pr}_\phi z^+ \quad \text{When } z^+ < z_0^+ \quad (C-30)$$

$$u^+ = \frac{\sigma_\phi}{\kappa} \ln(E_\phi z^+) \quad \text{When } z^+ > z_0^+ \quad (C-31)$$

$\text{Pr}$  is the Prandtl number defined as:

$$\text{Pr}_\phi = \frac{\mu}{\Gamma_\phi} \quad (C-32)$$

And:

$$\phi^+ = \frac{(\rho \cdot \tau_w)^{1/2}}{J_\phi} (\phi_w - \phi) \quad (\text{C-33})$$

Where  $J_\phi$  is the flux at the wall, and  $\phi_w$  is the value of the scalar at the wall.

$$J_\phi = \left( \frac{\partial \phi}{\partial n} \right)_w \quad (\text{C-34})$$

$E_\phi$  is calculated using the following equation:

$$E_\phi = E \exp \left( 9.0 \kappa \left( \left( \frac{\text{Pr}}{\sigma_\phi} \right)^{0.75} - 1 \right) \left( 1 + 0.28 \exp \left( -0.007 \frac{\text{Pr}}{\sigma_\phi} \right) \right) \right) \quad (\text{C-35})$$

## APPENDIX D. ERRORS AND GRID INDEPENDENCE

---

## **D.1. Errors in CFD Simulations**

There are a number of errors inherent in CFD simulations, some recognizable; others implicit in the assumptions of the flow field and some unacknowledged errors associated with programming or usage errors. A classification and description of the acknowledged errors, NPARC (2003), are given below.

- Physical approximation error
- Computer round-off error
- Iterative convergence error
- Discretization error
- Computer programming errors
- Usage errors

### **D.1.1. Physical approximation error**

These errors are associated with assumptions made in order to simplify the model or to improve computational efficiency of the solution. Errors due to assumptions in the flow field come about through incomplete knowledge of a particular problem, uncertainty of the magnitude of certain parameters of a model, simplification errors and the lack of experimental confirmation of a particular flow situation. Assessment of physical approximation errors is achieved through validation studies, which focus on certain known aspects of the model, verifiable through comparison with experimental or analytical solutions.

### **D.1.2. Computer round-off errors**

Round-off errors occur due to truncation of calculated values associated with the accuracy required in a computational flow package. These errors are usually considered insignificant when compared with other errors. If round-off errors are suspected of being significant, a test run using a higher precision is possible.

### **D.1.3. Iterative convergence error**

Convergence errors exist at the completion of a particular run and scale to the variation in the solution.

### **D.1.4. Discretization errors**

The governing flow equations are represented by algebraic equations in a discrete domain of space and time. Discretization errors are associated with the methods used for these representations. These are also known as numerical errors. The discrete spatial domain is known as the grid or mesh, and as this mesh is refined the solution should tend towards the continuum value and become less dependant on the size of the grid spacing. This process is known as grid convergence, and the solution is said to be grid independent if a variation in grid spacing does not significantly alter the values of variables from one grid to a successively refined grid. Discretization errors are of primary concern in CFD applications as they are dependant on the quality of the grid.

### **D.1.5. Computer programming errors**

Programming errors occur due to errors in programming of a particular code, and are discovered by thorough verification of subprograms and the entire code.

### **D.1.6. Usage errors**

As the name suggests usage errors are associated with incorrect use of a particular program. These errors can often manifest as modelling and discretization errors. Minimising of such errors only happens through proper training and experience with particular codes of flow modelling packages.

## D.2. Grid independence

In order to show that the solution is independent of the grid, three successive refinements of the grid are necessary. The solution is then extrapolated for a value of a significant flow variable using the results from the three refined solutions in the following manner, Thiart (2000), based on Richardson extrapolation:

$$\phi \approx \phi_h + \alpha h^n \quad (\text{D-1})$$

Where n in the above equation is:

$$n = \log_2 \left( \frac{\phi_{2h} - \phi_{4h}}{\phi_h - \phi_{2h}} \right) \quad (\text{D-2})$$

$$\alpha h^n = \frac{\phi_h - \phi_{2h}}{2^n - 1} \quad (\text{D-3})$$

If the argument for n in the above equation is negative, this means that the value of n is an imaginary number and that the value of  $\phi$ , does not change monotonically with refinement of the grid but oscillates with either increasing or decreasing amplitude. With substitution of n into equation D-2, the method can still be used. The result of this substitution follows below:

$$\alpha h^n = \frac{(\phi_h - \phi_{2h})^2}{2\phi_{2h} - \phi_h - \phi_{4h}} \quad (\text{D-4})$$

Further substitution of equation D-4, into equation D-1, gives the following relationship for the zero grid solution:

$$\phi \approx \frac{\phi_{2h}^2 - \phi_h \phi_{4h}}{2\phi_{2h} - \phi_h - \phi_{4h}} \quad (\text{D-5})$$

The value for n is an indicator of whether the value of  $\phi$  is converging or diverging. The criteria below must be met for convergence:

$$\left| \frac{\phi_{2h} - \phi_{4h}}{\phi_h - \phi_{2h}} \right| > 1 \quad (\text{D-6})$$

It is not necessary to halve the grid points in each co-ordinate system in order to get a finer grid, NPARC (2003). Non-integer grid refinement might be desirable in order to keep the solution within computational limits. However, it is important to keep the same grid generation parameters for each of the refined grids. This is usually done in significant area, i.e. normal to the wall, flow boundaries or stagnation zones and areas with large curvature.

## APPENDIX E. ENERGY EQUATION

---



## E.1. Energy Equation in terms of Potential Temperature

The energy equation can be defined in terms of the potential temperature. It can be seen that a simple conduction/convection transport equation is derived for the potential temperature. Starting from the first law of thermodynamics and the ideal gas law:

$$du = c_v dT = dh - pd\alpha \quad (\text{E-1})$$

$$p\alpha = RT \quad (\text{E-2})$$

Taking the derivatives of pressure, specific volume and temperature of the ideal gas law, and combining like terms gives the following equation:

$$pd\alpha + \alpha dp = RdT \quad (\text{E-3})$$

$$\frac{dp}{p} = \frac{R}{p\alpha} dT - \frac{d\alpha}{\alpha} \quad (\text{E-4})$$

From the definition of potential temperature, and deriving the equation in terms of temperature and pressure:

$$\theta = T \left( \frac{p_o}{p} \right)^{R/c_p} \quad \text{Definition of potential temperature} \quad (\text{E-5})$$

$$\frac{d\theta}{\theta} = \frac{dT}{T} - \frac{R}{c_p} \frac{dp}{p} = \frac{dT}{T} - \frac{R}{c_p} \left( \frac{R}{p\alpha} dT - \frac{d\alpha}{\alpha} \right) \quad (\text{E-6})$$

Substituting the first law equation in terms of the specific volume term obtained above, gives the following equation:

$$\frac{d\theta}{\theta} = \frac{dT}{T} - \frac{R}{c_p} \frac{dp}{p} = \frac{dT}{T} - \frac{R}{c_p} \left( \frac{R}{p\alpha} dT - \frac{dh - c_v dT}{p\alpha} \right) \quad (\text{E-7})$$

Further substitution of the relationship between specific heats of a fluid and the gas constant into the above equation for the derivative of potential temperature:

$$c_p = c_v + R \quad (\text{E-8})$$

$$\frac{d\theta}{\theta} = \frac{dT}{T} \left(1 - \frac{R}{c_p}\right) - \frac{R}{c_p} \left(\frac{c_v dT}{RT} + \frac{dh}{p\alpha}\right) = \frac{R}{c_p} \frac{dh}{p\alpha} \quad (\text{E-9})$$

For a transient process, the equation above simplifies to an equation for the changes of energy in terms of the potential temperature:

$$\frac{d\theta}{dt} = \frac{R}{c_p} \frac{\theta}{p\alpha} \frac{dh}{dt} = \frac{1}{c_p} \frac{\theta}{T} \frac{dh}{dt} \quad (\text{E-10})$$

It can be shown, Montavon (1998), that the right-hand side of the equation represents the non-adiabatic heat exchanges. Finally obtaining the energy equation in flux form:

$$\frac{\partial}{\partial t}(\rho\theta) + \vec{\nabla}(\vec{v}\rho\theta) = \rho \underbrace{\left[ \frac{\partial}{\partial t}\theta + \vec{v}\vec{\nabla}(\theta) \right]}_{\frac{d\theta}{dt}} + \theta \underbrace{\left[ \frac{\partial}{\partial t}\rho + \vec{\nabla}(\vec{v}\rho) \right]}_{=0, \text{continuity}} \quad (\text{E-11})$$

$$\frac{\partial}{\partial t}(\rho\theta) + \vec{\nabla}(\vec{v}\rho\theta) = \rho \frac{d\theta}{dt} = \rho \frac{1}{c_p} \frac{\theta}{T} \frac{dh}{dt} \quad (\text{E-12})$$

It can be seen that the energy equation, for purely adiabatic processes, is simply an advection diffusion equation in terms of potential temperature with a vanishing diffusion co-efficient. Diffusion is included during turbulent mixing.

## APPENDIX F. USER FORTRAN ROUTINES

---

The FORTRAN routines shown below have been edited from the original files in order to facilitate ease of understanding of the routines involved. In some cases the dummy arguments for utility routines have been condensed. The usual FORTRAN comments for the routines have been highlighted. For further information on the exact specification of dummy arguments for the FORTRAN routines it is necessary to consult CFX 4-4 (2001).

## F.1. Hydrostatic Density Profile

The density used in the calculations in CFX 4-4 is stated as a function only of height, with the assumption of a dry adiabatic lapse rate temperature profile throughout the height of the flow domain.

```
SUBROUTINE USRDEN
```

*Hydrostatic reference pressure based on DALR set as a function of height*

```
PHYDRO(I) = 101300.00*(1-0.00975*XP(I)/300.00)**3.5
```

*Real temperature profile based on DALR*

```
TREAL(I) = 300.00 - 0.00975*XP(I)
```

*Set hydrostatic density profile based on given real temperature profile*

```
CALL GETVAR('USRDEN','DEN ',IDEN)
```

*Single phase flow*

```
IPHS = 1
```

*Set constant value for R\_AIR*

```
RUNIV = 8314.00 !Universal gas constant
```

```
AIR_MOL_MASS = 28.95 !Molecular mass for air
```

```
R_AIR = RUNIV/AIR_MOL_MASS
```

*Loop over cell centres*

*Use IPALL to find 1D addresses of all cell centres in blocks*

```
CALL IPALL('*', '*', 'BLOCK', 'CENTRES', IPT, NPT, CWORK, IWORK)
```

*DRHODP at constant T*

```
DO I = 1, NPT
```

```
    INODE = IPT(I)
```

*Use function for real temperature*

```
DRHOPT = 1.0 / (R_AIR*TREAL(INODE))
```

*Set new density and use function for hydrostatic pressure*

```
DENN(INODE,IPHS) = DRHOPT*PHYDRO(INODE)
```

```
ENDDO
```

*Set density on all patches*

```
CALL IPALL('*', '*', 'PATCH', 'CENTRES', IPT, NPT, CWORK, IWORK)
```

```
DO I=1, NPT
```

```
    INODE = IPT(I)
```

```
    DRHOPT = 1.0 / (R_AIR*TREAL(INODE))
```

*Set new density*

```
DENN(INODE,IPHS) = DRHOPT*PHYDRO(INODE)
```

```
ENDDO
```

```
END
```

## F.2. Specification of Potential Temperature Diffusivity

This subroutine is used to specify the diffusivity of the potential temperature USER SCALAR in terms of the Prandtl number for the potential temperature and the turbulent viscosity in the flow field.

```
SUBROUTINE USRDIF
```

*Obtain variable number for the potential temperature user scalar*

```
CALL GETVAR('USRDIF', 'SCAL ', ISC)
```

```
CALL GETSCA('POTTEMP', ISCAL1, CWORK)
```

```
ISC1 = ISC + ISCAL1 - 1
```

*Find variable number for Prandtl number*

```
CALL GETADD('USRDIF', 'RTURB ', 'PRT ', ILEVEL, JPRT)
```

*Define constant molecular viscosity at 300K*

```
VIS_MOL = 1.843E-06
```

*Get the variable for the turbulent viscosity*

```
CALL GETVAR('USRDIF', 'VIS ', IVIS)
```

*If the diffusivity of the potential temperature is calculated then change*

IF (IEQN.EQ.ISC1) THEN

*Set for single phase flow*

IPHS = 1

*Set the diffusivity of the potential temperature for all cells*

DO INODE = 1,NCELL

*Set the diffusivity of the potential temperature based on turbulence*

*Turbulent Prandtl number for potential temperature*

PRANPT = WORK(JPRT + ISC1 - 1)

*Turbulent viscosity*

VISTURB = VIS(INODE,IPHS)

*Diffusivity*

DIFFPT = VISTURB/PRANPT

GAMMA(INODE,IPHS,1) = DIFFPT

END

### F.3. Addition of Source Terms in the Transport Equations

User routine USRSRC used in order to specify buoyancy source term in the u-momentum equation in terms of the potential temperature. This routine is also utilised in the application of source terms in the k equation for buoyant production of turbulent kinetic energy and the  $\epsilon$  equation, as well as the addition of the transport equation in the  $\epsilon$  equation.

SUBROUTINE USRSRC

*Hydrostatic reference pressure function for the DALR*

PHYDRO(I) = 101300.00\*(1-0.00975\*XP(I)/300.00)\*\*3.5

*Real temperature profile based on the DALR*

TREAL(I) = 300.00 - 0.00975\*XP(I)

*Potential temperature reference value*

FPOTTEMP(I) = 300.00

*Addition of momentum source term based on potential temperature*

***Definition of Cp and Rair and GRAV***

CP\_AIR = 1005.00 *!At 300K, from MILLS(1995)*

RUNIV = 8314.00 *!Universal gas constant*

RM\_AIR = 28.95 *!Molecular mass of air at 300K*

GRAV = 9.8 *!Acceleration due to gravity*

***Define R\_AIR = RUNIV/MM\_AIR Air gas constant***

R\_AIR = RUNIV/RM\_AIR

***Use IPALL to find addresses of block for momentum equation***

CALL IPALL('\*', '\*', 'BLOCK', 'CENTRES', IPT, NPT, CWORK, IWORK)

***Call variable number for the U momentum equation***

CALL GETVAR('USRSRC', 'U', IU)

***Call scalar number for potential temperature and USRDCC\_SOURCE***

CALL GETSCA('POTTEMP', ICS1, CWORK)

***If u-momentum equation then add source term based on pottemp***

IF (IU.EQ.IEQN) THEN

***Set IPHS for single-phase flow***

IPHS = 1

***Loop over all blocks***

DO I = 1, NPT

***Use statement function IPT to get addresses***

INODE = IPT(I)

***Define the hydrostatic potential temperature as function of x-height temporary values***

PHYDROTEMP = PHYDRO(INODE) *!Hydrostatic pressure at height*

***XP(INODE)***

TREALTEMP = TREAL(INODE) *!Real temperature profile at height*

***XP(INODE)***

***Combine R\_AIR and CP\_AIR into R\_over\_Cp***

R\_over\_Cp = R\_AIR/CP\_AIR

***Define P\_GROUND, pressure at ground level***

P\_GROUND = 101300.00 !pa

***Hydrostatic potential temperature***

POTTEMP\_HYDRO = 300.00

*Constant potential temperature for DALR hydrostatic condition*

*Hydrostatic density value at height XP(INODE)*

HYDRODEN =PHYDROTEMP/(R\_AIR\*TREALTEMP)

*Assign temporary value for the potential temperature scalar at XP(INODE)*

TEMPPOTTEMP = SCAL(INODE,IPHS,ICS1)

*Define the source term based on potential temperature*

TEMPSOURCE =

+ HYDRODEN\*(TEMPPOTTEMP  
POTTEMP\_HYDRO)/POTTEMP\_HYDRO

*Buoyancy source*

BSCPT = GRAV\*(TEMPSOURCE)

*Add source terms depending on difference from hydrostatic*

SOURCU = BSCPT

*Addition of potential temperature source term to U-momentum*

SU(INODE,IPHS) = SU(INODE,1) + SOURCU\*VOL(INODE)

ENDDO

ENDIF !IEQN.EQ.IU

*Introduction of buoyancy source term in the 'K' equation*

*Negative part is introduced implicitly to avoid that  $K < 0$*

*Positive part is introduced explicitly See Duynkerek(1988)*

*Find variable number for turb kinetic energy*

CALL GETVAR('USRSRC','TE ',ITE) *!Variable number of k*

CALL GETVAR('USRSRC','SCAL ',ISC) *!Variable number for user scalar*

CALL GETSCA('POTTEMP',ISCAL1,CWORK) *!Scalar 1 is potential  
temperature*

ISC1 = ISC + ISCAL1 - 1

*If TE equation then add source term*

IF (IEQN.EQ.ITE) THEN

*Reserve real workspace for potential temperature gradients*

CALL SETWRK('USRSRC','WORK ', 'GRADPT',3\*NCELL,JGRAPT)



*Compute potential temperature gradients*

CALL GRADS

*Find variable number for Prandtl number*

CALL GETADD('USRSRC','RTURB ','PRT ',ILEVEL,JPRT)

*Find variable number for old value of k, TE*

CALL GETADD('USRSRC','VAROLD','TE ',ILEVEL,JTEOLD)

*Find variable number for old value of  $\varepsilon$ , ED*

CALL GETADD('USRSRC','VAROLD','ED ',ILEVEL,JEDOLD)

*Loop over patch*

DO I = 1,NPT

*Use statement function IPT to get addresses*

INODE = IPT(I)

*Vertical component of potential temperature gradient*

DPOTX = WORK(JGRAPT + INODE - 1)

*Prandtl number for potential temperature*

PRANPT = WORK(JPRT + ISC1 - 1)

*Compute buoyancy production term for K (positive for unstable stratification i.e. DPOTX < 0)*

GBUOY = -VIS(INODE,IPHS)/PRANPT  
+ \*ABS(GRAV)\*DPOTX/FPOTTEMP(INODE)

*Split buoyancy term into positive and negative representation*

BUOPOS = 0.5\*(GBUOY + ABS(GBUOY))

BUONEG = 0.5\*(GBUOY - ABS(GBUOY))

TEOLD = WORK(JTEOLD + INODE - 1)

TEOINV = 1/(TEOLD + SMALL)

SOURCU = BUOPOS

SOURCP = BUONEG\*TEOINV

*Add source term, depending on the vertical pot temp gradients*

SU(INODE,IPHS) = SU(INODE,IPHS) + SOURCU\*VOL(INODE)

SP(INODE,IPHS) = SP(INODE,IPHS) + SOURCP\*VOL(INODE)

ENDDO

*Delete workspace for gradients when finished*

```
CALL DELWRK('USRSRC','WORK ', 'GRADPT')
```

```
ENDIF !ITE = IEQN
```

*Buoyancy source term in the epsilon equation, only active when +ve*

*Source term depending on the vertical diffusion of the TKE, only +ve*

*Find variable number for turbulent dissipation rate*

```
CALL GETVAR('USRSRC','ED ', IED)
```

*If dissipation equation then add source term*

```
IF (IEQN.EQ.IED) THEN
```

*Find variable number for Prandtl number*

```
CALL GETADD('USRSRC','RTURB ', 'PRT ', ILEVEL, JPRT)
```

*Find variable number for old value of TE*

```
CALL GETADD('USRSRC','VAROLD','TE ', ILEVEL, JTEOLD)
```

*Find variable number for old value of ED*

```
CALL GETADD('USRSRC','VAROLD','ED ', ILEVEL, JEDOLD)
```

*Reserve workspace for potential temperature gradients*

*kinetic energy gradients*

*gradient of the 'inner term',  $\partial k / \partial x_i$*

```
CALL SETWRK('USRSRC','WORK ', 'GRADTE', 3*NCELL, JGRATE)
```

```
CALL SETWRK('USRSRC','WORK ', 'GRADPT', 3*NCELL, JGRAPT)
```

```
CALL SETWRK('USRSRC','WORK ', 'GRATE2', 3*NCELL, JGRTE2)
```

```
CALL SETWRK('USRSRC','WORK ', 'GRDINT', NNODE, JGRINT)
```

*Compute potential temperature gradients*

```
CALL GRADS
```

*Compute k gradients*

```
CALL GRADS
```

*Loop over patch to assign to work(JGRINT) the x component of JGATE multiplied by*

*VIS/PRANTL*

*Prandtl number*

```
PRANTE = WORK(JPRT + ITE - 1)
```

*Loop over block*

```
DO I = I,NPT
```

**Use statement function IPT**

INODE = IPT(I)

**Assign values to the new work**

WORK(JGRINT + INODE - 1) = VIS(INODE,IPHS)/PRANTE  
+ \* WORK(JGRATE + INODE - 1)  
ENDDO

**Loop over boundaries**

CALL IPALL('\*', '\*', 'PATCH', 'CENTRES', IPT, NPT, CWORK, IWORK)  
DO M = 1, NPT

**Boundary node global-node-number**

INODE = IPT(M)  
IBDRY = INODE - NCELL  
INODE1 = IPNODB(IBDRY, 1)  
INODE2 = IPNODB(IBDRY, 2)  
WORK(JGRINT + INODE - 1) = VIS(INODE2, IPHS)/PRANTE  
+ \* WORK(JGRATE + INODE2 - 1)  
ENDDO

**Compute gradients of the inner term,**

**Term is stored in the array WORK(JGRATE+NCELL)**

CALL GRADS  
CALL IPALL('\*', '\*', 'BLOCK', 'CENTRES', IPT, NPT, CWORK, IWORK)

**Loop over patch adding buoyancy part**

DO I = 1, NPT  
INODE = IPT(I)

**Compute vertical potential temperature gradients**

DPOTX = WORK(JGRAPT + INODE - 1)

**Prandtl number for potential temperature**

PRANPT = WORK(JPRT + ISC1 - 1)

**Compute buoyancy production term for K (positive for unstable stratification i.e. DPOTX < 0)**

GBUOY = -VIS(INODE, IPHS)/PRANPT  
+ \* ABS(GRAV) \* DPOTX / FPOTTEMP(INODE)

*Split buoyancy term into positive representation, negative ignored*

BUOPOS = 0.5\*(GBUOY + ABS(GBUOY))

TEOLD = WORK(JTEOLD + INODE - 1)

TEOINV = 1/(TEOLD + SMALL)

EDOLD = WORK(JEDOLD + INODE - 1)

*Add term relative to the diffusion of TKE only when > 0*

TRSPKE = WORK(JGRTE2 + INODE - 1)

TRSPOS = 0.5\*(TRSPKE + ABS(TRSPKE))

*Add source term only when positive*

C1 = 1.46 *!Model constants for k-e model*

SOURCU = C1\*(BUOPOS)\*EDOLD\*TEOINV

SU(INODE,IPHS) = SU(INODE,IPHS) + SOURCU\*VOL(INODE)

ENDDO

*Delete workspace in reverse order*

CALL DELWRK('USRSRC','WORK ','GRDINT')

CALL DELWRK('USRSRC','WORK ','GRATE2')

CALL DELWRK('USRSRC','WORK ','GRADPT')

CALL DELWRK('USRSRC','WORK ','GRADTE')

ENDIF *!IED = IEQN*

END